Extending Quota models to nitrogen-limited growth of phytoplankton populations

Thesis submitted by

Martino Edoardo Malerba

BSc James Cook University

BSc (Hons) James Cook University

In December 2015

For the degree of **Doctor of Philosophy**

In the College of Marine and Environmental Science

James Cook University

Acknowledgements

First and foremost, I want to thank Prof. Sean R. Connolly for his endless and unconditional support. You have been a mentor throughout my entire student career. Thank you for giving me a chance. I will always look back at all your teachings.

Thank you very much Kirsten for all your time and effort, without which this project would have not been possible. When I first started I knew little about working in a microbiology laboratory. I will now pass your wisdom to others.

Thank you to all members of the Ecological Modelling Laboratory and the North Queensland Algal Identification Facility, for insightful feedback and for the team spirit provided throughout these few years. Special thanks to Dr. Loic Thibaut, for feedback on computer codes, and Dr. Shane Blowes, for comments on manuscripts. I also want to thank Stan Hutson and Florian Berner for their guidance with laboratory practices.

I am very thankful to the Australian Institute of Marine Science, the AIMS@JCU scholarship program, and James Cook University for financial and logistical support. I also want to thank Dr. Lyndon Llewellyn, Savita Francis, Dr. Mia Hoogenboom, Dr. Christian Lonborg, Prof. James Burnell, Prof. Bruce Bowden, Dr. Samuel Circes for help provided along the way. Finally, I want to thank Carlo Mattone and Dr. Chiara Pisapia, my inseparable coffee companions.

Statement of Contribution of Others

Chapter 2: Martino Malerba conceived the project, co-designed and performed the analyses, and wrote multiple drafts of the manuscript. Sean Connolly assisted in developing the approach and argument, assisted in the interpretation of the results, and made suggestions and edits to multiple drafts of the paper. Kirsten Heimann assisted in developing the laboratory protocols, assisted in the approach and the argument, and made suggestions and edits to multiple drafts of the paper.

Chapter 3: Martino Malerba conceived the project, co-designed and performed the analyses, and wrote multiple drafts of the manuscript. Sean Connolly assisted in developing the approach and argument, assisted in the interpretation of the results, and made suggestions and edits to multiple drafts of the paper. Kirsten Heimann assisted in the approach and the argument, and made suggestions and edits to multiple drafts of the paper.

Chapter 4: Martino Malerba conceived the project, co-designed and performed the analyses, and wrote multiple drafts of the manuscript. Sean Connolly assisted in developing the approach and argument, assisted in the interpretation of the results, and made suggestions and edits to multiple drafts of the paper. Kirsten Heimann assisted in developing the laboratory protocols, in the approach and the argument, and made suggestions and edits to multiple drafts of the paper.

Chapter 5: Martino Malerba conceived the project, co-designed and performed the analyses, and wrote multiple drafts of the manuscript. Sean Connolly assisted in developing the approach and argument, assisted in the interpretation of the results, and made suggestions and edits to multiple drafts of the paper. Kirsten

Heimann assisted in developing the argument and made suggestions and edits to multiple drafts of the paper.

Abstract

Almost all life on earth is directly or indirectly dependent on phytoplankton primary productivity. In many aquatic systems, phytoplankton primary production is limited by the availability of nitrogen in the environment. Therefore, studying the dynamics of nitrogen uptake and assimilation by phytoplankton cells is critically important for understanding many ecosystem services and global biogeochemical cycles. Mathematical models are particularly powerful tools for analyzing dynamic processes in many areas of ecology, but so far their employment with phytoplankton time-series has been limited. Specifically, published phytoplankton models are unable to explicitly account for the role of different nitrogen forms on cell division and can only be calibrated with time-consuming and impractical monitoring of specific variables. Overall, this thesis aimed to expand previous models by incorporating important processes regulating nitrogen utilization in phytoplankton cells, and by improving their calibration with proxy data routinely monitored in experimental studies.

Nitrate and ammonium are the two most important sources of inorganic nitrogen driving phytoplankton primary productivity. The performance of phytoplankton species changes when reared with either of these two forms of nitrogen individually, as well as when they are both present, or when cells have experienced previous periods of nitrogen starvation. However, current functional responses are unable to capture transient and interactive dynamics of nitrate and ammonium uptake, nor can they capture how these two forms of nitrogen differently influence cell division. Hence, in chapter 2, I designed and empirically

tested a new process-based model that includes uptake of both nitrate and ammonium, as well as the effects of starvation length and inhibition of nitrate uptake by ammonium on phytoplankton cell division. Results for the green alga *Chlorella* sp. showed that a single parameterization of the model performed well across data from laboratory cultures started at 12 different initial conditions. This new model allowed for the first time the quantification of nitrate-ammonium utilization traits of a phytoplankton species. This contributes to a more comprehensive understanding of the factors underpinning the high variation in nitrate-ammonium assimilation observed in natural and engineered systems.

Characterizing resource utilization traits of a species is particularly important for identifying processes promoting biodiversity and ecosystem functioning in nature. Most trait-based studies define species by their mean trait values and assume intraspecific trait variability to be negligible compared to interspecific differences. However, phenotypic plasticity may be an important source of variation in phytoplankton species, which are well known for their ability to rapidly adjust their cell size according to biotic and abiotic conditions. In chapter 3, I used the model designed in chapter 2 to evaluate the effects of cell size plasticity on the nitrogen utilization traits of the green alga *Desmodesmus armatus*, reared under different nitrogen sources (nitrate, ammonium, or both) and nitrogen histories (N-replete and N-deplete). Results showed that nitrate-ammonium utilization traits depended substantially on mean cell size and nitrogen history and that representing phytoplankton species by their mean trait values (as per traditional approaches) could underestimate the actual performance of a species by as much as one order of magnitude. These results highlight the ecological importance of intraspecific

variability in determining the ability of a species to adjust to new environmental conditions.

Biologically, it is well-known that the internal concentration of the most limiting nutrient (cell "quota") is what determines the growth rate of a cell. Given the critical importance of nitrogen for phytoplankton cell division, monitoring nitrogen quota is important to understand aquatic primary productivity, phytoplankton ecology, eutrophication and algal blooms. However, current methods to directly monitor nitrogen quota remain inaccurate, expensive, destructive, and time-consuming. Thus, in chapter 4, I tested the hypothesis that optical changes in single cells, which can be rapidly and accurately monitored with a standard flow cytometer, can provide reliable proxies for per-cell internal nitrogen. Results from four freshwater phytoplankton species showed that cellular nitrogen quota could be estimated accurately ($R^2 = 0.9$) from cell optical properties and medium nitrogen, and that the relationship did not change among different species or different initial conditions. In particular, red chlorophyll autofluorescence (from here on simply "red fluorescence") was the most important variable explaining 77% of the total variability in total cell nitrogen. These results indicate that optical flow cytometric variables are a reliable and non-destructive method to estimate nitrogen quota in phytoplankton cells.

Finding an efficient proxy to evaluate cell nitrogen quota is particularly valuable for extending the applicability of phytoplankton models. The internal nitrogen status of a cell is critical to analyze the dynamics of nitrogen-limited phytoplankton populations, but accounting for this process in phytoplankton models requires monitoring per-cell nitrogen quota, which is time-consuming, inaccurate,

and destructive. Instead, the method I proposed in chapter 4 to quantify nitrogen quota using the optical properties of individual cells is rapid, precise, accurate, and non-destructive. Hence, in chapter 5, I evaluated a new way to model phytoplankton populations, consisting in explicitly including cell optical properties as a proxy for nitrogen quota within phytoplankton Quota models. Results showed that accounting for cell optical properties could improve the performance of phytoplankton population models while still accounting for the biologically important process of cell nitrogen storage. More broadly, these findings highlight the importance of identifying proxy variables for the internal condition of an organism when using population models to analyze species dynamics.

The overarching aim of my thesis was to improve current phytoplankton models for the analysis of phytoplankton nitrogen utilization. This was achieved by presenting and calibrating a new mathematical framework describing the dynamics of nitrate-ammonium utilization in phytoplankton populations (chapter 2), by evaluating the effect of mean cell size and previous nitrogen history in determining the nitrogen utilization of a cell (chapter 3), and by documenting the importance of cell optical properties for explaining the dynamics of phytoplankton populations (chapters 4 and 5). These findings improve our ability to identify, analyze, and understand the relationships between nitrogen concentrations in the environment and phytoplankton populations. More broadly, this thesis offers new mathematical tools to better investigate the processes regulating phytoplankton primary productivity in nature and engineered systems.

Table of contents

List of Tables

List of Figures

Dedicated to the ones I love.

To my dad, mum, brother, and grandmother, for always encouraging me to follow my dreams, even when they take you so far away from home.

To my beloved partner, Maria del Mar Palacios, my island of peace and happiness.

Chapter 1: General Introduction

Phytoplankton Nitrogen Assimilation

All life depends on nitrogen. It is the building block from which nature assembles essential biomolecules, including amino acids, proteins, and nucleic acids (Crawford *et al.* 2000; Capone *et al.* 2008). The Earth's atmosphere is composed of 78% nitrogen, but for the most part it is in a form that is not directly usable by most organisms (Wayne 1993; Carpenter & Capone 2008). Only a minority of specialized organisms (e.g. N_2-fixing cyanobacteria and proteobacteria) are able to convert and deliver nitrogen from the atmosphere to the rest of the biosphere (Carpenter *et al.* 2008). Overall, phytoplankton cells contribute around 70% to global nitrogen assimilation, and they are responsible for 30-40% of the primary productivity on Earth (Duarte & Cebrian 1996; Collos & Berges 2002). Hence, investigating the processes regulating phytoplankton nitrogen utilization is critically important for global nitrogen cycles, ecosystem management, and ecological processes.

Scientific interest in phytoplankton nitrogen utilization has risen consistently in the past few decades, especially due to certain emerging key issues. Firstly, economic development is profoundly altering nitrogen fertilization regimes, both in terms of total concentrations and also relative abundance of different nitrogen types (Domingues *et al.* 2011; Fowler *et al.* 2013). The impacts are predicted to increase in freshwater and coastal systems, especially near highly populated areas, with effects that are difficult to forecast (Fowler *et al.* 2013). Secondly, there is considerable evidence showing that altering total and relative nitrogen fertilization

can destabilize natural food webs and affect ecosystem functioning and plant community structure (Folke *et al.* 2004; Schimel & Bennett 2004; Boudsocq *et al.* 2012). For instance, whole-lake experiments have shown that changing fertilization rates can shift an aquatic system characterized by clear-water and nutrient recycling, to an alternative stable state of turbid-water, dominated by toxic cyanobacteria, and with anoxic events and high fish mortality (Smith 1998; Folke *et al.* 2004). Thirdly, microalgal biotechnology is emerging as an important source of energy and primary metabolites (e.g. sugars, oils and lipids; Mata, Martins & Caetano 2010; Gimpel *et al.* 2013). The economic sustainability of phytoplankton industrial production also relies on ensuring optimal regimes of nitrogen fertilization of the biomass, avoiding limited growth while reducing excess nutrients in wastewaters (Lardon *et al.* 2009; Yang *et al.* 2011). Thus, the interaction between phytoplankton and nitrogen is critically important in many areas of conservation, ecology, and economics.

Nitrate and Ammonium

Phytoplankton assimilation of nitrate and ammonium quantitatively dominates the nitrogen cycle (Gruber 2008). However, the assimilation of these two forms of nitrogen differs. Ammonium is easier to assimilate because most amino acids are in the same oxidation state; in contrast, nitrate must first be reduced to ammonium, by means of specialized enzymes, before assimilation can occur (Dortch 1990; Crawford *et al.* 2000; Gruber 2008). These physiological differences in the assimilation of nitrate and ammonium lead to transitory uptake dynamics in the environment. For instance, phytoplankton cells tend to favor ammonium over nitrate when both are present (Dortch 1990; Domingues *et al.* 2011). Also, cells recovering from nitrogen starvation require an acclimatization period before they

can assimilate nitrate, while ammonium uptake is not affected (Dortch *et al.* 1982; Martinez 1991; De La Rocha *et al.* 2010). Therefore, transitory and interactive processes affect the way in which phytoplankton cells uptake and assimilate nitrate and ammonium from the environment.

Quota Models

Fitting process-based models to time-series is a particularly powerful way to analyze nitrogen utilization in phytoplankton cultures. The main advantage of analyzing culture dynamics with process-based models is that it uses functional responses to analyze correlated changes in multiple state variables (i.e. rate of population growth depends on changes in nitrogen uptake and internal storage), conversely to phenomenological (statistical) curve-fitting methods where each state variable is analyzed in isolation. Also, process-based models are built on prior knowledge about how a system works, making their assumptions more transparent. Furthermore, these modeling techniques can account for transient dynamics of a cell, by explicitly incorporating the effect of time in the culture, which is particularly important for phytoplankton systems that are not at equilibrium (Hilborn & Mangel 1997; Bolker 2008; Cuddington *et al.* 2013).

The Quota model, first introduced by Droop (1968), is today the most successful type of process-based model to describe nitrogen-limited growth in phytoplankton populations (Pahlow & Oschlies 2013). The major innovation of Quota models is that stored nutrients within a cell can allow cell division even in the absence of sufficient external nutrients, as opposed to previous models where instead cell division depended directly on external nutrient concentrations (Droop 1983; Droop 2003; Leadbeater 2006). This assumption of Quota models is largely

biologically justified: phytoplankton cells are adapted to respond to nutrient-limited conditions by relocating resources from storage molecules (e.g. lipids, carbohydrates, proteins, pigments, RNA) to vital metabolic functions (e.g. cell division; Dortch *et al.* 1984). Today Quota models are used both for theoretical analysis of phytoplankton dynamics (e.g. Klausmeier *et al.* 2004; Grover 2011), and for analyzing nutrient utilization of algal species in the field or in laboratory conditions (e.g. Solidoro *et al.* 1997; Ducobu *et al.* 1998). The main advantage of using Quota models to analyze nitrogen utilization from time-series of phytoplankton dynamics is that it allows calibrating functional responses based on all variables in the system, therefore quantifying the flows of nitrogen between the environment (i.e. ambient nitrate and ammonium concentrations), the pre-existing biomass (i.e. intracellular nitrogen storages), and the newly produced biomass (i.e. cell division).

Improving Phytoplankton Quota Models

Multiple Nitrogen Types

Phytoplankton quota models have been extended to multiple nitrogen sources to improve current oceanographic models (e.g. Moore et al. 2002, Litchman et al. 2006). However, these more complex models have never been directly calibrated to experimental data. Instead, their parameters have been inferred from literature surveys. Quota models that have been calibrated to phytoplankton nutrient-utilization data have been, so far, overwhelmingly limited to a single source of ambient nitrogen (but see Malerba, Connolly & Heimann 2012). In particular, their formulation cannot distinguish between the different effects of nitrate and ammonium on cell division. Current analytical methods for the analysis of nitrate-

ammonium utilization in phytoplankton cells are phenomenological. They mainly consist of calculating per-cell rates by dividing depleted medium nitrogen by cell density at two successive points in time, and then fitting a functional response with least-squares techniques (e.g. Dortch 1990; Maguer *et al.* 2007; Laws *et al.* 2011; Tantanasarit, Englande & Babel 2013). While convenient for the analysis of systems at equilibrium, these traditional approaches are unable to characterize the mechanism of cell specific growth rate as a function of per-cell nitrogen assimilation. Phenomenological models can estimate how the assimilation of a cell or its growth rate change as a function of nutrient concentrations, but they cannot characterize nitrogen dynamics among the different compartments in the system (i.e. from the medium to the internal quota of a cell and to the newly produced cells). Also, the precision of these approaches is limited, since each point is calculated from two observations only. A different way to analyze phytoplankton nutrient utilization is by fitting process-based models to time-series observations. Differently to phenomenological models, process-based models explicitly characterize changes in response variables (biomass, ambient nitrogen, etc.) as functions of events that drive those changes (nitrogen uptake, assimilation, cell proliferation, etc.). This makes possible calibration of species-specific functional responses on data from all variables at once, thereby characterizing how flows of nitrogen among ambient nitrate and ammonium, internal nitrogen quota, and population density influence one another. Hence, in the first part of this thesis, I developed an alternative mathematical framework for the analysis of nitrate-ammonium utilization in phytoplankton dynamics. To do this, I extended the classic formulation of the Quota model to explicitly account for two different nitrogen sources (i.e. nitrate and ammonium), and to characterize how each one affects

population dynamics. By designing and fitting a new Quota model, it was possible to quantify the different contributions of nitrate and ammonium to the overall rate of cell division in phytoplankton populations. Furthermore, this approach allowed accounting for two factors that are important to regulate nitrate and ammonium assimilation: the transient effect of nitrogen starvation length on nitrate uptake, and the inhibitory effects of ammonium uptake on nitrate uptake.

Possessing a process-based method for quantifying phytoplankton nitrate-ammonium utilization in phytoplankton species also allows investigating what factors regulate nitrogen assimilation in single cells. For instance, the size of a cell is often considered the "master" trait in phytoplankton species (Litchman & Klausmeier 2008). This is mainly because the ability of a cell to assimilate nutrients, photosynthesize, or divide is constrained by its surface-to-volume ratio by first principles of physics and chemistry (Litchman *et al.* 2008; Barton *et al.* 2013). However, phytoplankton cells are also known for their remarkable ability to rapidly respond to changes in environmental conditions by adjusting their cell size (Duarte *et al.* 1996). Potentially, this means that the nitrogen utilization of a species will change depending on the size of the cell. Therefore, chapter 3 tested the hypothesis that phenotypic plasticity in cell size influences the nitrogen utilization of phytoplankton species. I tested this hypothesis by fitting alternative parameterizations of the Quota model designed in chapter 2 to time-series collected from a different phytoplankton species.

Optical Proxies for Per-Cell Nitrogen Status

It has long been recognized that phytoplankton cells experiencing nutrient limitation divide at a rate that is proportional to the internal supply of the most

limiting nutrient, and only indirectly dependent on ambient nutrient availability (Caperon 1968; Droop 1968). As a consequence, any attempt to model phytoplankton nitrogen-limited dynamics requires explicit characterization of the dynamics of the internal nitrogen concentration within a cell (Caperon & Meyer 1972; Droop 2003). The traditional approach to estimate nitrogen status in phytoplankton cells is mainly by direct elemental analysis (Shelly, Holland & Beardall 2010). However, these protocols are usually time-consuming, require specialized laboratory equipment, and cannot differentiate between elements derived from live and dead cells or inorganic particles, which can substantially overestimate per-cell nutrient composition (Beardall, Young & Roberts 2001; Shelly *et al.* 2010). Dynamics of internal nitrogen can sometimes be inferred based on changes in population density and ambient nitrogen depletion (Fujimoto *et al.* 1997; De La Rocha *et al.* 2010). Previous experiments showed that phytoplankton Quota models could be fitted to laboratory time-series data even when internal quota is not directly monitored (Ducobu *et al.* 1998; Malerba *et al.* 2012). However, this approach is limited to closed and highly controlled laboratory settings, and it generally requires more data and more complex experimental designs. In chapter 4, I explored an alternative method to monitor the per-cell nitrogen concentrations within phytoplankton cells. Specifically, I tested the hypothesis that the cell nitrogen status leads to systematic changes in the optical properties of a cell, which can provide a quantifiable proxy for cell nitrogen concentrations that is non-destructive and more precise to measure than traditional methods.

Using optical analysis to estimate internal nitrogen status in phytoplankton cells can be particularly useful for modeling phytoplankton nutrient-limited dynamics. Calibrating Quota models to data usually requires time-series of daily

observations of multiple state variables. This task becomes particularly time-consuming when, together with ambient nitrogen and population density, also internal cell nitrogen needs to be monitored. Flow cytometric optical analysis of phytoplankton cells is instantaneous, non-destructive, precise, and can be monitored through automated programmable instruments (Collier 2000; Dubelaar & Jonker 2000; Veldhuis & Kraay 2000). Therefore, monitoring the optical information of a culture for calibrating nitrogen-limited Quota models can be vastly more efficient than directly quantifying nitrogen concentrations within cells. In chapter 5, I assess the feasibility and precision of calibrating Quota models to phytoplankton time-series where optical information are employed as a proxy of internal nitrogen.

Thesis Structure

The overarching aim of this thesis is to improve the design and broaden the applicability of Quota models for understanding nitrogen utilization in phytoplankton cells. The data chapters in this thesis are divided in two thematic sections, each consisting of two chapters. The aims of each chapter are presented below:

Part I: Nitrate-ammonium utilization in phytoplankton cells

- Chapter 1: The aim is to formulate, calibrate, and test a new Quota model that quantifies the nitrate-ammonium utilization of phytoplankton populations, also accounting for transient and interactive effects of starvation length and ammonium inhibition on the nitrate uptake.
- Chapter 2: The aim is to test whether changes in mean population cell size can affect nitrate-ammonium utilization traits of phytoplankton cells.

Part II: Optical proxy for internal nitrogen status in single phytoplankton cells

- Chapter 3: The aim is to investigate whether cell optical properties can be used as an accurate predictor of nitrogen quota in laboratory phytoplankton cultures.
- Chapter 4: The aim is to evaluate the reliability of explicitly accounting for cell red fluorescence as a proxy for internal nutrient status in phytoplankton nitrogen-limited models.

Publication Details

Each data chapter is presented as a stand-alone scientific article. As a result, the contextualization of the work in each chapter was broadened to fit the scope of the target journal. Chapter 2 of my thesis is published in Ecological Modelling (Malerba, Connolly & Heimann 2015). Chapter 4 is published in the Journal of Applied Phycology (Malerba, Connolly & Heimann, 2016). Chapters 3 is *in press* in Functional Ecology. Chapter 5 is currently under review in Journal of Theoretical Ecology (JTB-S-15-01491).

Chapter 2: An experimentally validated nitrate-ammonium-phytoplankton model including effects of starvation length and ammonium inhibition on nitrate uptake

Introduction

All living organisms require nitrogen (N) for the production of new biomass. While heterotrophic organisms rely exclusively on organic N from their diet, autotrophic organisms can also absorb inorganic N from the environment (Crawford *et al.* 2000). Ammonium and nitrate are the two most common ionic (reactive) forms of inorganic N, and their assimilation by plants and photosynthetic algae quantitatively dominates the nitrogen cycle (Zehr & Ward 2002; Gruber 2008). However, the way autotrophic organisms incorporate these two N forms differs. Ammonium is easier to assimilate because most amino acids are in the same oxidation state; in contrast, nitrate must be first reduced to ammonium by means of specialized enzymes and then assimilated (Guerrero, Vega & Losada 1981; Syrett 1981; Berges 1997). This key difference between nitrate and ammonium assimilation leads to different assimilation kinetics in autotrophic organisms, which have far reaching implications in many areas, including understanding changes in species competition (Jackson, Schimel & Firestone 1989; Donald *et al.* 2011), evaluating the effects of eutrophication (Cox *et al.* 2009), quantifying fluxes of the nitrogen cycle (Fowler *et al.* 2013), and analyzing optimal fertilization for industrial production (Michalczyk *et al.* 2014).

Assimilation of nitrate and ammonium is particularly important for phytoplankton, estimated to be responsible for around 30-40 % of global primary productivity (Duarte *et al.* 1996). Nitrate and ammonium concentrations in natural environments affect phytoplankton ecology, by selecting for different phytoplankton species (Donald *et al.* 2011) or modifying the risk for algal bloom formation (Dugdale *et al.* 2007). Because of the importance of nitrogen sources in phytoplankton ecology, numerous studies over the last 40 years have documented a range of processes regulating nitrate-ammonium assimilation kinetics in phytoplankton cells (Dortch 1990; Flynn, Fasham & Hipkin 1997b). Firstly, phytoplankton cells can display different degrees of specialization toward ammonium or nitrate by presenting better kinetic parameters when reared with either source of nitrogen (here referred to as "preference"; reviewed in Dortch 1990). Secondly, supplying ammonium can repress the nitrate uptake of a cell by either altering the activity of specific transport enzymes or by preventing their synthesis ("inhibition"; Morris & Syrett 1963; Berges 1997; L'Helguen, Maguer & Caradec 2008; although not all species are affected, Mulholland & Lomas 2008). Physiological studies have determined that the observed ammonium-induced inhibition is a product of the ammonium assimilation pathway, which often impairs the ability of a cell to assimilate nitrate (Syrett & Morris 1963; Rigano *et al.* 1979). Thirdly, periods of nitrogen starvation can lead to an initial delay in nitrate assimilation and cell division ("starvation"; Dortch *et al.* 1982; Martinez 1991; De La Rocha *et al.* 2010). However, our understanding of these phenomena is incomplete; in particular, we do not know how processes of preference, starvation and inhibition can interact to simultaneously influence phytoplankton dynamics under different nitrate and ammonium concentrations. This aspect can be important

in multiple fields. In nature, phytoplankton communities can be exposed to periods of N starvation with episodic and cyclic resupplies of nitrate or ammonium (Priddle *et al.* 1997; Young & Beardall 2003a). In aquaculture, imposing periods of nitrogen limitation can increase the quality of the final product by increasing the specific lipid content in the biomass (Griffiths, van Hille & Harrison 2014). Finally, managing aquatic environments also involve regulating nitrate-polluting (e.g. land clearing, agriculture) and ammonium-polluting activities (e.g. human waste discharge, intensive livestock) in order to minimize risks of algal bloom formation (Domingues *et al.* 2011).

Some time ago, Dortch (1990) called for an improved approach for quantifying nitrogen (N) utilization in single species to make better sense of phytoplankton dynamics in nature. Molecular methods of measuring the activity of assimilatory enzymes can provide important information about N utilization (Fan *et al.* 2003; Lomas 2004), but quantifying nitrogen uptake and its conversion into producer biomass still requires monitoring total phytoplankton assimilation (either directly with isotope techniques, or indirectly from ambient N depletion) and producer population densities (Bronk *et al.* 2007). Typically, species-specific kinetic estimates for per-cell nitrogen uptake are calculated by dividing N consumed by cell density at successive points in time, and then fitting a saturating Michaelis-Menten functional response (Maguer *et al.* 2007; Laws *et al.* 2011; Tantanasarit, Englande & Babel 2013). While convenient when analyzing rates of N utilization under constant nutrient regimes, this technique cannot tractably capture the functional relationships that govern important processes, such as interactions between nitrate and ammonium uptake and acclimatization following extended starvation periods. Furthermore, the precision of this technique is limited by the fact

that each estimate for per capita uptake rate is based on only two observations at successive times. One way forward is to develop a more process-oriented framework for modeling nitrate and ammonium utilization in phytoplankton also accounting for the interactive and transient dynamics involved in this process.

In this study, we develop, calibrate, and test a model to characterize nitrate-ammonium utilization of phytoplankton populations reared in laboratory conditions, including transient effects of preference, starvation, and inhibition. The only previous models describing nitrate-ammonium utilization in phytoplankton cells (without the effect of starvation) are very detailed, explicitly characterizing the main biochemical processes that regulate the flows between multiple internal pools of different N forms (Flynn and Fasham 1997; Flynn et al. 1997) . Such a modeling approach requires estimates of biochemical rate parameters that can only be obtained from expensive and time-consuming measurements that are very rarely made in nitrogen utilization experiments. For example, the ANIM model of Flynn et al. (1997) requires estimates of the shape parameters for the size of the glutamine pool that stops NH_4 uptake (*NH4mGLN*), for the maximum size of the nitrate and ammonium internal pools assuming a maximum biomass N:C ratio (*NO3Pm*, *NH4Pm*), and for the curve characterizing glutamine suppression of nitrate-nitrite reductase synthesis (*NNiRhGLN*). Indeed, as yet, no comprehensive set of parameter estimates for any such model has been obtained for any species. Our goal here is to sacrifice the explicit characterization of the dynamics of multiple intracellular nitrogen pools, and instead to construct more tractable models whose best-fit parameter values and 95% confidence limits can be estimated from time-series of external nutrient concentrations and population size, variables that are commonly measured in phytoplankton laboratory cultures. Our results show that transient and

interactive processes between nitrate and ammonium uptake play an important role determining the dynamics of our species. The present approach contributes to a more comprehensive understanding of the factors underpinning the high variation in nitrate-ammonium assimilation observed in natural and experimental systems.

Materials and Methods

Model

To analyze nitrate-ammonium utilization in *Chlorella* sp., we first design a process-based model derived from our current understanding of the biological processes acting on the study system (see Table 2.1 for parameter definitions and units). Our model extends the commonly used "Quota" model for a single nitrogen source, to explicitly account for two different nitrogen sources (i.e. nitrate and ammonium) and how they drive cell division. In the original Quota model, cells are assumed to assimilate a single generic form of nitrogen and divide at a rate that is proportional to their internal nitrogen concentration as follows:

$$\frac{dN}{dt} = -f_N\big(N(t)\big)\times B(t) \qquad \text{(eq. 2.1 a)}$$

$$\frac{dQ}{dt} = f_N\big(N(t)\big) - \mu_{max}\times\left(1-\frac{Q_{min}}{Q(t)}\right)\times Q(t) \qquad \text{(eq. 2.1 b)}$$

$$\frac{dB}{dt} = \mu_{max}\times\left(1-\frac{Q_{min}}{Q(t)}\right)\times B(t) \qquad \text{(eq. 2.1 c)}$$

where $N(t)$, $Q(t)$, and $B(t)$ represent external nitrogen, internal nitrogen within each cell, and population density respectively as a function of time, $f_N\big(N(t)\big)$ represents the functional response quantifying uptake rate as a function of medium nitrogen concentration, μ_{max} is the growth rate of a cell at infinite internal nitrogen, and Q_{min} is the threshold of internal nitrogen concentration at which no cell division occurs.

Our formulation extends this framework by allowing nitrogen to be assimilated as either nitrate or ammonium. In doing so, we account for the main

interactions known to regulate nitrate and ammonium utilization in phytoplankton cells (Dortch 1990). We use two saturating functional responses for each nitrogen type:

$$f_{NO3}\big(NO_3(t), NH_4(t)\big) = v_{NO3} \times \frac{NO_3(t)}{NO_3(t) + k_{NO3}}$$

$$\times I_{sNO3}(r_{NO3}, t) \times I_{inh}(NH_4(t)) \qquad \text{(eq. 2.2 a)}$$

$$f_{NH4}(NH_4(t)) = v_{NH4} \times \frac{NH_4(t)}{NH_4(t) + k_{NH4}} \qquad \text{(eq. 2.2 b)}$$

where v_{NO3} and v_{NH4} represent the maximum feasible per-cell uptake rate, and k_{NO3} and k_{NH4} specify the half-saturation constants, for nitrate and ammonium respectively. $I_{sNO3}(r_{NO3}, t)$ and $I_{inh}(NH_4(t))$ are indicator functions (i.e. functions whose values are either 0 or 1). $I_{sNO3}(r_{NO3}, t)$ indicates whether or not recovery from starvation has occurred and depends on the starvation status of the cell (r_{NO3}). Finally, $I_{inh}(NH_4(t))$ indicates whether ammonium-induced nitrate uptake inhibition is occurring.

Studies on nitrate assimilation have found that, when a culture is N starved, the conversion of NO_3^- into assimilated N can require some time to be reactivated. This is because non-constitutive enzymes (e.g. nitrate reductase) need an induction period after extended lack of use. Hence, upon resupply of nitrate, there can be an initial time lag required for a cell to reactivate the N assimilation pathways (Martinez 1991). Previous studies have also found that extended starvation lengths are associated with an increasingly long period required for the culture to acclimatize to nitrate repletion (Martinez 1991; De La Rocha *et al.* 2010). To reproduce this behavior, we assume that each cell can withstand a period of length

d_{NO3} without displaying starvation symptoms for nitrate. Further increases in starvation time (t_{st}) will require a proportionally longer rehabilitation period r_{NO3}:

$$r_{NO3} = \begin{cases} 0 \quad if \quad t_{st} < d_{NO3} \\ c_{NO3} \times (\, t_{st} - d_{NO3}) \quad otherwise \end{cases} \qquad \text{(eq. 2.3)}$$

where c_{NO3} is the sensitivity of the rehabilitation period to starvation time. During the rehabilitation period cells cannot assimilate nitrogen ($I_{sNO3} = 0$), and they return to normal assimilation once rehabilitated ($I_{sNO3} = 1$), as per:

$$I_{sNO3}(r_{NO3}, t) = \begin{cases} 0 \quad when\ t < r_{NO3} \\ 1 \quad otherwise \end{cases} \qquad \text{(eq. 2.4)}$$

Eq. 2.4 imposes a step-function in nitrogen uptake: it is either zero, or equal to its normal predicted uptake. We considered smoother (sigmoid) transition functions, but in practice, the transition from zero to approximately normal uptake was rapid, relative to our daily sampling interval, which meant that the step-function was adequate to characterize the response in our experiments.

Most previous models have assumed the process of ammonium inhibition on nitrate uptake to be a function of ambient ammonium concentration. However, physiological studies have documented that is the assimilation of ammonium (not its external concentration) that inhibits the nitrate uptake of a cell. Furthermore, the form of functional response for ammonium inhibition over nitrate uptake changes depending on the species (Dortch 1990; L'Helguen *et al.* 2008). In Chlorophyceae and Cyanophyceae, ammonium addition often causes an immediate cessation of nitrate utilization (Syrett *et al.* 1963; Thacker & Syrett 1972; Pistorius, Funkhouser & Voss 1978; Cullimore & Sims 1981). Hence, in this study nitrate uptake inhibition is assumed to follow a step-function, where the uptake of ammonium above a critical level (f_{NH4_crit}) fully represses nitrate uptake:

$$I_{inh}(NH_4(t)) = \begin{cases} 1 & if\ f_{NH4}(\mathrm{NH_4}(t)) < f_{NH4\_crit} \\ 0 & otherwise \end{cases} \qquad \text{(eq. 2.5)}$$

However, alternative functional responses representing a linear or an exponentially decreasing inhibition may be more suitable for diatoms (Parker 1993), coccolithophores (Varela & Harrison 1999) or dinoflagellate species (Collos *et al.* 2004), and could readily be accommodated within the modeling framework presented here.

The full structure of our nitrate-ammonium model for batch cultures is:

$$\frac{dNO_3}{dt} = -f_{NO3}\big(NO_3(t), NH_4(t)\big)\times B(t) \qquad \text{(eq. 2.6 a)}$$

$$\frac{dNH_4}{dt} = -f_{NH4}\big(NH_4(t)\big)\times B(t) \qquad \text{(eq. 2.6 b)}$$

$$\frac{dQ}{dt} = \big[f_{NO3}\big(NO_3(t), NH_4(t)\big) + f_{NH4}\big(NH_4(t)\big)\big] - \mu_{max}\times\left(1 - \frac{Q_{min}}{Q(t)}\right)\times Q(t) \qquad \text{(eq. 2.6 c)}$$

$$\frac{dB}{dt} = \mu_{max}\times\left(1 - \frac{Q_{min}}{Q(t)}\right)\times B(t) \qquad \text{(eq. 2.6 d)}$$

where $f_{NO3}\big(NO_3(t), NH_4(t)\big)$ and $f_{NH4}\big(NH_4(t)\big)$ are specified by eq. 2.2-2.5 (see Fig. 2.1 for conceptual diagram and Table 2.1 for a summary table of model parameters). In this model, assimilated nitrate and ammonium are jointly stored in an internal nitrogen quota compartment whose concentration determines the rate at which the cell divides. Note that, because all parameters in eq. 2.6 c also appear in one of the other equations, it is possible to calibrate the model using only observations on phytoplankton population size and external nitrate and ammonium concentrations, and to infer changes in internal nitrogen from the fitted parameter

values (De La Rocha *et al.* 2010; Malerba *et al.* 2012). Specifically, these fitted parameters determine the concentration of internal nitrogen at which cell division stops (Q_{min}) and the initial quota concentrations at the start of each experiment (Q_{init}). For experiments in which cells were experimentally starved, Q_{init} was set at Q_{min}.

Overall, there are some physiological differences between nitrate and ammonium assimilation in phytoplankton cells that our model had to simplify in order to allow calibration from observations of only medium nitrogen and population size. For instance, assimilated ammonium can only be stored as organic nitrogen (mainly amino acids or N-containing pigments), and therefore its assimilation rate is influenced by the carbon availability of the cell (Crawford *et al.* 2000). Conversely, nitrate can also be stored in its inorganic form, but its assimilation is dependent on photosynthetic electron transport for the production of reduced ferredoxin (Collos *et al.* 2002). We experimentally controlled for the influence of carbon limitation by ensuring pH levels below 7, using magnetic stirrers to continuously suspend the cultures, supplying air, and by collecting data at the same time in the diel cycle. Furthermore, high concentrations of ammonium have been shown to become cytotoxic due to formation of un-ionized ammonia from the ammonium ion in response to photosynthesis-induced high culture pH (Kallqvist & Svenson 2003; Yoshiyama & Sharp 2006). In this study, ammonium-derived ammonia toxicity was avoided by maintaining culture pH below 7. The absence of ammonium-induced ammonia toxicity was confirmed in a specific experiment (see *N starvation followed by NH_4^+ repletion* in the *Calibration Experiments* section).

Experimental Design

Monoclonal 1.2 L batch cultures of the ecologically ubiquitous and commercially important green alga *Chlorella* sp. (Kallqvist *et al.* 2003; Yoshiyama *et al.* 2006; culture accession NQAIF 305, sourced from the North Queensland Algal Culturing and Identification Facility at James Cook University, Townsville, QLD) were reared in standard Bold Basal Medium (BBM; Nichols 1973). Nitrogen was set as the limiting factor for growth in all experimental cultures, supplied at 1/8 and 1/4 the recommended BBM concentration either as sodium nitrate ($NaNO_3$) for nitrate-BBM, or ammonium chloride (NH_4Cl) for ammonium-BBM, or both (see specific experiment descriptions below). Furthermore, dissociation of ammonium ion (NH_4^+) into volatile un-ionised ammonia (NH_3) was minimized by ensuring pH levels below 7 by buffering the modified nitrate-BBM and ammonium-BBM media with *4-(2-hydroxyethyl)-1-piperazineethanesulfonic acid* (HEPES) at 8 mmol L^{-1} and $NaHCO_3$ at 2.38 mmol L^{-1} (Vaddella, Ndegwa & Jiang 2011). Cultures were kept in a temperature-controlled room at 27±3°C with a 14-10 h day-night cycle at a light intensity of 45 µmol photons m^2 s^{-1}. Cultures were continuously mixed with magnetic stirrers at 300 rpm (IKA RCT Basic, IKA Labortechnik, Germany) and aerated with 0.45 µm filtered air (Durapore, Millipore). For all experiments, daily triplicate measurements for cell numbers were collected by flowcytometry (Guava, Millipore, Hayward, CA, USA) and for nitrogen concentrations with the auto-analyser EasyChem Plus (Systea S.p.A., Anagni, Italy), following the manufacturer's EPA-approved and certified protocols (Systea User Manual, 2011). Glassware was acid-washed (10% HCl) and all culturing materials were autoclaved and handled aseptically in a laminar-flow cabinet (Alternative Environmental

Solutions fitted with high-efficiency particulate arresting filter, Australia Standards 4260, National Association of Testing Authorities certified).

Time series were collected from 14 different initial conditions of medium NO_3^- and/or NH_4^+, starvation treatment, and initial population size across five different experiments: data from the first 4 experiments were used to calibrate the model, while those collected in the last experiment were used for model validation (i.e. confronting the parameterized model with a new dataset not used for calibration). Experimental designs and starting conditions used for the different experiments were as follows:

Calibration experiments

Single nitrogen source utilization - To observe the behavior of the species when reared with either nitrate- or ammonium-BBM, two mother cultures were grown in modified BBM medium with the corresponding nitrogen forms and inoculated at 2.5×10^6 cells mL^{-1} (n=3). Initial nitrogen concentration was standardized at 400 µmol N L^{-1} of either NO_3^- or NH_4^+.

NO_3^- + NH_4^+ utilization - To observe growth and nitrogen assimilation response to simultaneous and equally concentrated medium nitrate- and ammonium-N, a single nitrogen-replete mother culture was reared in nitrate-BBM and used to inoculate 3 independent replicate cultures. Cultures were inoculated with 4.5×10^6 cells mL^{-1} and nitrogen was supplied at 400 µmol N-NH_4^+ and 400 µmol N-NO_3^-.

N starvation followed by NO_3^- repletion - To test for the effect of nitrogen starvation length on the performance of the nitrate uptake system, a single mother culture reared in nitrate-BBM was starved for 6, 8, 11, 14, and 17 days; for each

starvation period a culture was inoculated with 5×10^6 cells mL^{-1} and 400 µmol N-NO_3^- L^{-1} and monitored until stationary phase.

N starvation followed by NH_4^+ repletion – To confirm that starvation only affected nitrate assimilation, but not ammonium assimilation, and that our range of ammonium concentrations did not produce cytotoxic effects (both processes not included in the model), a single mother culture reared in ammonium-BBM was used to inoculate 4 independent cultures at 5×10^6 cells mL^{-1}, with a factorial design of 2 levels of starvation (0 and 17 days), each with 2 levels of initial ammonium concentration (200 and 800 µmol N-NH_4^+ L^{-1}). The experiment confirmed that NH_4^+ was assimilated immediately, irrespective of starvation status, and that rates for the highest population growth did not differ between low and high ammonium concentrations (data not shown).

Validation experiments

Ammonium-acclimatization after N starvation - To test whether acclimatizing cells with nitrogen resupplied as ammonium could eliminate the starvation effect on initial nitrate assimilation, a single 17-day starved mother culture was used to inoculate 3 independent cultures at an initial density of 5×10^6 cells mL^{-1} and 500 µmol N-NH_4^+ L^{-1}. When ammonium was depleted, an additional 1000 - 1500 µmol N-NO_3^- L^{-1} was supplied to test the response of the same culture under repleted conditions. These trajectories were compared to 2 additional equally inoculated cultures that did not receive ammonium acclimatization but an equal concentration of 500 µmol N-NO_3^- L^{-1}.

Model Calibration

We used maximum likelihood methods to fit eq. 2.6 to data from the first four experiments simultaneously. This way, model predictions generated from a single set of parameters were confronted with time series from 12 different combinations of initial nitrate, ammonium, population density, and starvation length. Note that all of the parameters that influence the dynamics of the unobserved state (internal quota, $Q(t)$) also appear in the equations for the dynamics of one of the observed states. Flux into the quota can be inferred from changes to medium nitrate and ammonium, while flux out of the quota can be inferred from changes in population density. Note that this would not be true if we had multiple internal pools *sensu* Flynn *et al.* (1997a) or Flynn *et al.* (1997b), with fluxes between them. Indeed, when we explored a model with a glutamine pool between inorganic nitrogen uptake and a fully assimilated internal quota, numerical algorithms failed to converge on best-fit parameters because compensatory changes in model parameters involving the flux between the glutamine pool and the internal quota produced equally good fit to the data (results not shown).

Two different sources of error can affect parameter calibration from time-series data: process noise and observation error (Hilborn *et al.* 1997; Bolker 2008). Process noise refers to unexplained variation due to natural stochasticity in the culture dynamics, while observation error refers to unexplained variation caused by measurement error. The appropriate way to fit the model and calculate parameter best estimates depends on which type of error dominates in the system. When process noise dominates over observation error, then measurements for the state variables will generally be much closer to the system's true state than the predicted

values, so observed states at time *t* should be used to predict states at time *t*+1. Conversely, when observation error dominates over process error, then model predictions are likely to be closer to the true values of the state variables than the measured values, so predicted states at time *t* should be used to predict states at time *t*+1.

For highly controlled microbial laboratory systems, observation error is often quite small, and it is reasonable to assume that process noise dominates the random variation in the data (Bolker 2008). Indeed, in our data, there was strong evidence that this was the case: the standard deviation from the triplicate independent readings offers an independent estimate of the magnitude of the observation error and was usually less than 5% of the total error calculated from model calibration. Consequently, standard one-step ahead techniques were employed to account for process noise during parameter calibration (Hilborn *et al.* 1997; Bolker 2008). For our dataset, the function for the negative log-likelihood score (-*L*) assuming normally-distributed process noise is:

$$-L_{t,i}\left\{Y_{t,i}\middle|f\left(Y_{t-1,i}\right),\sigma_i^2\right\} = -\frac{n}{2}\ln(2\pi) - \frac{n}{2}\ln(\sigma_i^2) - \frac{1}{2\sigma_i^2}\times\left(Y_{t,i} - f\left(Y_{t-1,i}\right)\right)^2 \quad \text{(eq. 2.7)}$$

where *i* indexes each state variable (i.e. nitrate, ammonium, and population density), *t* indicates time (days since the start of the experiment), *n* is the length of the time series, σ_i^2 is the variance of state variable *i*, and $Y_{t,i}$ and $f\left(Y_{t-1,i}\right)$ are the observed value of state variable *i* at time *t*, and the corresponding model predicted value (calculated from eq. 2.6 based on the observed state at time *t* -1), respectively. Maximum likelihood parameter estimates were obtained by minimizing eq. 2.7 summed across all *t*, all *i*, and all calibration experiments using the unconstrained

general-purpose optimization function *nlminb* in the software program R (R Core Team 2014).

Model Selection

To assess how the parameterization of individual functional responses contributed to the model fit, we compared the fit of the fully parameterized model against reduced versions, where particular functional responses were simplified or excluded. We used Akaike's Information Criterion (AIC) to select the best fitting model. The best model was the one that minimized the formula $-2\times L + 2\times k$, where L is the log-likelihood score and k is the total number of calibrated parameters (Bozdogan 1987). The model with the lowest AIC is the estimated best model. In general, models within 2 AIC units of the best model should be considered as having significant statistical support (Burnham & Anderson 2002). We also confirmed that alternative model selection techniques of Bayesian Information Criterion (BIC) and Likelihood Ratio Testing produced the same conclusions as AIC. For the best model, we calculated 95% profile likelihood confidence intervals for each of the estimated parameters and we evaluated the model's goodness of fit by inspecting how evenly the residuals were distributed across replicate cultures for each day of the different experiments.

Model Validation

While experiments including different degrees of starvation or simultaneous exposure to nitrate and ammonium include unique information about the behavior of the species, single nitrogen utilization and acclimatization experiments include information also present in at least one other experiment. Time-series from the

acclimatization experiment (see section *Acclimatization after N-Starvation*) represent the most novel and challenging set of initial conditions. Therefore, the data from this experiment were excluded from model calibration and were instead used for model validation: after using data from the first 4 experiments to select the best model, and to estimate the maximum likelihood parameter estimates for that model, the same parameter values were used to predict the trajectories of the 5 other independent cultures inoculated with 17-day starved cells, re-supplied with either ammonium (n=3) or nitrate (n=2), and finally supplied with a pulse of new nitrate. To quantify the fit, a standard coefficient of determination (R^2_{pred}) between the model prediction and the observed values for each state variable of each experiment was calculated as follows:

$$R^2_{pred} = 1 - \frac{\sum_{c=1}^{n}\sum_{d=1}^{7}\left(y_{c,d}-\hat{y}_{c,d}\right)^2}{\sum_{c=1}^{n}\sum_{d=1}^{7}\left(y_{c,d}-\bar{y}_c\right)^2} \qquad \text{(eq. 2.8)}$$

where *c* indexes the independent cultures, *d* indexes the observations for each day within each culture, $y_{c,d}$ is the observed value from culture *c* at day *d*, $\hat{y}_{c,d}$ is the corresponding predicted value generated by the calibrated model with eq. 2.6, and $\bar{y}_c$ is the mean value from culture *c* across the time-series (Turchin 1996; Lindstrom *et al.* 1999). To further evaluate the predictive ability of the model, we also report the R^2_{pred} coefficients from the only other possible cross-validation configuration, where the *single nitrogen source utilization* experiments were used as validating datasets, and all other data were used as training datasets.

Results

Model calibration and model selection

The model described the data for our first four experiments reasonably well (Figs. 2.2-2.4). Model selections with AIC and BIC both indicated that observations of *Chlorella* sp. were best described by a model assuming linear nitrate and ammonium assimilation and incorporating nitrate starvation and ammonium-induced nitrate uptake inhibition (Table 2.2). Alternative model selection technique of Likelihood Ratio Testing produced identical conclusions (results not shown). Maximum likelihood estimates and 95% confidence limits were successfully identified for all model parameters, and they indicate that *Chlorella* sp. exhibited a higher per-cell uptake rate for nitrate over ammonium (compare w_{NO3} and w_{NH4} in Table 2.1).

The first experiments with nitrate- and ammonium-only tested the model against data from two single-N experiments, and showed that, in the absence of starvation or multiple N sources, observed trajectories are well characterized by the model: residual variation was small compared to the mean and symmetrically distributed around zero (Fig. 2.2), except during days 3 and 4 for the ammonium cultures, where ammonium uptake rates were consistently lower than those predicted by the model. This is apparent in Fig. 2.2 C by arrowheads (model predictions) pointing consistently below observed values at days 3 and 4, yielding positive residuals across all replicates for those days. The second experiment tested the model against time-series of *Chlorella* sp. reared with nitrate and ammonium simultaneously, which the model also captured reasonably well (Fig. 2.3). This included up to an approximately one-day delay in nitrate uptake due to fast rates of

ammonium uptake, followed by a return to rapid nitrate uptake by the second day (initial horizontal trajectories, followed by rapid declines in Fig. 2.3 A). There was a time delay between N assimilation and population growth that the model did not capture: the rapid increase in population density resulting from the substantial NO_3^- + NH_4^+ uptake at day 2 was predicted to take place at day 3, but was mainly observed at days 4 and 5. This is apparent by arrowheads pointing above the observed values (all negative residuals) at day 3, while pointing consistently below the observed values (all positive residuals) at days 4 and 5 (Fig 2.3 C). However, the overall good fit indicates that the model was able to simultaneously (i.e., with the same fitted parameters) explain both nitrate- and ammonium-only growth, as well as growth with the two nutrients in equal quantities, with relatively small errors in the timing of when the most rapid changes occurred.

N starvation had an important effect on nitrate uptake in *Chlorella* sp. (Fig. 2.4 A-B). Model selection favored a functional response in which activation of the nitrate uptake system is delayed by a brief (<1 day) period that is proportional to the length of starvation experienced before the experiment (Table 2.2), which the model captured well across all starvation treatments (residuals approximately evenly spread among negative and positive values in Fig. 2.4 A). Data on population growth for N-starved cultures resupplied with nitrate showed evidence of temporal correlation in the residuals. Population size trajectories were under-predicted by the model, with arrowheads consistently pointing below observed values (mostly positive residuals in Fig. 2.4 B). This indicates that cells displayed greater efficiency in converting N into new cells than the model could capture. Starvation only affected nitrate uptake, as ammonium assimilation did not show any delays, even after 17 days of starvation (data not shown).

Model validation

Using parameter estimates from fits of the previous four experiments, data from acclimatization experiments (see section *Acclimatization after N starvation* in material and methods) were used to test the predictive power of the model. R^2_{pred} coefficients were generally very high (0.86-0.99; Fig. 2.5). Acclimatizing 17-day starved cultures with a preliminary pulse of ammonium removed any initial delay in nitrate assimilation (no nitrate uptake delay after day 5 in Fig. 2.5 B). Conversely, acclimatizing equivalently starved cells with nitrate showed an initial 24-hour delay in nitrate uptake and cell division that is consistent with nitrate starvation experiments (cf. horizontal orange arrows at day 0 for 17-day starved treatment in Fig. 2.4 A with two horizontal arrows at day 0 in Fig. 2.5 E). Once cells recovered from starvation, the rate of per-cell nitrate assimilation did not differ between nitrate- and ammonium-acclimatized cultures (comparable uptake at day 5 between Fig. 2.5 B and 2.5 E). The only lack of fit occurred between days 1 and 3, where the model predicted a slower rate of ammonium depletion (arrows pointing consistently above observed values, yielding negative residuals for these days in Fig. 2.5 C) than occurred in the cultures. Finally, the excellent prediction ability of the model was further confirmed by repeating cross-validation using the *single nitrogen utilization experiments* as validating datasets and all other experiments as training datasets: R^2_{pred} for all state variables were between 0.85 and 0.99, very similar to the R^2_{pred} values reported in our original validation experiment (Fig. 2.5). Because fitted and predicted trajectories in this second exercise were virtually identical to those shown in Figs. 2.2-2.5, we have not reproduced them here.

Table 2.1: Summary table of model state variables and parameters. Maximum likelihood estimates are reported only for those parameters in the model selected by AIC (cf. Table 2.2 for AIC scores). Hence, parameter best estimates for the functional response for the hyperbolic nitrogen uptake were not reported as the best-fitting model has a linear uptake. Also d_{NO3} was not reported, as the best-fitting model does not have delayed nitrate starvation.

Variables	Definition (units)	
NO_3	Nitrate in medium (µmol NO_3^- L^{-1})	
NH_4	Ammonium in medium (µmol NH_4^+ L^{-1})	
Q	Nitrogen quota (µmol N $cell^{-1}$)	
B	Population density (cell L^{-1})	
Parameters	**Definition (units)**	**Mean (± 95% CI)**
v_{NO3}	Maximum per-capita nitrate uptake rate (µmol NO_3^- $cell^{-1}$ day^{-1})	--
k_{NO3}	Nitrate half-saturation constant (µmol NO_3^- L^{-1})	--
w_{NO3}	Rate of daily per-capita nitrate uptake ($cell^{-1}$ day^{-1})	9.82 (9.03-10.5) $\times 10^{-11}$
v_{NH4}	Maximum per-capita ammonium uptake rate (µmol NH_4^+ $cell^{-1}$ day^{-1})	--
k_{NH4}	Ammonium half-saturation constant (µmol NH_4^+ L^{-1})	--
w_{NH4}	Rate of daily per-capita ammonium uptake ($cell^{-1}$ day^{-1})	6.74 (5.88-7.17) $\times 10^{-11}$
c_{NO3}	Recovery rate of the nitrate assimilation systems following a period of nitrogen starvation ($days^{-1}$)	0.088 (0.074-0.093)
d_{NO3}	Length of nitrogen starvation that a cell can withstand without displaying negative effects on nitrate assimilation systems (days)	--
f_{NH4_crit}	Critical ammonium uptake rate above which the nitrate uptake of a cell is repressed (µmol NH_4^+ L^{-1} day^{-1})	1.08 (1.02-1.21) $\times 10^{-8}$
Q_{min}	Per-capita minimum nitrogen quota (µmol N $cell^{-1}$)	3.10 (2.36-3.67) $\times 10^{-8}$
μ_{max}	Growth rate at infinite nutrient storage (day^{-1})	16.10 (9.02-19.1)
t_{st}	Experimental period of nitrogen starvation imposed on the culture before the experiment (days)	Fixed experimentally
r_{NO3}	Length of starvation-induced delay before a cell can resume nitrate uptake (days)	Calculated via eq. 2.3 from c_{NO3}, d_{NO3}, and t_{st}

Table 2.2: Formal model selection with Akaike Information Criterion (AIC) and Bayesian Information Criterion (BIC) between functional responses for nitrate and ammonium uptake (f_N), rehabilitation time following nitrogen starvation (r_N), and ammonium-induced inhibition on nitrate uptake (I_{inh}). We compared the fit of the full model against reduced versions, where particular functional responses were simplified or excluded from the fully parameterized model. Biological interpretation and scores for maximum negative log-likelihood (-*L*), AIC, difference in AIC (ΔAIC), BIC, difference in BIC (ΔBIC) are reported between competing models for each functional response (FR), with their corresponding number of calibrated parameters in brackets (# pars). Boldface indicates the estimated best-fitting model and therefore the one employed for parameter estimation. *See* eq. 2.2-2.5 for full functional responses, Model Selection section in Material and Methods, and Table 2.1 for parameter definitions, units, and calibrated values.

FR		*Competing models for each FR* [*# pars*]	*Nitrate ($N=NO_3$)* -L	AIC	ΔAIC	BIC	ΔBIC	*Ammonium ($N=NH_4$)* -L	AIC	ΔAIC	BIC	ΔBIC	*Biological Interpretation*
f_N	(1)	$w_N \times N(t)$ [23]	**-3068**	**6182**	**0**	**6277**	**0**	**-3068**	**6182**	**0**	**6277**	**0**	*Functional response for the uptake of a single cell:*
	(2)	v_N [23]	-3156	6358	176	6453	176	-3189	6424	242	6519	242	(1) Increases linearly with N
	(3)	$v_N \times \frac{N(t)}{N(t)+k_N}$ [24]	-3068	6184	2	6283	6	-3068	6184	2	6283	6	(2) Fix for any N (3) Saturates at high N
r_{NO3}	(1)	$\begin{cases} 0 & if\ t_{st} < d_{NO3} \\ c_{NO3} \times (t_{st} - d_{NO3}) & otherwise \end{cases}$ [24]	-3068	6184	2	6283	6						*Starvation-induced delay on nitrate uptake* (1) Linearly proportional to starvation length after d_N days of starvation
	(2)	$\begin{cases} 0 & if\ t_{st} < d_{NO3} \\ c_{NO3} \times t_{st} & otherwise \end{cases}$ [23]	**-3068**	**6182**	**0**	**6277**	**0**						(2) Linearly proportional to starvation length
	(3)	0 [22]	-3133	6310	128	6401	124						(3) No starvation effect
I_{inh}	(1)	$\begin{cases} 1 & if\ f_{NH4}(\mathrm{NH_4}(t)) < f_{NH4\_crit} \\ 0 & otherwise \end{cases}$ [24]						**-3068**	**6184**	**0**	**6283**	**0**	*Ammonium-induced inhibition on nitrate uptake:* (1) Threshold at f_{NH4_crit}
	(2)	1 [23]						-3093	6232	48	6327	44	(2) No Inhibition

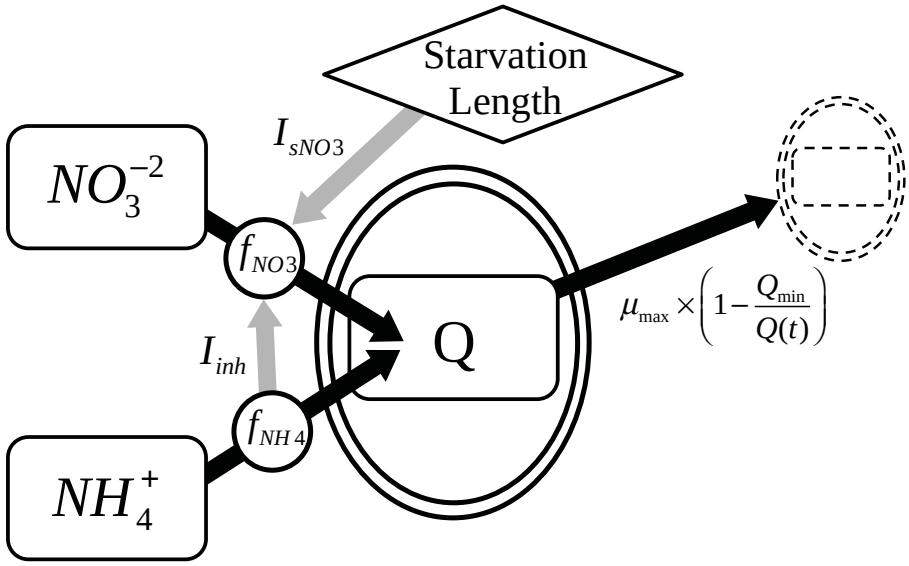

Figure 2.1: Model diagram for nitrate (NO_3^{-2}) and ammonium (NH_4^+) utilization in phytoplankton cells. The double-lined ellipse represents the cell wall of a single cell. Squares indicate the state variables for the different forms of nitrogen, either in the medium or inside the cell. The diamond represents the starvation length. Black arrows describe nitrogen flows in the system. Grey arrows indicate inhibitor mechanisms on the per-cell nitrate uptake rate. Nitrate and ammonium are taken up through the membrane and stored inside the cell. The production of new cells (dashed lines) is a saturating function of internal nitrogen concentration (Q), whose shape is determined by the parameters for maximum growth rate (μ_{max}) and minimum internal nitrogen (Q_{min}). See Table 2.1 and eq. 2.1-2.6 for details on model formulation.

a

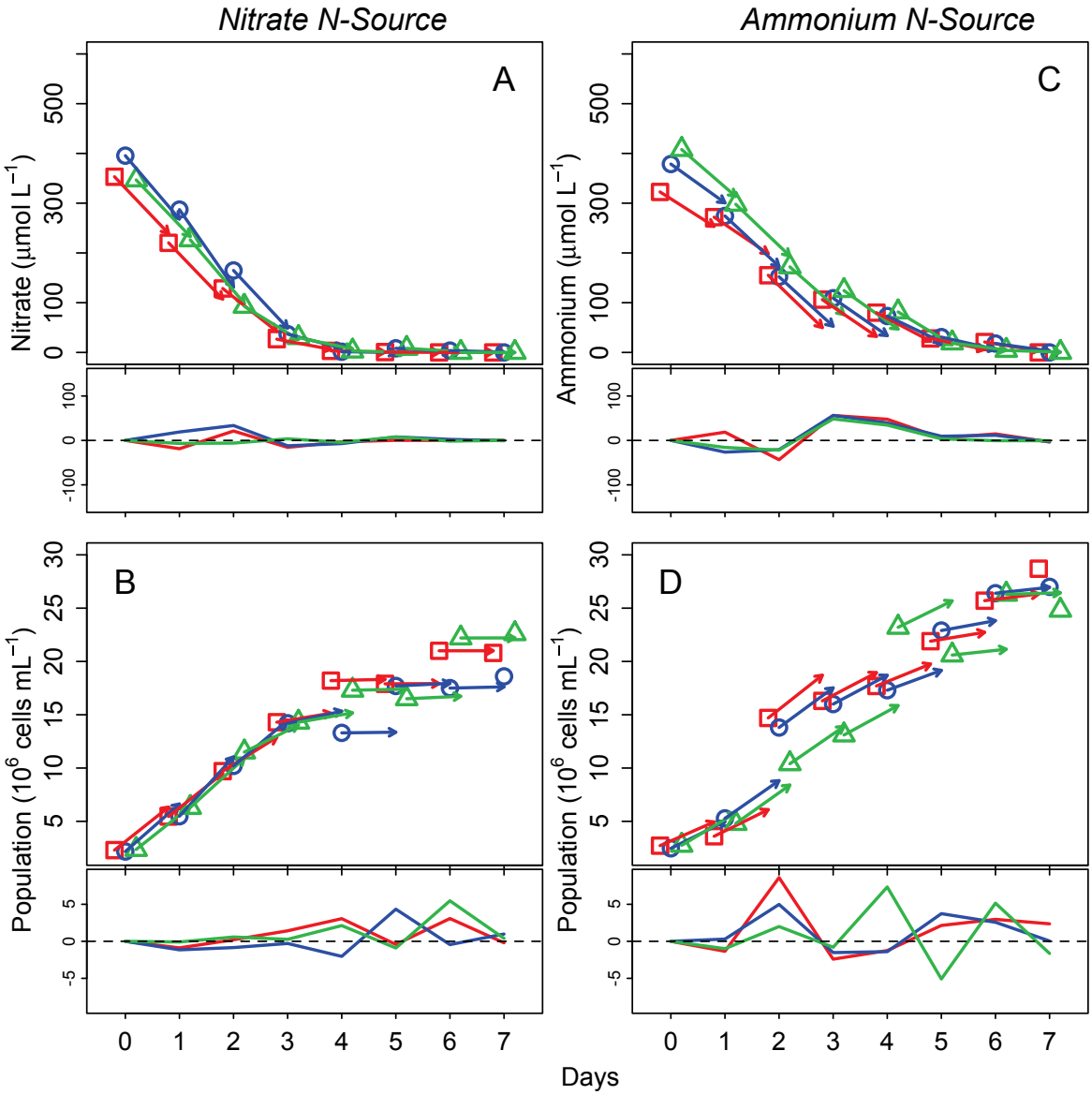

Figure 2.2: Time-series for medium nitrogen (A, C) and population size (B, D) for *Chlorella* sp. reared in batch culture with either nitrate (A, B) or ammonium (C, D) as the only nitrogen sources. Each symbol type is an independent replicate culture and each point is the mean between three replicate measurements for that culture. Arrows show one-step ahead predictions for the best-fit model assuming process noise, where the observed values at time *t* (base of arrows) are used in eq. 2.6 to predict values at time *t* + 1 (arrowheads; see calibration section). Line graphs

beneath each panel connect the residuals between model predictions and observations for each day and are color coded for each culture. Vertical axes are scaled consistently across the two sub-panels.

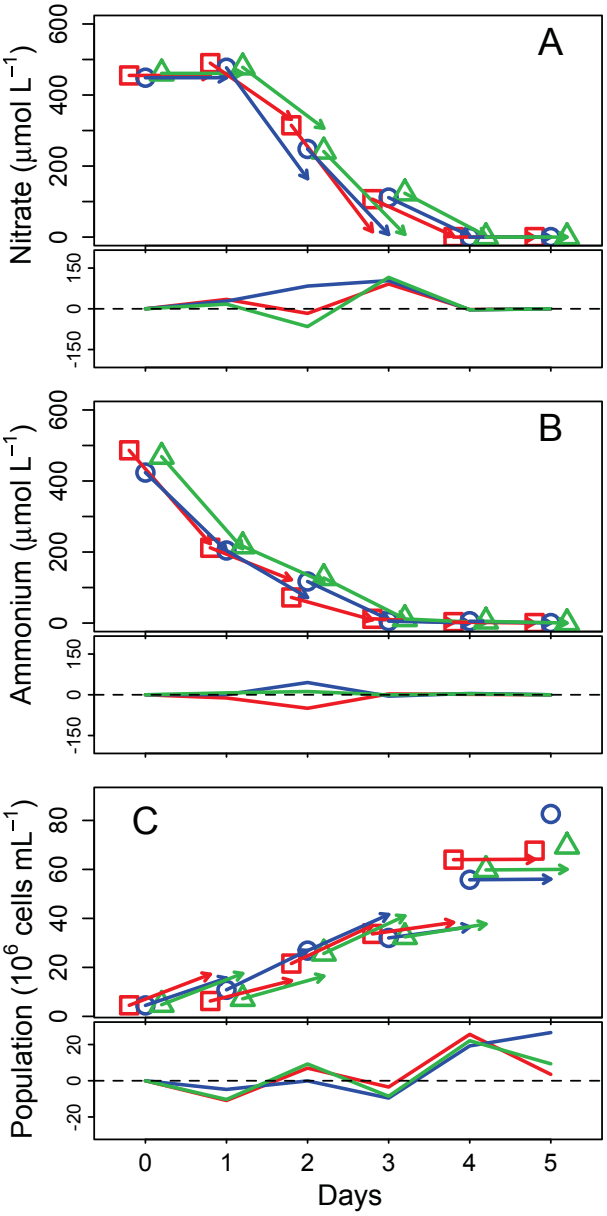

Figure 2.3: Time-series and model fit for medium nitrate (A), medium ammonium (B), and population size (C) for *Chlorella* sp. reared in the presence of both forms of nitrogen. Each symbol type is an independent replicate culture and each point is the mean between three replicate measurements for that culture. Arrows (top panel) and lines (bottom panel) show the predicted values for the best-fit model and its residuals. See Fig. 2.2 legend for further details.

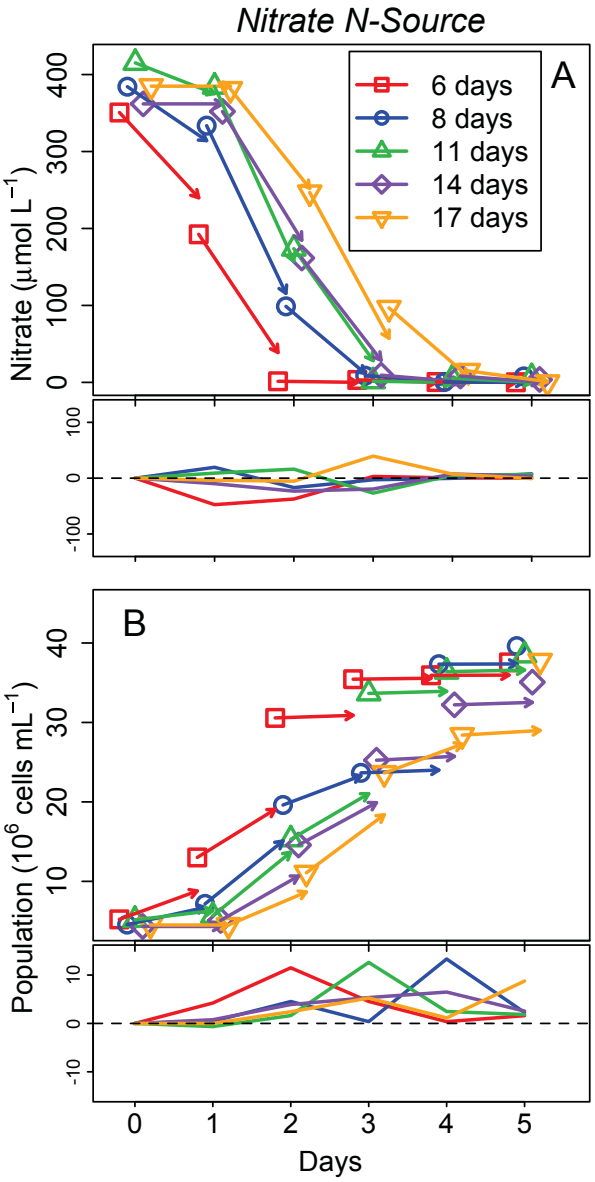

Figure 2.4: Time-series and model fit for medium nitrate (A) and population size (B) of a nitrogen-starved inoculum of *Chlorella* sp. resupplied with nitrate. Legend indicates the length (days) of starvation imposed before starting the experiment. Each point represents the mean between three replicate measurements for each culture. Arrows (top panel) and lines (bottom panel) show the predicted values for the best-fit model and its residuals. See Fig. 2.2 legend for further details.

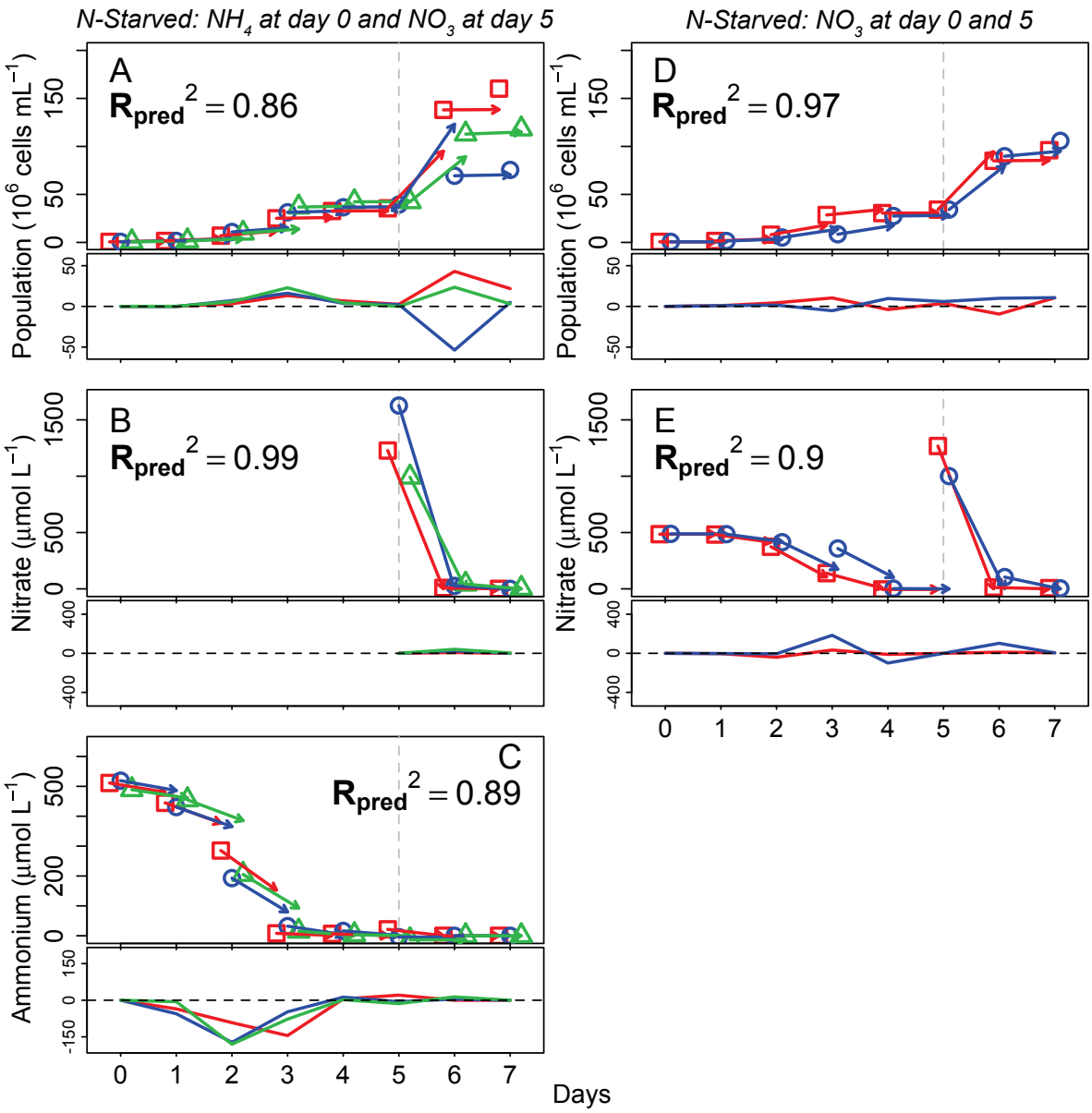

Figure 2.5: Model validation with time-series from a 17-day starved inoculum of *Chlorella* sp. not included during model calibration. Left column – Time-series for population size (A) resupplied at day 0 with ammonium (B) and at day 5 with nitrate (grey dashed vertical line in C). Right column – Time-series for population size (D) resupplied with nitrate (E) both at day 0 and at day 5. Each symbol type is an independent replicate culture and each point is the mean between three replicate measurements for that culture. Arrows (top panel) and lines (bottom panel) show

the predicted values for the best-fit model and its residuals. See Fig. 2.2 legend for further details.

Discussion

Our results show that a single set of model parameters can characterize well the coupled dynamics between nitrate and ammonium uptake and cell division in the green algal species *Chlorella* sp. reared in batch culture under a wide range of initial conditions. Analyzing nitrate-ammonium utilization with the present model allowed us to quantify functional responses for assimilation of nitrate and ammonium individually or combined, as well as effects of nitrogen starvation or ammonium-induced nitrate uptake inhibition on nitrate uptake. Furthermore, high R^2_{pred} scores recorded during model validation suggest that the model describes culture trajectories well even under novel experimental conditions.

While previous studies have quantified assimilation responses to a few particular starvation lengths, the present study is the first to calibrate a functional response quantifying delay in nitrate uptake as a continuous function of starvation length. The physiological reason for such delay is a slow recovery in nitrate-reductase activity following nitrogen starvation, which acts as the limiting step for nitrate assimilation and amino acid incorporation into proteins (Dortch *et al.* 1982). This explanation is also consistent with our observed absence in a delay for ammonium uptake following starvation, as no enzymatic reduction is required for its assimilation (Crawford *et al.* 2000). Proteins involved in the reduction of nitrate to organic nitrogen were recorded to decrease by 60-90% in the diatom *Thalassiosira pseudonana* at the onset of nitrogen starvation (Hockin *et al.* 2012). Different species display variable delay times to starvation: 1 and >2.5 hours delays

for 3 and 4 days of starvation (Martinez 1991) and 2 hours for 3 days of starvation for the diatom *Skeletonema costatum* (Dortch *et al.* 1982), 8 hours for 3 days of starvation for the dinoflagellate *Amphidinium carterae* (Dortch *et al.* 1982), and no delay for the green alga *Dunaliela tetriolecta* (Dortch *et al.* 1982). These observed delay times are comparable with presently calibrated functional responses for *Chlorella* sp., where 3 and 4 days of starvation would correspond to 5 and 7 hours of delay, respectively. In nature, some species, mostly diatoms, form fortnightly algal blooms near estuaries correlated with tidal cycles (Parsons *et al.* 1983; Zamon 2002). One potential explanation is that, within phytoplankton communities, some species are adapted to respond quickly to nutrient fluxes after extended starvation periods (Largier 1993). This hypothesis could be tested by calibrating and comparing the shapes of the functional responses for the recovery rate of nitrate uptake to nitrogen starvation (r_{NO3}) for species that commonly produce algal blooms, and those that do not.

Interestingly, the effect of starvation on nitrate assimilation was removed when starved cultures were first acclimated with ammonium before supplying nitrate (Fig. 2.4). This result is consistent with earlier work on *Chlorella vulgaris*, where the production of nitrate reductase, a specific enzyme required for nitrate assimilation, increased when cells were reared in ammonium following N starvation (Morris & Syrett 1965). Also the marine haptophyte *Isocrysis galbana* registered a low but constant production of nitrate reductase when reared with ammonium as the only nitrogen source (Flynn *et al.* 1993). In contrast, synthesis of nitrate reductase did not occur in cells of the freshwater rhodophyte *Cyanidium caldarium* grown in ammonium-based media (Rigano & Violante 1973). The lack of a clear trend across

species poses further complications in our understanding of the general role of nitrate and ammonium fluctuations in the regulation of phytoplankton communities.

Analyzing episodes in which the model failed to reproduce observed trajectories can indicate mis-specification of functional forms or implicate biological responses not explicitly incorporated in the model. For instance, discrepancies between the data and our model indicated that the rate at which assimilated nitrogen was converted into new cells was more rapid in cultures recovering from nitrogen starvation compared to replete conditions (mostly positive residuals in Fig 2.3B). A possible explanation is that cells with insufficient nitrogen for production of new biomass will channel excess carbon produced from photosynthesis into storage molecules such as triglyceride or starch (Zhang *et al.* 2013). This produces an increase in the C:N ratio that can enhance growth rate following nitrogen resupply (Bittar *et al.* 2013). *Chlorella* sp. has been documented to display a significant increase in lipid and carbohydrate contents in response to nitrogen starvation conditions (Zhang *et al.* 2013). Thus, one area for refinement for our model would be to explicitly account for the relationship between nitrogen starvation, carbon content of a cell, and per-cell rate of population growth.

Despite decades of research, the role of different nitrogen sources on the ecology of autotrophic communities remains unclear (Schimel *et al.* 2004; Boudsocq *et al.* 2012). For phytoplankton, this problem has implications for a broad range of aquatic systems: from coastal areas, where seasonal precipitation or tidal regimes drive large fluctuations in nitrogen availability at multiple scales, to inland basins, experiencing temporally variable anthropologic nitrogen release from fertilizers or waste-water discharge (Domingues *et al.* 2011). The present data on

nitrate and ammonium assimilation clearly show that there are major differences in how cells take up and assimilate these two different nitrogen sources. The modeling approach presented and tested here can contribute to our understanding of how different nitrogen supplies influence growth and interactions of phytoplankton communities in nature.

Chapter 3: Intraspecific cell size plasticity influences phytoplankton nitrate-ammonium utilization traits

Introduction

Explaining ecological communities and ecosystem functioning requires considering how multiple morphological and functional characteristics of a wide range of species change along various environmental gradients (McGill *et al.* 2006). Therefore, in ecology it is often advantageous to describe species not by their taxonomic identity, but rather by well-defined, measurable properties of a species that determine its performance ("functional traits"; McGill *et al.* 2006; Albert *et al.* 2010). When examining the distribution of a species and how it changes with biotic and abiotic factors, trait-based approaches allow far greater generality and predictability (e.g. plants with dense canopy are more temperature-tolerant) compared to more traditional nomenclature approaches focusing on species identities (e.g. species X grows better at temperature Y; Lavorel *et al.* 1997; Violle *et al.* 2007).

Ecological studies have often assumed that intraspecific variability in functional traits is negligible compared to interspecific differences (Albert *et al.* 2010; Albert *et al.* 2011). However, a growing number of studies challenge this assumption. In particular, phenotypic plasticity, a major source of intraspecific variability in species traits, has often been documented to play an important role in species' ability to cope with changing environmental conditions (Bolnick *et al.* 2002; Albert *et al.* 2010). For example, leaves of several plant species inhabiting

wet habitats have adapted mechanisms to rapidly increase oxygenation and better cope with flooding events (Mommer *et al.* 2006). Furthermore, the phytoplankton species *Scenedesmus subspicatus* is able to increase cell size, form larger colonies, and develop spines to reduce grazing mortality a few hours after being exposed to new biotic and abiotic conditions (Hessen & Vandonk 1993; Donk, Lürling & Lampert 1999). Hence, not accounting for intraspecific trait variability due to phenotypic plasticity risks underestimating the actual ability of a species to persist under changing biotic and abiotic conditions, and thus potentially to overestimate community turnover along environmental gradients.

The influence of phenotypic plasticity on intraspecific trait variability has the potential to be particularly important in phytoplankton ecology. Functional traits are commonly used to explain species trade-offs, optimal size, or size structure in phytoplankton communities (Irwin *et al.* 2006; Litchman *et al.* 2007). For example, phytoplankton nitrogen utilization traits, such as the maximum uptake rate, the maximum growth rate, and the ability to store nutrients, can be directly linked to the performance of the population, as well as its competitive ability within the community, and its contribution to nitrogen fluxes within the ecosystem (Falkowski, Barber & Smetacek 1998; Field *et al.* 1998; Edwards *et al.* 2012). Furthermore, there is now considerable evidence showing that phytoplankton nutrient-utilization traits change systematically with a species mean cell size (Stolte & Riegman 1995; Litchman *et al.* 2007; Edwards *et al.* 2012). Specifically, small species show higher specific population growth rates and assimilation efficiencies, while large species show higher nutrient uptake rates and greater ability to store nutrients (Stolte & Riegman 1996; Litchman *et al.* 2008; Edwards *et al.* 2012). However, phytoplankton cells are also known for their remarkable ability to rapidly

respond to changes in environmental conditions by adjusting their cell size (Duarte, Agusti & Canfield 1990; Dassow, Chepurnov & Armbrust 2006; Lyczkowski & Karp-Boss 2014). To our knowledge, no study has quantified the effects of intraspecific cell size plasticity on the nutrient utilization traits of a species. If fluctuations in cell size were to substantially influence the nutrient utilization traits of a species, then characterizing phytoplankton trait distribution solely by inter-specific allometric relationships is likely to underpredict a species' ability to respond and adjust to environmental fluctuations (Duarte *et al.* 1990). Hence, quantifying the effects of intraspecific cell size plasticity on nutrient utilization traits, particularly relative to interspecific variability in such traits, is important to assess the reliability of using species-level mean trait values in assessments of trait variability in phytoplankton.

In this study, we test the hypothesis that changes in mean cell size are correlated with the nitrate-ammonium utilization dynamics of the widespread freshwater phytoplankton species *Desmodesmus armatus* (Chlorophyta). The nutrient utilization traits under analysis are: the per-capita rates for nitrate and ammonium assimilation, the maximum division rate, and the minimum storage of nitrogen. The experiment monitored the performance of the species under different nitrogen sources (nitrate, ammonium, or both) and nutrient histories (N-replete and N-deplete). The effects of temporal changes in mean cell size, and of nutrient histories, on the nitrate-ammonium utilization of the species were evaluated by fitting dynamic models. Specifically, four alternative Quota-type models were designed and fitted to data by assuming different relationships between cell size and nutrient traits: (1) traits are independent of nutrient history and cell size ("baseline" model); (2) traits depend only on nutrient history ("N-history" model), or (3) only

on cell size ("allometric" model); and (4) traits depend on both cell size and nutrient history ("allometric N-history" model). Results show that the effects of cell size and N-history on nutrient utilization dynamics in *Desmodesmus armatus* depends on the trait: ammonium uptake, maximum growth rate, and minimum internal N quota vary systematically with changes in cell size and previous N-history, while nitrate uptake is less related to both factors. This is the first study to quantify the importance of intraspecific trait variability on the population and nutrient-uptake dynamics of a species.

Materials and Methods

Process-based models

Model presentation

The nitrate-ammonium-phytoplankton model proposed by Malerba *et al.* (2015) was fitted to time-series of *Desmodesmus armatus* reared in laboratory conditions across treatments of nitrogen types (nitrate, ammonium, or both) and N-history (N-replete or N-deplete). The model followed the general assumptions of the original "Quota" model, first proposed by Droop (1974): cells take up nitrogen from the environment and divide at a cell-specific rate that is proportional to their internal nitrogen concentration. Malerba *et al.* (2015) extended this model to explicitly account for the dynamics of two specific types of nitrogen sources, with cells dividing after taking up either nitrate or ammonium or both. The main feature of the model is that phytoplankton cells can display different degrees of specialization toward ammonium or nitrate by presenting better kinetic parameters when reared with either source of nitrogen. Moreover, the model accounts for the interaction

between nitrate and ammonium assimilation: high rates of ammonium uptake are known to repress nitrate uptake of a cell, by either altering the activity of specific transport enzymes or by preventing their synthesis (Syrett *et al.* 1963). The structure of the model was as follows (see Table 3.1 for definitions of state variables and parameters):

$$\frac{dNO_3}{dt} = -f_{NO3}\big(NO_3(t)\big)\times f_{inhib}\big(NH_4(t)\big)\times B(t) \quad \text{(eq. 3.1 a)}$$

$$\frac{dNH_4}{dt} = -f_{NH4}\big(NH_4(t)\big)\times B(t) \quad \text{(eq. 3.1 b)}$$

$$\frac{dQ}{dt} = \big[f_{NO3}\big(NO_3(t)\big)\times f_{inhib}\big(NH_4(t)\big) + f_{NH4}\big(NH_4(t)\big)\big] - g(Q(t))\times Q(t) \quad \text{(eq. 3.1 c)}$$

$$\frac{dB}{dt} = g(Q(t))\times B(t) \quad \text{(eq. 3.1 d)}$$

with the four differential equations describing changes in nitrate $(NO_3(t))$, ammonium $(NH_4(t))$, internal cell nitrogen $(\mathrm{Q}(t))$, and total population size $(\mathrm{B}(t))$. The functional responses for $f_{NO3}(NO_3(t))$ and $f_{NH4}(NH_4(t))$ represent per-cell uptake of nitrate and ammonium, respectively, with $f_{inhib}(NH_4(t))$ quantifying the inhibition of ammonium uptake on nitrate uptake. Finally, $g(Q(t))$ represents the functional response regulating the specific daily growth rate of a cell as a function of its internal nitrogen concentration.

Traditionally, the per-capita nitrogen uptake rate of a cell is assumed to follow a saturable Michaelis-Menten functional response of the form $f_N = v_{max}\times\frac{N(t)}{N(t)+k_N}$, where v_{max} is the maximum per-capita uptake rate and k_N is the half-saturation constant. However, preliminary experiments showed that the per-capita nitrogen uptake for the study species is linearly proportional to the nutrient concentration in the environment, for the range of concentrations considered here. A linear

functional response for per-cell nitrogen assimilation is consistent with physiological studies. Phytoplankton cells have evolved two alternative assimilatory systems to better cope with fluctuating nutrient availabilities (Collos *et al.* 1997; Flynn 1999; Collos, Vaquer & Souchu 2005). High nutrient concentrations (~100-1000 µmol-N) induce the expression of a low-affinity system, which is linearly proportional to external nitrogen (Crawford *et al.* 2000). Conversely, low nutrient concentrations (1-100 µmol-N) induce a high-affinity system, which follows a saturable function of external nitrogen concentration (Crawford *et al.* 2000). Hence, per-cell nitrate and ammonium assimilation was modeled as a linear functional of medium nitrogen:

$$f_{NO3}(NO_3(t)) = w_{NO3} \times NO_3(t) \qquad \text{(eq. 3.2 a)}$$

$$f_{NH4}(NH_4(t)) = w_{NH4} \times NH_4(t) \qquad \text{(eq. 3.2 b)}$$

where w_{NO3} and w_{NH4} are the per-cell nitrate and ammonium uptake rates, respectively (units of cell^{-1} day^{-1}).

Physiological studies have shown that ammonium inhibition on nitrate uptake depends on the per-cell ammonium uptake rate (not of the external ammonium concentration) (Syrett *et al.* 1963). The specific form of this functional response can depend on the species and the experimental conditions, ranging from an immediate cessation of nitrate utilization in the presence of ammonium, to a less abrupt transition, or even to the absence of any interactions between ammonium and nitrate uptake. A general and flexible way to parameterize the effect of ammonium inhibition on nitrate uptake is using a negative exponential functional response between 0 (fully inhibited) and 1 (no inhibition), as:

$$f_{inhib}\big(NH_4(t)\big) = e^{-a \times f_{NH4}(NH_4(t))^b} \qquad \text{(eq. 3.3)}$$

with *a* and *b* regulating the shape of the curve.

Finally, the function $g(Q)$ regulates the growth rate of a cell as a function of its internal nitrogen concentration. For phytoplankton species this relationship is commonly represented with a non-linear rectangular hyperbola of the form:

$$g\big(Q(t)\big) = \mu_{max} \times \left(1 - \frac{Q_{min}}{Q(t)}\right) \quad \text{(eq. 3.4)}$$

where μ_{max} indicates the growth rate at infinite internal quota and Q_{min} indicates the concentration of per-cell internal nitrogen at which no cell division occurs (with $Q(t) \geq Q_{min}$).

Alternative models

Four alternative models were derived assuming different functional responses for describing the traits for the species. The first model ("baseline model") assumes that all traits in eq. 3.2 a-b and eq. 3.4 (i.e. w_{NO3} , w_{NH4} , μ_{max}, and Q_{min}) are fixed species-specific terms. The second model ("N-history model") instead assumes that the traits of the species differ with nitrogen status. Empirical studies have documented that N-deplete cells often respond to new nitrogen availability with higher nitrogen uptake rates and lower division rates (Cochlan & Harrison 1991; Sinclair *et al.* 2006). Hence, this model includes two independent sets of parameters to describe the species' traits for nitrogen uptake and growth rate: one to represent experiments whose inoculum was previously N-replete (w_{NO3_rep} , w_{NH4_rep} , and $\mu_{\max\ \_rep}$) and another for experiments whose inoculum was N-deplete (w_{NO3_dep} , w_{NH4_dep} , and $\mu_{\max\ \_dep}$). There is no biological reason to assume that cells change their minimum internal nitrogen requirement between nitrogen replete and deplete conditions, so the parameter Q_{min} was fixed, independent of nitrogen history. We

checked that including two independent Q_{min} parameters for different nitrogen histories did not change the interpretation of the results. Overall, the "N-history" model included 7 estimated parameters. The third alternative model ("allometric model") assumed that N-utilization traits of a species are a power-law function of the mean cell size in the population. For example, the trait for the nitrate uptake rate of a cell now becomes:

$$w_{NO3}(size(t)) = w_{NO3\_coef} \times size(t)^{w_{NO3\_exp}} \quad \text{(eq. 3.5)}$$

with w_{NO3_coef} and w_{NO3_exp} as tuneable parameters regulating the shape of the relationship. In this way, each demographic parameter in the "baseline model" became an allometric function of cell size, for a total of 8 estimated parameters. Because there is strong biological evidence indicating that phytoplankton cells assimilate nitrogen at a rate that is proportional to their cell surface area (Aksnes & Egge 1991), both w_{NO3_exp} and w_{NH4_exp} were constrained to be positive. Also Q_{min_exp} was constrained to be positive, as the minimum internal nitrogen of a cell is directly proportional to the cell area (Shuter 1978; Edwards *et al.* 2012). We also checked that removing these constraints did not change the interpretation of the results. Notice that the slope between the size and the maximum growth rate of a cell was left unconstrained, as this relationship can either be positive or negative depending on the mean cell size of the species (Wirtz 2011; Maranon *et al.* 2013). Finally, the fourth "allometric N-history" model merges the assumptions of the "allometric model" and the "N-history" model: each trait in the "N-history" model follows an allometric function of mean population cell size. Hence, this parameterization assumes that the effect of cell size changes depending on whether

the inoculum was N-replete or N-deplete before the experiment, with a total of 14 estimated demographic parameters.

Data Collection

Culture maintenance

Monoclonal 1.2 L batch cultures of the green microalga *Desmodesmus armatus* (R. Chod.) Hegev. (culture accession: NQAIF301, sourced from the North Queensland Algal Culturing and Identification Facility at James Cook University, Townsville, QLD) were reared in standard Bold Basal Medium (BBM; Nichols 1973). Nitrogen was set as the limiting factor for growth in all experimental cultures, supplied between 4 to 8 times below the recommended BBM concentration with either sodium nitrate ($NaNO_3$) for nitrate-BBM, or ammonium chloride (NH_4Cl) for ammonium-BBM, or both. Phosphorous, iron, and all other nutrients were supplied at non-limiting concentrations. Furthermore, dissociation of ammonium ion (NH_4^+) into volatile un-ionised ammonia (NH_3) was minimized by ensuring pH levels below 7 by buffering the modified nitrate-BBM and ammonium-BBM media with *4-(2-hydroxyethyl)-1-piperazineethanesulfonic acid* (HEPES) at 8 mmol L^{-1} and $NaHCO_3$ at 2.38 mmol L^{-1} (Vaddella *et al.* 2011). Cultures were kept in a temperature-controlled room at 27 ± 3°C with a 14-10 day-night cycle at a light intensity of 70 µmol photons m^2 s^{-1}. Cultures were continuously suspended with magnetic stirrers at 300 rpm (IKA RCT Basic, IKA Labortechnik, Germany) and aerated with 0.45 µm filtered air (Durapore, Millipore).

Experimental design

The experimental set-up was a factorial design of two treatments of cell N-history (N-replete and N-deplete) crossed with three treatments of nitrogen type (nitrate, ammonium, or both), each replicated with three 1.2 L independent replicate cultures (see Fig. S3.1 for experimental design in Appendix Chapter 3). Initial medium nitrogen was standardized to 800 µM-N. Initial cell inoculation density was standardized at 1×10^9, which ensured between 4 to 8 days of rapid growth before reaching stable population densities. For N-replete cultures, exponentially growing cells were taken from a mother culture and inoculated into experimental cultures with fresh N-rich BBM medium. Data collection started immediately after inoculation. For N-deplete cultures, exponentially growing cells from the mother culture were inoculated into experimental cultures with N-free BBM medium. Cells were monitored until population density reached stationary growth, to ensure that all internal nitrogen was consumed before the beginning of the experiment (typically 3 to 4 days). Data collection started following fertilization of the N-free medium with nitrogen.

Population density and mean cell size

Three replicate measurements per culture were taken every day by loading 250 µL on a 96 well plate and measured with a Guava EasyCyte flow cytometer (Millipore, Hayward, CA, USA). To control for the effects of the 14-10 day-night photoperiod cycle on cell cycle, data collection was conducted daily at 13:00 (7 hours into the light period). Before cytometric analysis, each sample was diluted with DI water between 25 and 50 times to maintain the optimal precision range of the instrument (50 to 500 cells μL^{-1}). Population size was estimated after excluding

dead cells and inorganic particles characterized by low red fluorescence signals. Mean cell size was estimated optically through the forward light scatter recorded with the flow cytometer. Mullaney, Dilla and Coulter (1969) showed that the light refraction at small angles (i.e. forward light scatter) was proportional to the size of the particle, as predicted by Mie theory (Sharpless *et al.* 1975; Sharpless & Melamed 1976; Veldhuis *et al.* 2000; Shapiro 2005). Light microscopy validated the use of forward light scatter as an accurate linear proxy for mean cell size (cell area: $F_{1, 17} = 64.9$, $p<0.001$, $R^2 = 0.79$; cell perimeter: $F_{1, 17} = 49.6$, $p<0.001$, $R^2 = 0.66$). Instrument precision was periodically checked with Guava easyCheck beads (Catalog No. 4500-0025, Millipore), ensuring a coefficient of variation (CV) < 5% for all detectors.

Medium nitrogen analysis

Medium nitrate (NO_3^-) was quantified using the ultraviolet spectrometric screening method (Collos *et al.* 1999; Lanoul, Coleman & Asher 2002; Malerba *et al.* 2016). Three 1.25 mL replicate samples per culture of filtered supernatant were acidified with 25 µL 1N HCl to prevent interference from hydroxide or carbonate molecules (Clescerl, Greenberg & Eaton 1999). After vortexing, 250 µL was transferred onto a 96-wellplate (Ultraviolet-Star®, Greiner Bio-One GmbH) and optical density was measured at 230 nm (OD230; EnSpire® Multimode Plate Reader; Perkin-Elmer, Waltham MA, US). As certain types of dissolved organic matter can also absorb at 230 nm and NO_3^- does not absorb at 275 nm, a second measurement at 275 nm (OD275) was used to correct each OD230 reading (Clescerl *et al.* 1999). The standard curve for (OD230 - OD275) was linear across the range of nitrogen concentrations used in the experiments ($R^2 \geq 0.995$).

Model Calibration

We fitted the four process-based models to data for medium nitrogen and population density from all experiments. This way, model predictions generated from a single set of parameters were confronted with time series from 6 different combinations of nitrogen types and N-histories, with each treatment replicated 3 times. Quota dynamics were not experimentally measured but were instead inferred from the model fits: all of the parameters that influence the dynamics of the unobserved internal quota ($Q(t)$) also appear in the equations for the observed dynamics for nitrate depletion and biomass growth. Hence, flux into the quota can be inferred from changes in medium nitrate and ammonium, while flux out of the quota can be inferred from changes in population density (De La Rocha *et al.* 2010; Malerba *et al.* 2012; Malerba *et al.* 2015).

Two different sources of error can affect parameter calibration from time-series data: observation error and process noise (see Model Calibration in Chapter 2 for details; Hilborn *et al.* 1997; Bolker 2008). While highly controlled experimental systems are typically more consistent with process noise (Bolker 2008), the use of an optical proxy for mean cell size has the potential to increase the effects of observation error. Therefore, we adopted in this study the common approach of fitting two separate likelihood functions, one accounting for process error-only and a second one for observation error-only. We then checked that model selection and parameter estimation gave comparable results for the two methods, and supported the same conclusions (Malerba *et al.* 2012). Markov Chain Monte Carlo techniques, with Adaptive Mixture-Metropolis and Random Walk Metropolis and uniform priors, were used to fit all models, using package LaplacesDemon (Hall 2008) in the

software R (R Core Team 2015). To monitor for successful convergence, we visually inspected the iterated history, density plot, and correlation diagram for each of the parameters on four chains, and we checked for a potential scale reduction factor lower than 1.2 using Gelman and Rubin's MCMC convergence diagnostic (Gelman & Rubin 1992).

Model Selection

The goodness of fit for the "Baseline", "N-history", "Allometric", and "Allometric N-history" models were compared using Deviance Information Criteria (DIC) (Spiegelhalter *et al.* 2002; Hooten & Hobbs 2015). The model with the lowest DIC score is the estimated best-fitting model. In general, models separated by more than 5-10 DIC units from the best model should be considered as fitting the data substantially worse (Spiegelhalter *et al.* 2002). Model goodness of fit was also evaluated in two additional ways. Specifically, we calculated a standard coefficient of determination (R^2) for each state variable in each experiment, and we also inspected the distribution of residuals around predicted values.

Phenomenological models

The main advantage of fitting process-based models to our data is that it allows calibrating species-specific functional responses on data from all variables at once, thereby quantifying how flows of nitrogen among ambient nitrate and ammonium, internal nitrogen, and population density influence one another. However, most published demographic parameters for phytoplankton species have not been calculated in this way, but rather by calibrating each functional response independently, using more traditional least-squared regression between successive

points in time of each individual variable. Hence, we also tested if the conclusions from our dynamic model analysis were consistent with least-squared regressions from observed rates of per-cell nitrate and ammonium uptake and cell division (see Fig. S3.4 in Appendix Chapter 3).

Specific growth rates were computed for each day of each experiment as:

$$\mu_t = \ln(B_t) - \ln(B_{t-1}) \quad \text{(eq. 3.6)}$$

where *B* represents the total population density either at time *t* or *t*-1 (units of day^{-1}). Per-cell nitrogen uptake for nitrate and ammonium were computed for each day of each experiment as:

$$v_{NO3,t} = \frac{NO_3(t) - NO_3(t+1)}{mean(B(t), B(t+1))} \times \frac{1}{NO_3(t)} \quad \text{(eq. 3.7 a)}$$

$$v_{NH4,t} = \frac{NH_4(t) - NH_4(t+1)}{mean(B(t), B(t+1))} \times \frac{1}{NH_4(t)} \quad \text{(eq. 3.7 b)}$$

where NO_3 and NH_4 represent the mean nitrate and ammonium concentrations at time *t* or *t*+1. Hence, nitrogen uptake is computed as the total assimilated nitrogen divided by the mean population density (left fraction in eq. 3.7 a-b), and further divided for the mean nitrogen concentration (right fraction in eq. 3.7 a-b). In this way, v_{NO3} and v_{NH4} quantified per-cell nitrogen uptake rates while accounting for total medium nitrogen availability, with units of cell^{-1} day^{-1}.

RESULTS

Process-based models

The "Allometric N-history" model was selected as the best-fitting model by DIC model selection (Table 3.2). This model assumes that the species traits follow

two different allometric relationships with cell size, depending on the N-history of the cell. The “Baseline” model, which assumes that all demographic parameters are independent of cell size and N history, performed the worst (Table 3.2). The “Allometry” model, which assumes that demographic parameters vary with cell size, and the “N-history” model, assuming N-replete and N-deplete cells to display different size-independent demographic parameters, ranked in-between (Table 3.2). Furthermore, calibrating the model with either observation error-only or process noise-only likelihood functions produced equivalent conclusions, which indicate that the results are robust and independent of the assumptions about the source of error in the data (Table 3.2).

Except for the rates of per-cell nitrate uptake, all species traits show substantial differences when estimated with the “Allometric N-history” model (solid lines) compared to the size- and N-history-independent “Baseline” model (dashed lines; Fig. 3.1). Specifically, per-cell ammonium uptake was substantially influenced by mean cell size, and was higher in N-deplete cells than N-replete cells (Fig. 3.1 B). The maximum specific division rate increased with cell size for N-replete cells, but remained constant for N-deplete cells (Fig. 3.1 C). Finally, minimum internal nitrogen was higher when cells were larger (Fig. 3.1 D). Conversely, per-cell nitrate uptake was independent of cell size and was comparable between N-replete and N-deplete cells (Fig. 3.1 A). Functional responses calibrated by fitting the model with observation error-only or with process noise-only likelihood functions produced equivalent conclusions (compare Fig. 3.1 with Fig. S3.3 in Appendix Chapter 3).

Visually inspecting the fit for the four calibrated models revealed why the "Allometric N-history" model performed the best (Fig. 3.2-3.4). Because model selection (Table 3.2) and relationships of demographic and uptake parameters (Figures 3.1 and S3.3 in Appendix Chapter 3) were consistent between the process error-only and observation error-only models, we focus here only on observation error-only models. Cells that were previously N-replete and re-supplied with a single-nitrogen source showed smooth and gradual changes in nitrogen depletion (symbols in Fig. 3.2 A and 3.2 C), mean cell size (bars in Fig. 3.2 A and 3.2 C), and population density (Fig. 3.2 B and 3.2 D). In contrast, previously N-deplete cells reared under the same nitrogen regime showed faster initial nutrient depletion (symbols in Fig. 3.3 A and 3.3 C), an abrupt spike in mean cell size (bars in Fig. 3.3 A and 3.3 C), and a faster increase toward population carrying capacity (Fig. 3.3 B and 3.3 D). The same qualitative differences remained when cells were simultaneously supplied with both nitrate and ammonium: N-replete cells consistently displayed more regular transitions than N-deplete cells (compare Fig. 3.4 A-C with Fig. 3.4 D-F). Only the "Allometric N-history" model performed consistently well ($R^2 > 0.9$) with both smooth and abrupt dynamics from N-replete and N-deplete cells, respectively (dark blue line in Fig 3.2-3.4). The "Baseline" and "N-history" models performed well only with smooth N-replete dynamics (yellow and orange lines, respectively; Fig. 3.2, 3.4 A-C), instead showing clear lack of fit from data collected for N-deplete cultures (Fig. 3.3 B, 3.3 D and 3.4 F). Conversely, the "Allometric" model showed mostly good fits for abrupt N-deplete cultures (Fig. 3.3 and 3.4 D-F), but often failed to capture the smooth dynamics in N-replete cultures (Fig. 3.2 B-D and 3.4 C).

The explanation for the poor performance of the “Allometric” model with N-replete cells and of the “N-history” model with N-deplete cells lies in the observed mean cell sizes: N-deplete cells changed their size more suddenly than N-replete cells (compare bars in Fig. 3.2 A, 3.2 C, and Fig. 3.4 A against bars in Fig. 3.3 A, 3.3 C, and Fig. 3.4 D), mostly also recording higher peak values. The “Allometric” model can perform well with N-deplete cells because these rapid changes in cell size are indicative of imminent transitions in culture dynamics. However, this relationship between cell size and cell performances changed between N-replete and N-deplete cells. Consequently, forcing a single functional response for both N-deplete and N-replete cells (as assumed in the “Allometric” model) was inadequate and produced worse fits than the size-independent “baseline” and “N-history” models. This is the reason why the “Allometric N-history” model (assuming two different allometric relationship between N-replete and N-deplete cells) can combine the good performances of the “Allometric” model for N-deplete cells and of the “N-history” model for N-replete cells.

Overall, changes in mean cell size closely matched the transitions in medium nitrogen in the cultures: increasing cell size coincided with periods of high medium nitrogen, and decreasing cell size with periods of no available nitrogen (Fig. 3.2 A, C, Fig. 3.3 A, C, Fig. 3.4, A, D). Thus, it is not surprising that observations on population mean cell size and model-inferred internal nitrogen quota from the best-fitting “Allometric N-history” model were highly correlated (Spearman’s rho correlation: $r_s = 0.77$, $S = 6970$, $p > 0.001$, $N=57$; Fig. S3.2 in Appendix Chapter 3). Interestingly, however, the relationship was consistent for both N-replete and N-deplete cells (Fig. S3.2).

High ammonium concentrations produced a temporary phase of slow or absent nitrate assimilation (low nitrate depletion in the first 24 hours in Fig. 3.4 A, D). Most models captured this behavior well, which indicates that the deterministic structure of the model was adequate to describe ammonium-induced inhibition of nitrate uptake for this species.

Phenomenological models

Statistical linear models revealed a significant effect of cell size and nutrient history on the observed rates of nitrogen assimilation and specific growth rates, calculated between each two successive days with eq. 3.6 and 3.7 a-b. Specifically, nitrate uptake showed a weak positive effect of cell size ($F_{1,48}$ = 6.59, MS = 2.30, p=0.033), but no significant effect of nutrient history ($F_{1,48}$ = 0.97, MS = 0.34, p>0.5; Fig. S3.4 A in Appendix Chapter 3). Conversely, rates for ammonium uptake were significantly higher in N-deplete cells compared to N-replete cells ($F_{1,40}$ = 41.90, MS = 5.69, p<0.001) and displayed a significant positive effect of cell size ($F_{1,40}$ = 43.47, MS = 5.9, p<0.001; Fig. S3.4 B). The effect of cell size was constant across nutrient histories for both nitrate ($F_{1,48}$ = 0.27, MS = 0.1, p>0.05) and ammonium uptake ($F_{1,40}$ = 0.01, MS = 0.01, p>0.05; Fig. S3.4 A-B). Finally, growth rate increased with cell area at N-deplete conditions, not at N-replete conditions ($F_{1,149}$ = 8.07, MS = 0.51, p<0.01; Fig. S3.4 C). Overall, these results are mostly consistent with findings from fitting the process-based models. The only detectable difference is the effect of cell size on per-cell nitrate uptake, which was not detected by the process-based models. However, the very weak coefficient of determination (R^2<0.13) and the 95% confidence intervals for the slope coefficient almost

including zero (0.12 - 2.6) suggest some care should be taken in the interpretation of this result (Fig. S3.4 A).

Table 3.1: Best-estimates from the posterior distribution (median and upper and lower 95% credible intervals) of the parameters in the "allometric N-history" model with observation error-only likelihood function, which was the best-fitting model following DIC model selection (confront to Table 3.2 for DIC scores).

Variables	Definition (units)
NO_3	Nitrate in medium (μmol NO_3^- L^{-1})
NH_4	Ammonium in medium (μmol NH_4^+ L^{-1})
Q	Nitrogen quota (μmol N $cell^{-1}$)
B	Population density (cell L^{-1})

Parameters	Definition [Median (± 95% C.I.) units]
$w_{NO3\_coef\_rep}$	Scaling intercept for per-cell nitrate uptake in replete cells [1.99 (1.7-2.31) 10^{-9} $cell^{-1}$ cell $area^{-1}$ day^{-1}]
$w_{NO3\_exp\_rep}$	Scaling exponent for the per-cell nitrate uptake in replete cells [2.55 (1.7-3.69) 10^{-6} unitless]
$w_{NH4\_coef\_rep}$	Scaling intercept for the per-cell ammonium uptake in replete cells [5.52 (4.49-7.06) 10^{-21} $cell^{-1}$ cell $area^{-1}$ day^{-1}]
$w_{NH4\_exp\_rep}$	Scaling exponent for the per-cell ammonium uptake in replete cells [8.14 (8.04-8.20) unitless]
$\mu_{max\_coef\_rep}$	Scaling intercept for growth rate at infinite nutrient storage in replete cells [10.2 (8.50-13.7) 10^{-5} day^{-1} cell $area^{-1}$]
$\mu_{max\_exp\_rep}$	Scaling exponent for growth rate at infinite nutrient storage in replete cells [21 (19-22.2) unitless]
$w_{NO3\_coef\_dep}$	Scaling intercept for the per-cell nitrate uptake in deplete cells [6.75 (5.83-7.82) 10^{-10} $cell^{-1}$ cell $area^{-1}$ day^{-1}]
$w_{NO3\_exp\_dep}$	Scaling exponent for the per-cell nitrate uptake in deplete cells [1.09 (8.8-13.9) 10^{-8} unitless]
$w_{NH4\_coef\_dep}$	Scaling intercept for the per-cell ammonium uptake in deplete cells [2.09 (1.63-2.72) 10^{-10} $cell^{-1}$ cell $area^{-1}$ day^{-1}]
$w_{NH4\_exp\_dep}$	Scaling exponent for the per-cell ammonium uptake in deplete cells [0.55 (0.46-0.62) unitless]
$\mu_{max\_coef\_dep}$	Scaling intercept for growth rate at infinite nutrient storage in deplete cells [3.9 (3.18-4.88) day^{-1} cell $area^{-1}$]
$\mu_{max\_exp\_dep}$	Scaling exponent for growth rate at infinite nutrient storage in deplete cells [0.62 (0.57-0.66) unitless]
Q_{min_coef}	Scaling intercept for per-cell minimum nitrogen quota [1.32 (0.9-1.58) 10^{-9} μmol N $cell^{-1}$ cell $area^{-1}$]
Q_{min_exp}	Scaling exponent for per-cell minimum nitrogen quota [1.57 (1.49-1.68) unitless]

a	Shape parameters for the inhibition of ammonium uptake on per-cell nitrate uptake [2.49 (1.97-3.05) 10^{-14} unitless]
b	Shape parameters for the inhibition of ammonium uptake on per-cell nitrate uptake [6.98 (6.74-7.16) unitless]

Table 3.2: Formal model selection criteria between competing models with Deviance Information Criterion (DIC). Values represent the deviance (D(θ)), the DIC score, and the difference in DIC (ΔDIC) scores (thus, by definition, the best fit model has ΔDIC = 0), for models calibrated with either observation error-only or process noise-only likelihood functions. Boldface indicates the model with greater support from the data.

	Observation Error			*Process Error*		
Alternative Models	*D(θ)*	*DIC*	*ΔDIC*	*D(θ)*	*DIC*	*ΔDIC*
Allom. N-History	**9893**	**9946**	**0**	**9903**	**9930**	**0**
N-History	10014	10057	111	10007	10029	99
Allometry	10037	10080	134	10106	10131	201
Baseline	10101	10141	195	10138	10165	235

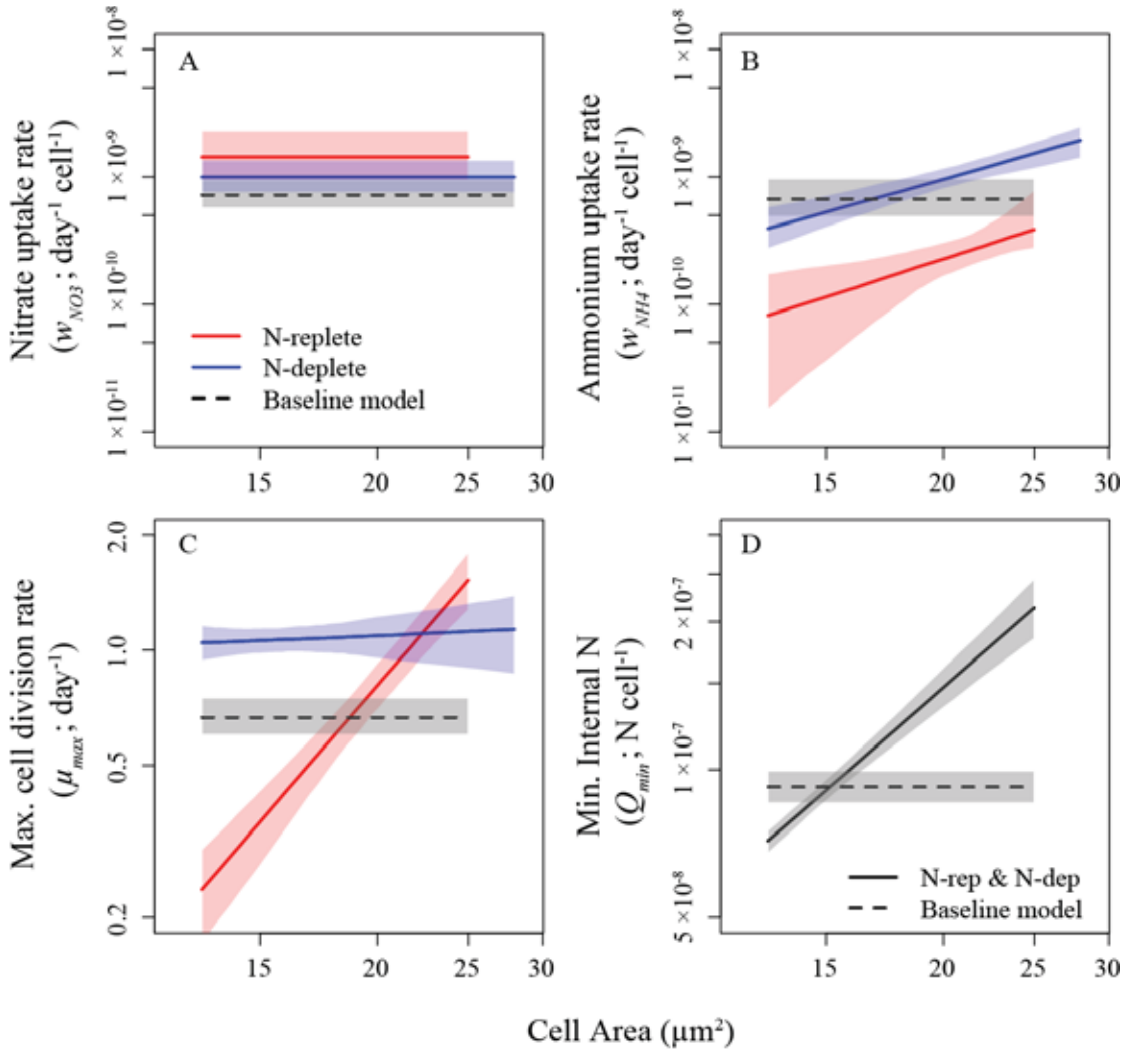

Figure 3.1: Comparison for the best-estimates for demographic parameters (median ±95% confidence intervals) calculated with the "baseline" model (dashed lines) and with the best-fitting "Allometric N-history" model (solid lines). Parameters were calculated using observation error-only likelihood functions and represent rate of per-cell uptake for nitrate (A) and ammonium (B), growth rate at infinite stored internal nitrogen (C), and minimum internal nitrogen (D). Two solid lines in the same pannel represent the effect of cell size on the demographic parameters between N-replete (red) and N-deplete (blue) previous N-history. Dashed line is the corresponsive parameter estimated with the "baseline" model,

which assumes independence with cell size and nutrient history. Notice that pannel D has only one solid line; this is because the functional response for minimum internal nitrogen in the “Allometric N-history” model was only designed as a function of cell size and independent of previous N-history of the culture. See Material and Methods, Table 3.1 for more details on model formulation and demographic parameters, and Fig. S3.3 in Appendix Chapter 3 for equivalent plot calculated with alternative process noise-only likelihood functions.

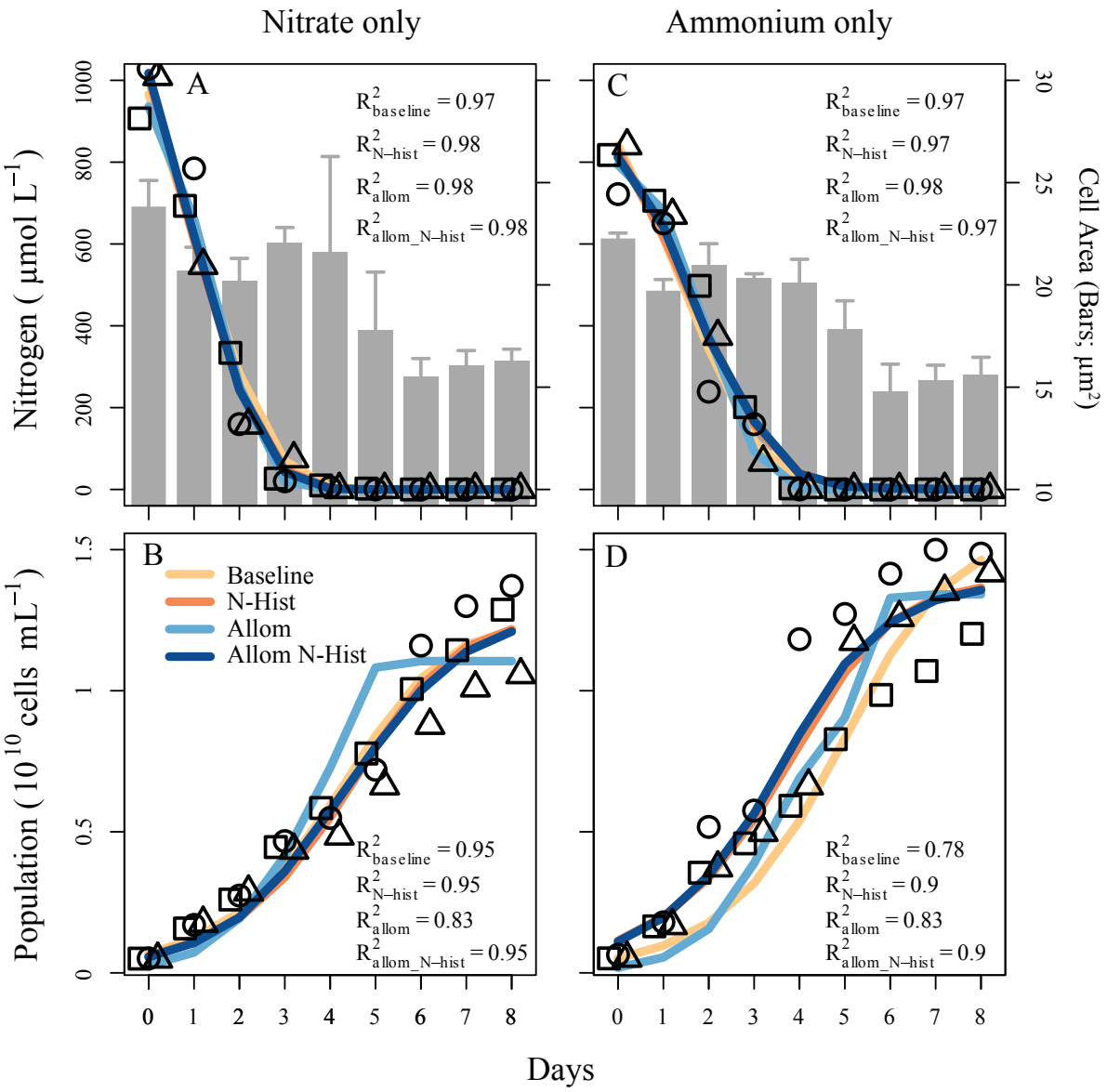

Figure 3.2: Time-series and model fits for nitrogen-replete culture dynamics grown with either nitrate (A, B) or ammonium (C, D) as the only nitrogen source. Plots show changes in medium nitrogen depletion (A, C) and population size (B, D) over the course of the experiments. Grey bars represent daily estimates for optical proxy for mean population cell size (+ St. Dev.; A, C). Different symbols represent the mean among three replicate measurments for each day for each of the three independent replicate culture. Colour lines represent model goodness-of-fit for the four competing models calibrated with observation error-only likelihood functions

(see Calibration section in Material and Methods). A coefficient of determination quantifies the goodness of fit for each competing model.

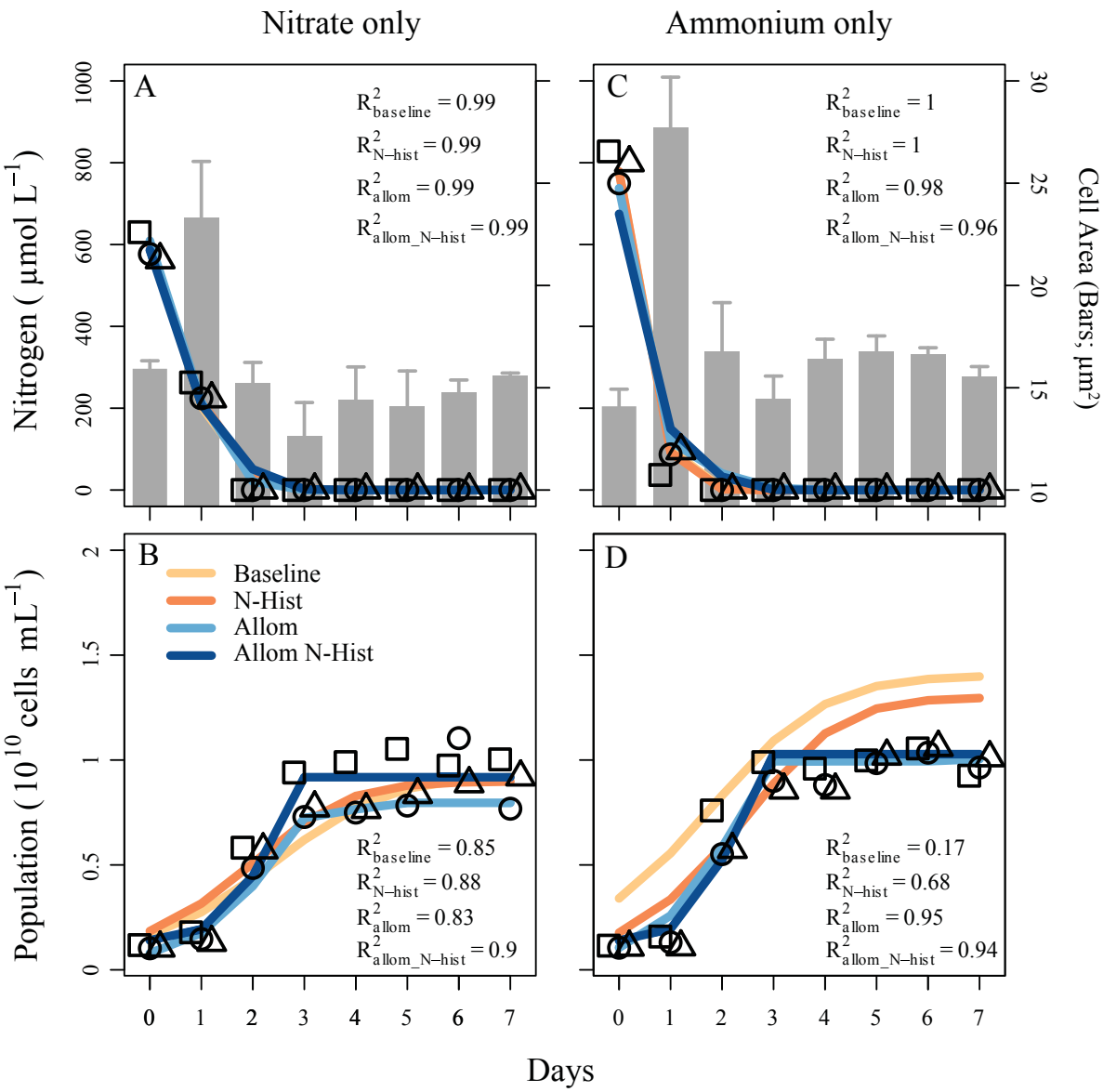

Figure 3.3: Time-series and model fits for nitrogen-deplete culture dynamics grown with either nitrate (A, B) or ammonium (C, D) as the only nitrogen source. Plots show changes in medium nitrogen depletion (A, C) and population size (B, D) over the course of the experiments. Grey bars represent daily estimates for optical proxy for mean (+ St. Dev.; A, C). Different symbols represent the mean among three replicate measurments for each day for each of the three independent replicate

culture. Model fits were calculated using observation error-only likelihood functions. See legend for Fig. 3.2 for more information.

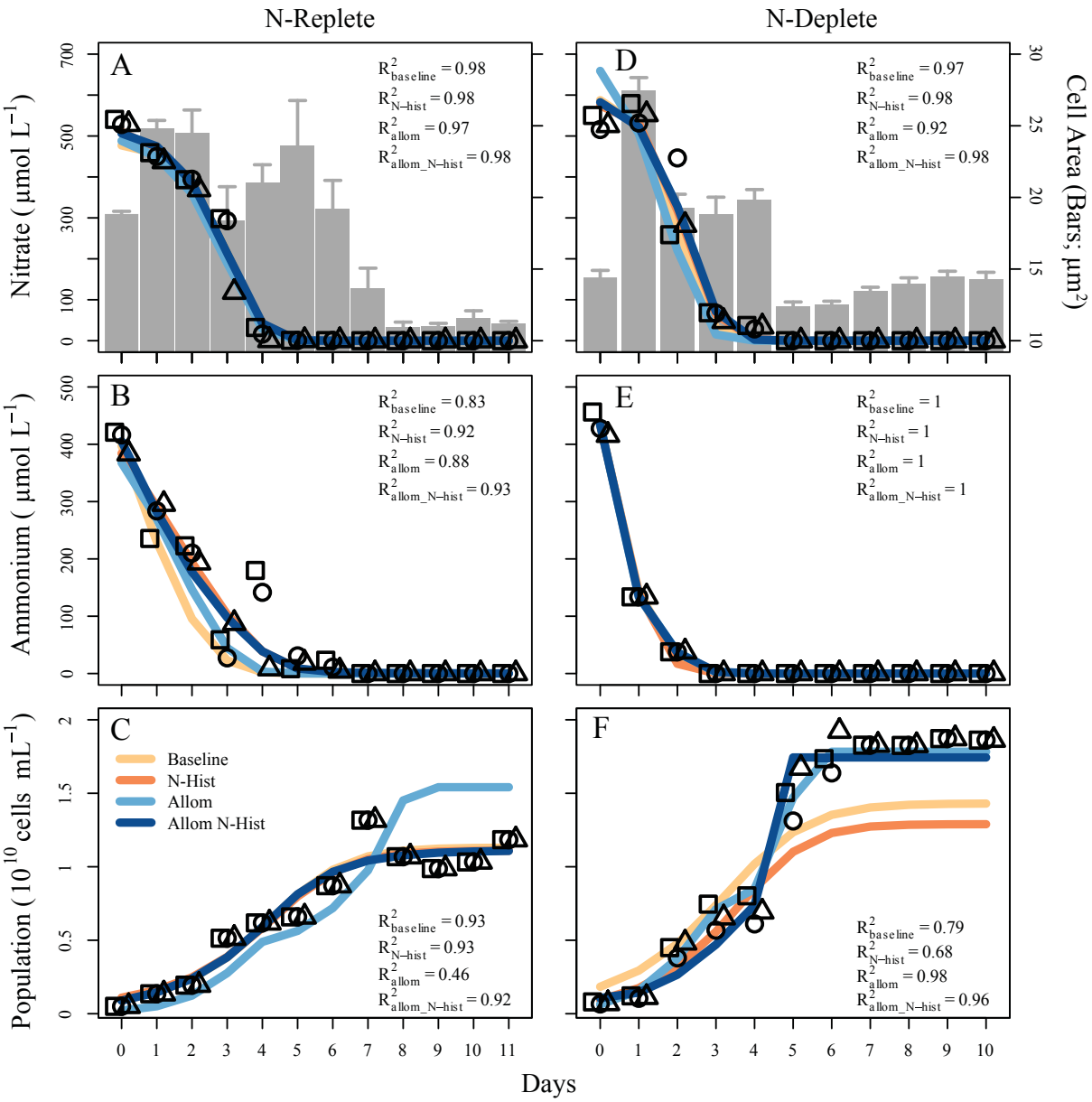

Figure 3.4: Time-series and model fits for nitrogen-replete (A-C) and nitrogen-deplete (D-F) cultures grown with both nitrate and ammonium as the only nitrogen source. Plots show changes in medium nitrogen depletion (A-B, D-E) and population size (C, F) over the course of the experiments. Grey bars represent daily estimates for optical proxy for mean (+ St. Dev.; A, D). Different symbols represent the mean among three replicate measurments for each day for each of the three independent replicate culture. Model fits were calculated using observation error-only likelihood functions. See legend for Fig. 3.2 for more information.

Discussion

The analysis supported our hypothesis that nutrient utilization dynamics of *Desmodesmus armatus* vary strongly with cell size and nutrient history. Overall, larger cells recorded higher ammonium uptake rate, maximum specific growth rate, and minimum internal nitrogen quota. Furthermore, rates of ammonium uptake were higher in cells recovering from N-depletion, while maximum cell growth rates increased with cell size more under N-replete than N-deplete conditions. Minimum cell quota increased with size under N-deplete conditions, but remained virtually constant under N-replete conditions. Finally, the positive relationship between mean cell size and (model-inferred) changes in internal nitrogen quota was consistent between N-replete and N-deplete cells across all experiments.

Our physiological understanding of the effect of N-stress in phytoplankton cells is consistent with an important role of mean cell size and previous N-history on phytoplankton nutrient utilization traits. For instance, our results show that rates of cell division were positively correlated with cell size under N-replete conditions. This is consistent with larger cells being at a more advanced stage of the cell division cycle (Hunter-Cevera *et al.* 2014), which explains the positive correlation with maximum cell division rates under N-replete conditions. Conversely, maximum cell division rates for N-deplete cells were independent of cell size due to faster rates recorded for small cells. When N availability inhibits cell division, cell size decreases and photosynthetic energy is diverted and stored in the form of lipids or carbohydrates (Rodolfi *et al.* 2009; Mata, Martins & Caetano 2010). When exposed to new nutrients, those energy stores can reactivate cell division at a rate that is temporarily enhanced (Bittar *et al.* 2013). Moreover, rates for ammonium

uptake were consistently higher for N-deplete than N-replete cells. This is likely because many species are adapted to exploit new supplies of a limiting nutrient by taking up more than would be required to sustain immediate growth (Sinclair *et al.* 2006). However, enhanced N uptake is more common when cells are supplied with ammonium, and less frequent with nitrate (Cochlan *et al.* 1991). This is also because ammonium is easier to assimilate, as most amino acids are in the same oxidation state. In contrast, nitrate can be assimilated only after being first reduced to ammonium, by means of specialized enzymes (Berges 1997). Overall, our results show that using single species-specific parameter values (i.e. "Baseline model") leads to a substantial underestimation of a species' ability to divide (up to 64 %), take up ammonium (up to 52 %) and nitrate (up to 63 %), and to store nitrogen intracellularly (up to 53 %), compared to accounting for variation due to cell size and N-history ("Allometric N-history model").

It is commonly assumed that within-species trait variability in phytoplankton species is negligible compared to between-species variability. However, this assumption is rarely tested. A way to estimate the relative importance of within-species sources of trait variation is by using information from published phytoplankton allometric relationships. We compared the range between minimum and maximum within-species trait values recorded here for each trait, against the standard deviation of the residuals in allometric scaling relationships across multiple species for the same trait. In this study, mean rates for nitrate uptake increased by up to 40%, while ammonium uptake, maximum growth rate, and minimum internal nitrogen increased between half and one and a half orders of magnitude. These ranges were low (within 1 standard deviation of between-species residual variation) for nitrate uptake, but were substantially higher (by more than three standard

deviations) for ammonium uptake, maximum growth rate, and minimum nitrogen quota when compared to the residual standard deviations in interspecific allometric N utilization traits for freshwater phytoplankton communities reported in Edwards *et al.* (2012). This indicates that for three of the four traits not accounting for phenotypic plasticity and intraspecific trait variability can lead to substantial uncertainty when calculating interspecific allometric relationships.

Overall, our findings are in agreement with the growing body of ecological literature highlighting the importance of phenotypic plasticity on species traits (Mommer *et al.* 2006; Violle *et al.* 2007). Phenotypic plasticity can provide an advantage to an individual by better adjusting to changes in abiotic conditions, while simultaneously decreasing interspecific competition by reducing niche overlap (Jung *et al.* 2010). In phytoplankton communities, the ability to modulate cell size can extend the geographic distribution of a species by adjusting for nutrient requirements in oligotrophic or fluctuating environmental conditions or by modifying grazing risks and sinking velocity in eutrophic environments (Duarte *et al.* 1990; Grover 1991; Maranon 2015). Similarly, plant communities occupying dynamic and unpredictable habitats, such as river floodplains, are dominated by species featuring wide phenotypic plasticity in traits determining gas exchange and submergence tolerance (Mommer *et al.* 2006; Jung *et al.* 2010). Another example is the common fruit fly *Drosophila melanogaster*, whose ability to thrive at different temperatures has large intraspecific variability, with the expression of heat-shock proteins depending on previous thermal regimes experienced throughout the life history of the individual (Krebs & Feder 1997). Further examples of intraspecific trait plasticity include relationships between mean clutch size and exposure to predators for the freshwater crustacean *Daphnia pulex* (DeWitt 1998) and between

development time and desiccation risk in the amphibian *Rana temporaria* (Merila, Laurila & Lindgren 2004).

In conclusion, our results show that the nutrient utilization dynamics of a phytoplankton species are functions of changes in mean cell size and previous nitrogen history. The importance of recognizing and quantifying trait plasticity in single species has become more urgent since a growing number of plant and animal studies use trait databases to investigate community patterns (Berg & Ellers 2010). Quantifying intraspecific trait plasticity is complex and most trait databases often report only fixed species-specific values for each life history trait (Vieira *et al.* 2006; Kleyer *et al.* 2008). Hence, it is important to recognize and distinguish between traits where interspecific variability is dominant, and traits where ignoring intraspecific trait plasticity will impair the explanatory power of trait-based analyses (Berg *et al.* 2010).

Chapter 4: Standard flow cytometry as a rapid and non-destructive proxy for cell nitrogen quota

Introduction

Identifying nitrogen limitation and quantifying the degree of nitrogen stress in phytoplankton cells is of primary importance in ecological and applied phytoplankton fields. Nitrogen is the nutrient required in highest amounts for cell division, and is often the first to become limiting. A limiting nutrient is defined as the element whose availability inside the cell is the lowest in relation to the cell's requirement (typically nitrogen, phosphorous, or iron; Howarth 1988). The capacity of a species to store internal nitrogen (here referred as "cell nitrogen quota") is a main determinant of primary productivity, nutrient competition outcomes, and a key mechanism for the maintenance of phytoplankton diversity (Grover 1991; Holt 2008). Furthermore, especially in oligotrophic waters, a sudden release of nitrogen can lead to increasing chances of an algal bloom, often with negative ecological and economic consequences (Cloern 2001). Therefore, substantial resources are allocated to monitor changes in phytoplankton nitrogen content, in order to regulate nitrogen loading budgets from anthropogenic activities (Shelly *et al.* 2010). Changes in phytoplankton nitrogen quotas are also routinely monitored in algal aquaculture practices: an intermediate degree of nitrogen limitation is needed to balance the quality (i.e. stress-related increase in lipid and carbohydrate contents) and quantity of the final product (Adams *et al.* 2013).

Current techniques to determine phytoplankton nitrogen status can be divided into direct and indirect methods, both with limited employability (Beardall *et al.* 2001; Shelly *et al.* 2010). The two most common direct methods are elemental analysis and digestion protocols. These techniques quantify the absolute and relative concentrations of single elements in biomass samples and infer the nitrogen quota of single cells (e.g. Raimbault *et al.* 1999a; Bertilsson *et al.* 2003; Li *et al.* 2014a). However, direct techniques tend to be costly, rely on sophisticated instruments and, most importantly, cannot differentiate between elements derived from live and dead cells or inorganic particles, which can substantially overestimate per-cell nutrient composition (Beardall *et al.* 2001). Alternatively, indirect methods to quantify nitrogen status consist of "bioassays" or "enrichment experiments", where the degree of nitrogen limitation is determined by comparing the response (usually growth rate, but also changes in protein content or specific enzymatic activities) of an indicator species (or of a community of species) in a sample when re-supplied with nitrogen (e.g. Hayes, Whitaker & Fogg 1984; Hecky & Kilham 1988; Dodds, Strauss & Lehmann 1993). Compared to direct methods, indirect techniques generally do not rely on costly equipment and can exclude the contribution from non-autotrophic particles. However, these experiments are more time consuming (lasting up to weeks) and their results are more controversial due to influences associated with extended confinement of natural assemblages in bottles (Graziano *et al.* 1996; Beardall *et al.* 2001; Shelly *et al.* 2010). Collectively, these shortcomings highlight the need for a reliable and more rapid method to quantify nitrogen status in phytoplankton communities.

An alternative way to improve current estimation techniques for phytoplankton nitrogen limitation is through the analysis of single-cell optical

properties. Nitrogen limitation influences many physiological and morphological aspects of phytoplankton cells such as cell volume, cell roundness, pigment composition, quantities of internal organelles, and concentrations of storage molecules (e.g. lipids, carbohydrates, proteins; Kolber, Zehr & Falkowski 1988; Rodolfi *et al.* 2009; Vanucci *et al.* 2010; Adams *et al.* 2013). The conventional way to quantify cell morphological features is with flow cytometers, which measure optical properties such as light refraction and fluorescence signals as a laser beam excites individual cells (Collier 2000; Veldhuis *et al.* 2000; Sosik, Olson & Armbrust 2010). In this way flow cytometric variables only depend on intrinsic properties of a cell without being influenced by total population size. Three types of flow cytometric optical signals directly relate to the anatomy and physiology of phytoplankton cells. The red fluorescence signal is proportional to the internal concentration of chlorophyll *a* inside the cell, and can be used to differentiate phytoplankton cells from chlorophyll-free particulate matter (Sosik, Chisholm & Olson 1989; Dubelaar *et al.* 2000). The forward light scatter represents the light travelling along the same axis of the laser beam and its intensity is proportional to the cell cross section (Dubelaar *et al.* 2000). Finally, the side light scatter represents the light travelling orthogonally to the incident laser beam and its intensity relates to the internal and external structures and granularity of the cell (Dubelaar *et al.* 2000). If the oncoming of nitrogen limitation leads to systematic anatomical and physiological changes within a cell, then a flow cytometric optical analysis should provide a quantifiable signal for evaluating cell nitrogen quota in ways that are instantaneous, non-destructive, precise, and practical to monitor with automatic programmable instruments.

Optical properties detected with flow cytometers have already been successfully used to infer specific features in phytoplankton cells (Balfoort *et al.* 1992). The red fluorescence signal accurately ($R^2 > 0.8$) predicted per-cell concentration of various pigments across different marine phytoplankton species (Cavender-Bares *et al.* 1999). Furthermore, analysis of forward light scatter signals provided information about the calcification level in coccolithophore cells (von Dassow *et al.* 2012). Regarding the relationship between optical proprieties and nitrogen status, flow cytometric red fluorescence of *Prochlorococcus*, *Synechococcus*, and picoeukaryotes showed a significant increase following nitrogen addition, which did not occur when supplied with non-limiting iron and phosphorous (Davey *et al.* 2008). Also *Microcystis aeruginosa* showed a positive relationship between flow cytometric red fluorescence and medium nitrogen availability (Brookes *et al.* 2000). Therefore, flow cytometric variables of red fluorescence, forward and side scatter all appear to be sensitive to changes in nitrogen status across different phytoplankton species and growth conditions.

It is important to consider and account for the effects of photoperiod when evaluating the use of optical properties as a proxy for nutrient status in phytoplankton cells (DuRand & Olson 1998; Mas *et al.* 2008). Photoperiod regulates the cell cycle: formation of cleavage furrows in the cell wall, organelle replication, increase in photosynthetic performance, and change in cell shape and size (Roenneberg & Mittag 1996; Luning 2005). As a result, optical properties of a cell also change depending on cell cycle relative to photoperiod (DuRand *et al.* 1998; DuRand *et al.* 2002). Hence, in order to eliminate diurnal effects, data collection was standardized with respect to sampling time.

The aim of this study was to investigate whether cell optical properties measured daily at 18:00 with a standard flow cytometer can be used as an accurate predictor of nitrogen quota in four nitrogen-limited microalgal species *Desmodesmus armatus*, *Mesotaenium* sp., *Scenedesmus obliquus*, and *Tetraedron* sp. grown in laboratory batch culture. In the experiment, nitrogen-limited cultures were re-supplied with nitrate and monitored daily until stationary phase across two treatments of initial inoculation densities. Our results demonstrate that flow cytometric optical properties can serve as excellent proxies for nitrogen quota in laboratory batch cultures.

Materials and Methods

Culture maintenance

Monoclonal 1.2 L batch cultures of three green microalgae, *Desmodesmus armatus* (R. Chodat) E. Hegewald (culture accession: NQAIF301), *Scenedesmus obliquus* (Turpin) Kützing (NQAIF299), and *Tetraedron* sp. (NQAIF295), and one charophyte, *Mesotaenium* sp. (NQAIF303), were sourced from the North Queensland Algal Culturing and Identification Facility at James Cook University (Townsville, QLD). The four species coexist in nature and are among the most common and resilient species in the area where they were originally isolated, at the Tarong ash-dam Power Station (Tarong, Queensland, Australia). Mother cultures were reared in standard Bold Basal Medium (BBM; Nichols 1973). All chemicals for culturing and nutrient analyses were purchased from Sigma-Aldrich. Nitrogen was set as the limiting factor for growth in all experimental cultures, by acclimatizing in nitrogen-free BBM prior to the beginning of the experiments until population density reached stationary phase, and successively supplying 1000

µmol-N L^{-1} of sodium nitrate ($NaNO_3$), which represents a third of the original BBM nitrogen concentration. Potential for carbon limitation was minimized by ensuring pH levels below 7 by buffering the modified nitrate-BBM with *4-(2-hydroxyethyl)-1-piperazineethanesulfonic acid* (HEPES) at 8 mmol L^{-1} and by supplying $NaHCO_3$ at 2.38 mmol L^{-1}. Cultures were kept in a temperature-controlled room at 27±3°C with a 14-10 day-night cycle at a light intensity of 70 µmol photons m^2 s^{-1}. Cultures were continuously mixed with magnetic stirrers at 300 rpm (IKA RCT Basic, IKA Labortechnik, Germany) and aerated with 0.45 µm filtered air (Durapore, Millipore). Glassware was acid-washed (10% HCl) and all culturing materials were autoclaved and handled aseptically in a laminar flow cabinet (Alternative Environmental Solutions fitted with High-Efficiency Particulate Arresting filter, Australia Standards 4260, National Association of Testing Authorities certified).

Experimental design

To test for the influence of light penetration and per-cell medium nitrogen availability, two independent replicate cultures for each of the four species were grown at two treatments of initial inoculation densities, leading to different per-cell nitrogen availabilities and mean light penetrations. Culture volume was standardized at 1 L. To standardize initial conditions for biomass and light penetration across species with different cell sizes, starting inoculation cell densities were set at optical densities of 0.01 for the low initial inoculation treatment and were increased 5-fold to 0.05 for the high initial inoculation treatments. Initial medium nitrogen was kept constant at 1000 µmol-N L^{-1}, which meant an approximate 5-fold difference in per-cell medium nitrogen availability between the

two treatments. Inoculation densities were based on preliminary analysis of the species to ensure from 3 to 6 days of fast nitrogen-driven population growth. Optical densities were measured at 750 nm on three 250 µL mother culture samples loaded on standard 96 well plates (EnSpire® Multimode Plate Reader; Perkin-Elmer, Waltham MA, US).

It is important to consider and account for the effects of photoperiod when evaluating the use of optical properties as a proxy for nutrient status in phytoplankton cells (DuRand *et al.* 1998; Mas *et al.* 2008). Photoperiod regulates the cell cycle: formation of cleavage furrows in the cell wall, organelle replication, increase in photosynthetic performance, and change in cell shape and size (Roenneberg *et al.* 1996; Luning 2005). As a result, optical properties of a cell also change depending on cell cycle relative to photoperiod (DuRand *et al.* 1998; DuRand *et al.* 2002). Hence, data collection was conducted every day at 18:00, in order to control for any diurnal fluctuations.

Flow cytometric analysis

Three replicate measurements per culture were taken every day at 18:00 loading 250 µL on a 96 well plate and measured with a Guava EasyCyte flow cytometer (Millipore, Hayward, CA, USA). Before cytometric analysis, each sample was diluted with DI water between 25 and 50 times to maintain the optimal precision range of the instrument (50 to 500 cells μL^{-1}). Optical variables are represented by the mean of the cytometric histograms for red fluorescence, forward scatter, and side scatter. The excitation light was a blue laser at 488 nm and 75 MW, and emission was recorded at 488 (± 6) nm for forward and side light scattering and at 690 (± 50) nm for red fluorescence as individual cells pass through a

microcapillary flowcell at 0.1 µL sec^{-1}. Population size and optical coefficients were estimated after excluding dead cells and inorganic particles characterized by low red fluorescence signals. Instrument precision was periodically checked with Guava easyCheck beads (Catalog No. 4500-0025, Millipore), ensuring a coefficient of variation (CV) < 5% for all detectors. Flow cytometric optical values are relative to the voltage applied to the photo-detector. We controlled for the sensitivity of the photo-detector by keeping it constant throughout all experiments and all species. Moreover, we facilitated result reproducibility by normalizing flow cytometric readings by the optical mean values of the easyCheck beads, a strategy already adopted by Durand and Olson (1996); DuRand *et al.* (1998) and Mas *et al.* (2008).

Medium nitrogen analysis

Phytoplankton cells can respond with nitrite (NO_2^-) excretion when initially exposed to a surge of ambient nitrate (NO_3^-; Malerba et al. 2012) . Hence, we quantified total medium nitrogen as the sum of nitrate and nitrite ambient concentrations with the ultraviolet spectrometric screening method (Lanoul *et al.* 2002). Three 1.25 mL replicate samples per culture of filtered supernatant were acidified with 25 µL 1N HCl to prevent interference from hydroxide or carbonate molecules (Clescerl *et al.* 1999). After vortexing, 250 µL was transferred onto a 96-wellplate (Ultraviolet-Star®, Greiner Bio-One GmbH) and optical density was measured at 230 nm wavelength (OD_{230}; EnSpire®). Also, because certain types of dissolved organic matter can also absorb at 230 nm and NO_3^- and NO_2^- do not absorb at 275 nm, a second measurement at 275 nm (OD_{275}) was used to correct each OD_{230} reading (Clescerl *et al.* 1999). The standard curve for (OD_{230} - OD_{275})

was linear across the range of nitrogen concentrations used in the experiments ($R^2 \geq$ 0.995).

Total Particulate Nitrogen and Cell Nitrogen Quota

Estimation of total particulate nitrogen content was performed by digesting biomass samples and oxidizing all nitrogen to nitrate following the persulfate oxidation method (Delia, Steudler & Corwin 1977; Solorzano & Sharp 1980; Eaton *et al.* 2005), and later estimating total nitrate-only concentration with the salicylate method (Cataldo *et al.* 1975). Cell nitrogen quota was then estimated for each sample by dividing total particulate organic nitrogen by the population size at each day of the experiment. The persulfate digestion required 2 reagent solutions: (1) 2.01 g of $K_2S_2O_8$ and 1.5 mL of 5M NaOH in 100 mL DI water (made fresh daily); (2) 6.18g H_3BO_3 and 0.8g NaOH in 100 mL DI water (stable solution). Nitrate determination with the salicylate protocol required two reagent solutions: (3) 0.5g of $C_7H_6O_3$ in 10 mL of conc. H_2SO_4 (made fresh daily); (4) 200 g NaOH in 1 L DI water (stable solution). Inorganic and organic standard nitrogen stocks were: (1) 1.011g KNO_3 in 1 L DI water for the inorganic control; (2) 0.75 g of glycine in 1 L DI water for the organic control.

The procedure for determining total particulate nitrogen consisted of three steps. Firstly, cells were separated from the supernatant by centrifuging between 2 to 14 mL of sample (depending on the total nitrogen content in the sample) at 3,000 g at 5 °C for 10 min (Eppendorf R 5810), gently removing 12 mL of supernatant, and re-suspending the biomass by diluting with DI water to a total volume of 14 mL. The procedure was repeated 4 times and, at the end of the fourth cycle, cells were concentrated in 2 mL. Secondly, biomass digestion was carried out by mixing

2 mL of reagent (1) with the concentrated biomass samples, autoclaving the solution for 30 min at 121°C, and allowing to rest in the autoclave overnight. We checked that increasing autoclaving time to 45 and to 60 min did not change the digestion efficiency. Thirdly, total nitrate was determined by mixing 300 µL of digested sample and 400 µL of reagent (3), vortexing, and incubating at room temperature for 20 min. Then, 5.7 mL of reagent (4) was added to the solution. Optical density was read at 410 nm after loading 350 µL on a 96 well plate (EnSpire®). For each sample, total nitrogen concentration was calculated based on a linear regression from a 7-point calibration curve, made daily from potassium nitrate stock ($R^2 >$ 0.99). A second 7-point calibration curve made daily from organic glycine and served as positive control for the persulfate oxidation method.

Statistical analysis

A multiple linear regression was carried out to examine daily changes in cellular internal nitrogen as a function of 5 continuous explanatory variables of per-cell red fluorescence, per-cell forward and side light scatters, medium N concentration, population size, and 2 categorical explanatory variables of the two experimental initial conditions and the four species. To ensure linearity, red fluorescence, forward light scatter, side light scatter, and population size were natural log-transformed, while medium N concentration was square root transformed. To satisfy the assumptions of generalized linear models, we avoided biases due to multicollinearity between main effects by setting a cut off variance inflation factor value of 5 (Zuur *et al.* 2009). In the data, all dynamics transitioned from states of high nitrogen-low population size to zero nitrogen-high population size; as a result, the variables for medium nitrogen and population size were highly

negatively correlated (variance inflation factor of 12) and could not both be included as explanatory variables in the same model. However, availability of medium nitrogen was clearly the underlying driver: a decrease in irradiance from increased population size and increased self-shading is expected to increase per-cell red fluorescence, due to higher pigmentation from photoacclimatization (Sosik *et al.* 1989). Conversely, a decrease in medium nitrogen availability should coincide with a decline in cell red fluorescence, due to reduced photosynthetic rate from factors such as reduced N-rich pigments, reduced thylakoid efficiency, decline in photosystem II density, reduction in light-harvesting complex, and a decline in enzymatic activities (Turpin 1991). Because we observed decreasing red fluorescence during the experiments, medium nitrogen is implicated as the driver. Hence, population size was removed from the initial full model and this reduced the maximum variance inflation factor score to 2.7, which was below the assumed cutoff value of 5.

Combinations between the 4 species and 2 initial inoculation densities could produce different interactive effects on optical properties, medium nitrogen, or total cell nitrogen. To account for this, 9 two-way interaction terms were included for all combinations between all continuous variables and the categorical explanatory variables of species and initial population size (also including an interaction term between the two categorical variables). Furthermore, 3 additional interaction terms were included between all combinations of optical properties with each other, to account for likely interactions between physical properties of a cell (e.g. fluctuations in red fluorescence can depend on changes in forward or side light scatters. When designing the initial model, we also considered adding quadratic terms for each of the continuous variables for the initial model. However, none of

the quadratic coefficients for the quadratic terms were significantly different from 0 (with alpha at 0.05) and were therefore omitted from the starting model. Overall, 31 estimated parameters were included in the initial full model, with a total of 89 residual degrees of freedom. Standard diagnostic plots on model residuals were examined to ensure normality (QQ plot), homoscedasticity (standardized residuals vs. fitted values), and absence of influential observations or outliers (Cook's distance < 0.5). Bayesian Information Criterion (BIC; Schwarz 1978) was adopted to determine the best-fitting model from all possible candidates, obtained by removing single or combination of parameters from the initial fully parameterized model. The best fitting model following BIC model selection is the one that minimizes the formula: $-2\times L + 2\times k\times(\ln(n) - \ln(2\pi))$, where L is the maximum likelihood score, k is the total number of calibrated parameters, and n is the sample size. ΔBIC was then calculated by subtracting the BIC score of the best model from all other scores (i.e., the ΔBIC for the best model is 0). In general, models with ΔBIC between 0 and 2 should be considered as having substantial empirical support (Kass & Raftery 1995; Strong *et al.* 1999). Model selection was carried out with the R package *MuMIn* (Barton 2014).

For the best-fitting model selected by BIC, the independent contribution of each explanatory term to the total explained variability was calculated with the hierarchical partitioning method (HPM) by Chevan and Sutherland (1991). The HPM method isolates the unique contribution of each single variable in a multiple regression analysis. For example, the contribution of variable *U* to the total R^2 of a multiple regression including *U*, *V*, *Y*, and *Z* is calculated by evaluating the incremental improvement in total explained variance (R^2_U) when introducing *U* to all possible model configurations, averaged within a certain model size (i.e. first-

order: *V*, *Y*, *Z*; second order: *VZ*, *YZ*, *VY*; third order: *VYZ*). Finally, the unique contribution of *U* to the total R^2 in the multiple regression is calculated by taking the average of the three R_U^2 scores across the first, second, and third orders of model sizes (Gromping 2006). The 95% confidence intervals (CI) for the relative contributions are calculated by ordinary non-parametric bootstrapping of all observations in the dataset (with replacement) 10^4 times and repeating the HPM method for each bootstrapped dataset (Gromping 2006). HPM and bootstrapped CI were calculated with R package *relaimpo* (Gromping 2006; Gromping 2007). Statistical computer software R and RStudio were used for all analyses and graphs (RStudio 2013; R Core Team 2014).

Results and Discussion

This study confirmed the hypothesis that flow cytometeric optical properties could reveal information about nitrogen quota in laboratory batch cultures. Of all the competing models derived from removing single or combinations of parameters from the starting full model, only one fell within the threshold level of $\Delta BIC<2$ (Table 4.1). This best-fitting model explained 90.2% of the changes in cell nitrogen quota as a function of the main effects for all three optical properties (i.e. red fluorescence, forward and side light scatters) and available medium nitrogen (Table 4.1). Model selection did not detect any important main or interactive effects of species (Table 4.1), implying that the effects of the main explanatory variables were consistent across all four species. Similarly, initial population size was not included in the best model (Table 4.1), indicating that any effects of different per-cell medium nitrogen availabilities were implicitly accounted for by optical properties and medium nitrogen. The best-fitting model performed very well across all four

species and for both initial nitrogen conditions (r = 0.87-0.94), showing no evidence of bias (Fig. 4.1). Red fluorescence had the highest explanatory power in the analysis. The total explained variability in the best-fitting model was 90%, but optical parameters of red fluorescence, forward scatter, and side scatter contributed to 88%, and only the remaining 2% was explained by medium nitrogen (Fig. 4.2). Indeed, a linear model including only the two most influential explanatory variables, red fluorescence and side scatter, could explain 87% of the total variability in total cell nitrogen (Fig. 4.3), of which the overwhelming majority (77%) could be explained with a simple linear regression only including red fluorescence (Fig. 4.4). Overall, these results strongly support the hypothesis that optical variables are a potential proxy for nitrogen quota for all four algal species reared in laboratory nitrogen-limited batch culture conditions.

The existence of a relationship between nitrogen quota and cell optical properties is consistent with our understanding of nutrient-limited growth in autotrophic cells. Together with carbon, nitrogen is the element in highest demand during cell division and, when nitrogen is in short supply, cells respond by relocating nitrogen from storage molecules to vital metabolic functions (Dortch *et al.* 1984; Mulholland *et al.* 2008). Hence, low nitrogen status usually coincides with a decline in N-rich pigments, density of internal organelles, and decrease in cell size, which are all related to the optical properties recorded with a flow cytometer: the intensity of the red fluorescence signal is mainly proportional to the total pigment concentration (especially chlorophyll *a*), forward light scatter is a proxy for cell cross-section and cell volume, and side light scatter is proportional to the general internal complexity of the cell (or its granularity; Dubelaar *et al.* 2000). In principle, similar mechanisms should also apply for cells limited by different

nutrients. For instance, positive trends in flow cytometric optical values have been recorded from nutrient-limited cultures resupplied with iron (Zettler *et al.* 1996; Timmermans *et al.* 2001; Davey *et al.* 2008; Liu & Qiu 2012), phosphorous (Cleveland & Perry 1987; Demers, Davis & Cucci 1989), and silicon (Demers *et al.* 1989).

This is the first documentation of flow cytometric optical properties as a quantifiable proxy for cell nitrogen quota in phytoplankton cells. These findings have implications for the way we monitor phytoplankton species. Firstly, optical properties are among the few measurements that can be quantified non-destructively from phytoplankton cells. This circumvents having to indirectly calculate per-cell concentrations by dividing two estimates for total elemental concentration and total population size, which inevitably leads to propagation and compounding of the uncertainty around the overall mean. Secondly, measuring optical properties in field or laboratory samples easily allow filtering out the contributions from all non-autotrophic particles through the intensity of the red fluorescence signal, which is mainly proportional to the concentration of pigments in photosynthetic tissues (Dubelaar *et al.* 2000). Moreover, it is now technologically feasible to measure phytoplankton optical properties from automated monitoring stations (Zhou *et al.* 2012; Thyssen *et al.* 2014). The temporal resolution from such flow-cytometric time series can provide important information about the influence of biotic and abiotic factors on nitrogen quota dynamics.

Introducing a protocol for flow cytometric analysis of nitrogen status can also benefit microalgal biotechnological production systems. Imposing a nitrogen-limited regime to a culture can substantially enhance the production of storage lipids

(e.g. triacylglycerols) and carbohydrates (mainly starch), leading to a significant increase in the specific value of the microalgal biomass (Ikaran *et al.* 2015). Today, conventional analytical methods are often implemented for monitoring and optimizing biomass quality, but with results only available considerable time after each sample is taken (da Silva, Roseiro & Reis 2012). Only recently, flow cytometric systems for continuous culture monitoring of lipid content, cell size, enzyme activity, and identification of microbial species are starting to emerge (da Silva *et al.* 2012; Hyka *et al.* 2013). While not common, such near-instantaneous methods have already produced some improvements in the productivity and the reproducibility of microalgal cultivation processes (de la Jara *et al.* 2003; Gouveia *et al.* 2009; Doan & Obbard 2011). Our approach can complement such applications of flow cytometry, by facilitating rapid assessments of culture nitrogen status.

It is important to quantify the variability of the relationship between optical properties and nitrogen quota across different species. Trends in optical properties mainly depend on the relative composition of different types of pigments within a cell (Sosik *et al.* 1989). Hence, it is likely that taxonomically related species will often show consistent relationships in optical properties. In this study, the calibrated relationship between nitrogen quota and cell optical properties was consistent across three chlorophytes and one charophyte species (BIC selected against species-specific coefficients; see Table 4.1). This means that an increase in internal nitrogen corresponded to the same response in optical properties across all four species. The extent to which this relationship remains consistent across more taxonomically disparate species, however, requires further investigation.

Future research should assess the reliability of optical properties as a proxy for nitrogen quota when extended from laboratory cultures to field samples of mixed assemblages. This requires analyzing the effects of additional covariates, such as the effects of multiple potentially limiting nutrients. Furthermore, cells can photoacclimatize and change their pigment concentrations when exposed to different light intensities (Jacquet *et al.* 1998; Dusenberry, Olson & Chisholm 1999; Collier 2000). Hence, the influence of light irradiance on the relationship between optical properties and nitrogen quota should be calibrated. Finally, optical characteristics also change throughout the diel cycle, usually increasing intensity throughout the light phase (DuRand *et al.* 1998; Mas *et al.* 2008), highlighting the need to standardize for time of sampling. Assessing each individual contribution from these factors can facilitate the comprehensive interpretation of time-series of per-cell optical properties with respect to nitrogen quota from field samples.

The capacity of phytoplankton cells to assimilate and store growth-limiting nutrients has important implications in nature and in engineered systems. Presently available techniques for directly measuring nitrogen quota in phytoplankton cells are difficult, and not feasible for monitoring frequently or over large areas (Shelly *et al.* 2010). The use of optical proxies has already revolutionized the scale and frequency of phytoplankton monitoring. For instance, the MODIS spectroradiometer installed on satellites Terra and Aqua documented, for the first time, patterns of global primary production on ocean surfaces by recording total chlorophyll fluorescence as a proxy for phytoplankton biomass (Bordi, Neeck & Scolese 1999). Today flow cytometers are installed in most oceanographic vessels and can even be designed as automated submersible units for continuous monitoring of natural phytoplankton assemblages or microalgal bioreactors (Yentsch *et al.*

1983; Olson, Shalapyonok & Sosik 2003). The results of the present study indicate that flow cytometeric data does not just indicate total population size, but also has the potential to provide information on nitrogen quota of phytoplankton cells.

Table 4.1: Summary table for the ten best models following Bayesian Information Criterion (BIC) model selection. Rows represent individual models ordered from lowest to highest BIC score. Columns indicate each model term (main effects or interactions that were selected at least once in the top ten models), coefficient of determination (R^2), degree of freedom (*df*), maximum log-likelihood score (*LogLik*), BIC score, ΔBIC, and cumulative weight. Presence for model terms is indicated with either its estimated parameter value for continuous variables or with a "+" sign for categorical variables. Models were judged based on ΔBIC, calculated by subtracting the overall best BIC score from the scores of each model (hence, by definition the ΔBIC of the best model is 0). "Exp." indicates the two initial conditions of starting population densities, "Fwd" is forward light scatter, "Red" is red fluorescence, "Side" is side light scatter, and "MdN" is the available medium nitrogen. Interaction terms between two variables are represented with the column sign (":").

	Model Terms																		
Model #	*(Intercept)*	*Exp.*	*log(Fwd)*	*log(Red)*	*log(Side)*	*Species*	*sqrt(MdN)*	*Exp:log(Side)*	*Exp:sqrt(MdN)*	*log(Fwd):log(Red)*	*log(Fwd):log(Side)*	*log(Fwd):Species*	*log(Red):log(Side)*	*log(Side):Species*	R^2	*df*	*LogLik*	*BIC*	*ΔBIC*	*Cum. Weight*
1	-17.77		0.32	0.90	0.35		0.01								0.90	6	16.38	-4.03	0.00	0.46
2	-18.21		-0.57	1.06	0.32		0.01			0.39					0.90	7	17.46	-1.42	2.61	0.12
3	-17.66	+	0.32	0.86	0.37		0.01								0.90	7	17.15	-0.79	3.23	0.09
4	-17.95			0.96	0.41		0.01								0.89	5	11.97	0.00	4.02	0.06
5	-18.00		0.36	0.98	0.15		0.01						0.07		0.90	7	16.75	0.01	4.04	0.06
6	-17.64	+	0.30	0.83	0.34		0.01	+							0.91	8	18.89	0.52	4.55	0.05
7	-17.74		0.45	0.90	0.37		0.01				0.08				0.90	7	16.42	0.68	4.71	0.04
8	-17.87	+	0.30	0.92	0.34		0.01		+						0.91	8	18.80	0.71	4.73	0.04
9	-19.09	+	0.90	1.23	-0.90	+	0.02		+			+	0.35	+	0.94	18	42.66	0.85	4.88	0.04
10	-17.87	+	0.28	0.89	0.30		0.01	+	+						0.91	9	20.92	1.26	5.28	0.03

Table 4.2: ANOVA table for the best-fitting multiple linear regression on total cell nitrogen following BIC model selection (see model #1 in Table 4.1).

Source (transformation)	*Sum of squares*	*d.f.*	*Mean square*	*F value*	*Prob(F)*
Red fluorescence ($\log_e$)	41.8	1	41.8	899.1	<0.0001
Side Scatter ($\log_e$)	5.6	1	5.6	119.6	<0.0001
Forward Scatter ($\log_e$)	0.5	1	0.5	11.1	<0.0001
Medium N (sqrt)	1.3	1	1.3	28.9	<0.0001
Residuals	5.3	115	0.05		

$F_{4,115} = 265$, Prob (F) < 0.0001; $R^2 = 0.902$, adj. $R^2 = 0.899$

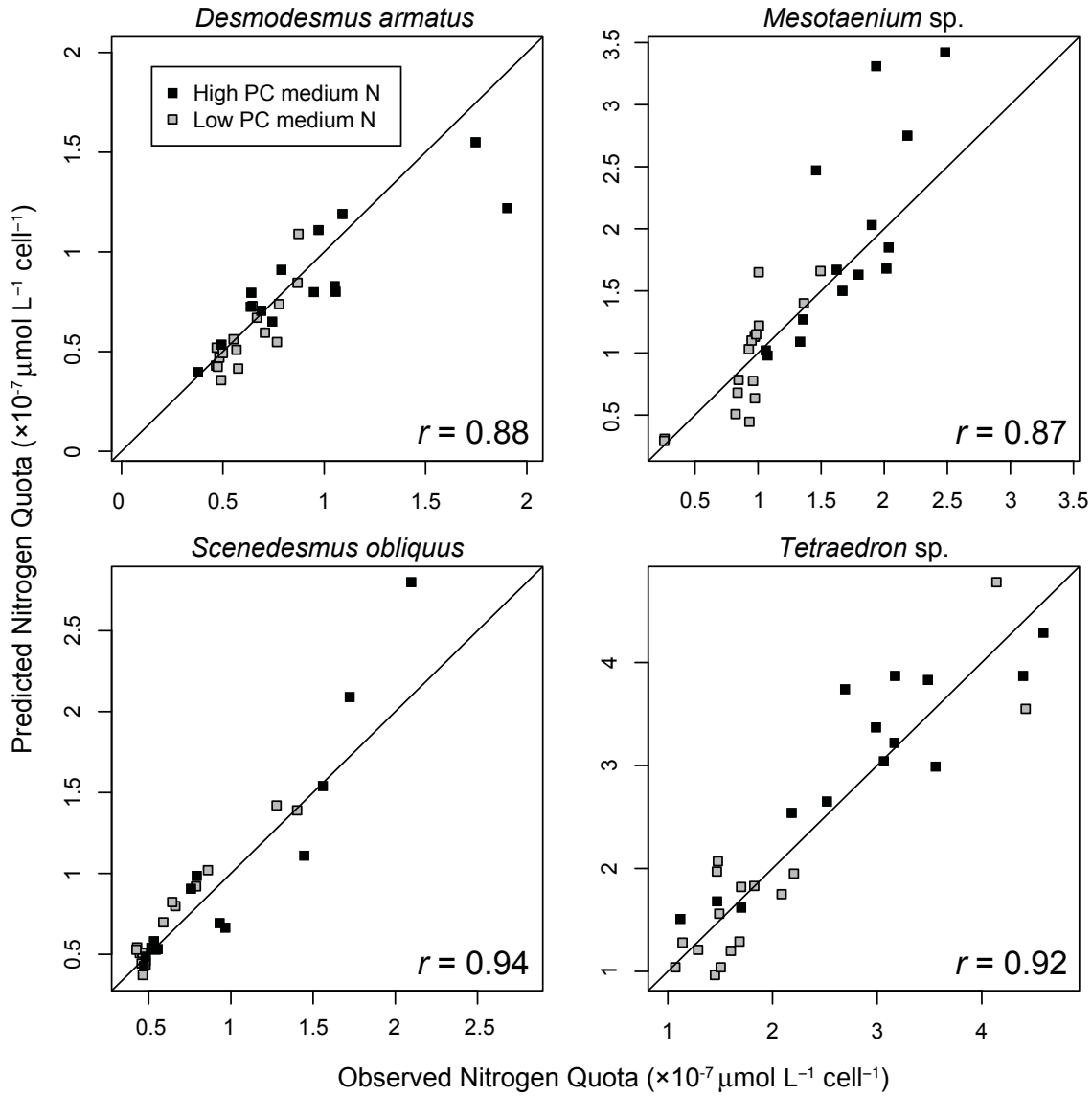

Figure 4.1: Observed and predicted nitrogen quota values extracted from the best-fitting model for each species. Each dot represents an independent culture for each day of the experiment, with different symbols indicating the two different initial per-cell nitrogen availabilities. The correlation coefficient quantifies the goodness of fit for each species pooled across both treatments of initial nitrogen. The diagonal line is the unity line, where observed and predicted values are equal

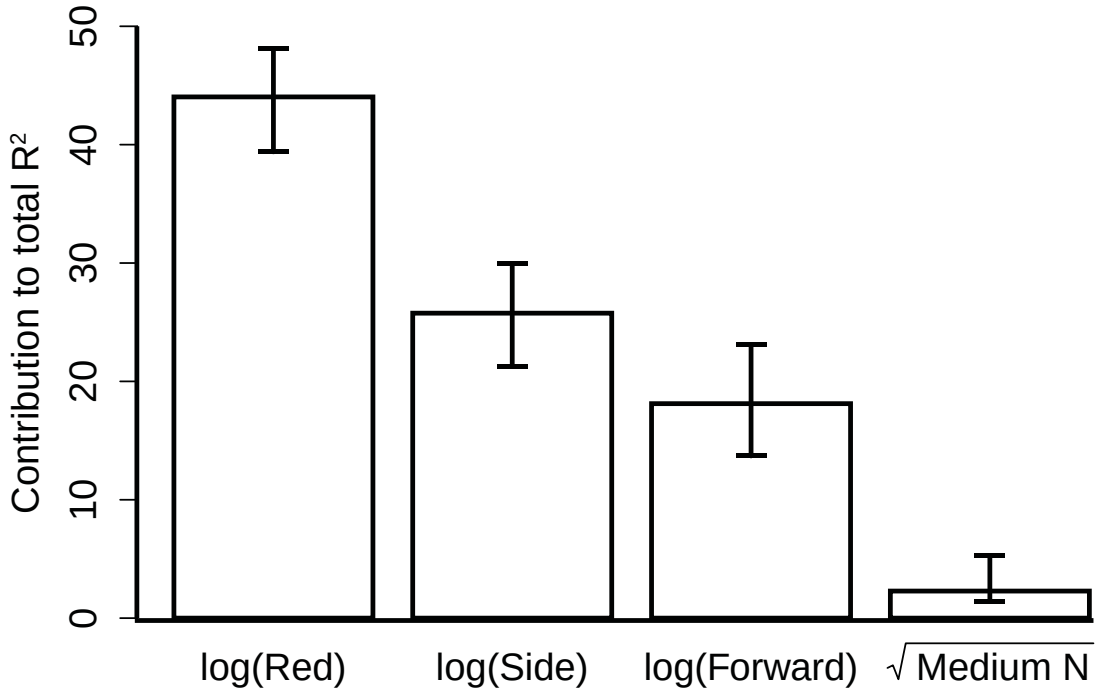

Figure 4.2: The unique contribution of explanatory variables for red fluorescence (“Red”), side light scatter (“Side”), forward light scatter (“Forward”), and medium nitrogen (“Medium N”) to the coefficient of determination (R^2 ± 95% bootstrapped confidence intervals) of the multiple regression model (see Table 4.1), as calculated by the hierarchical partitioning method (HPM). Total model explained variability (i.e. sum of the four unique contributions) was 90%

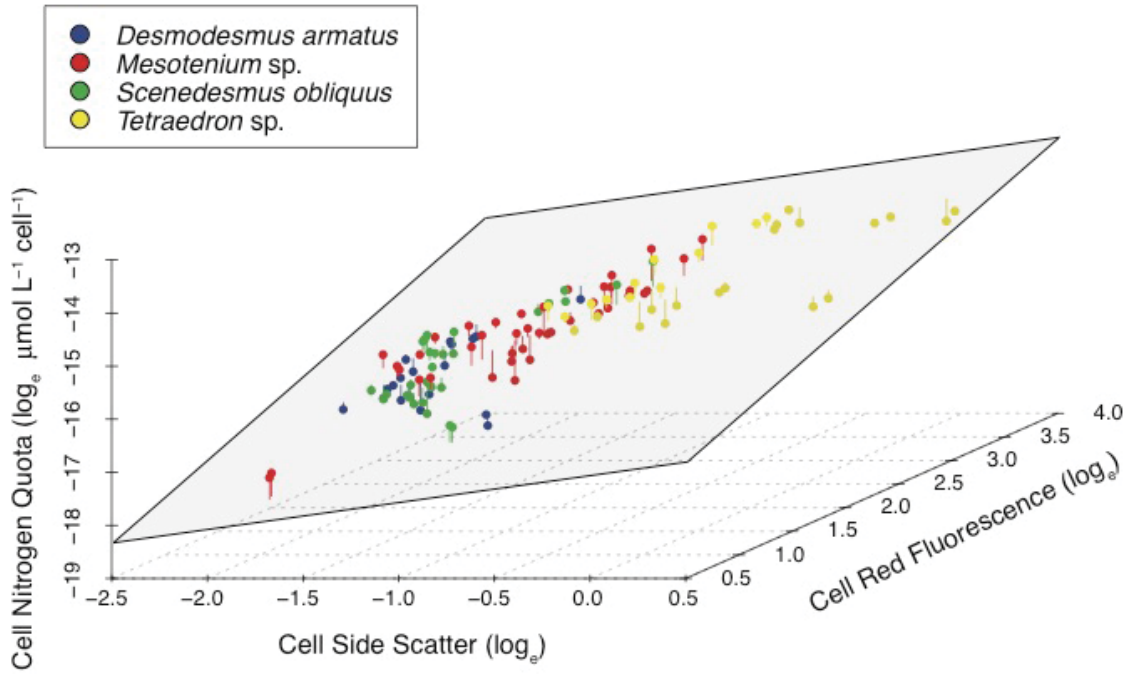

Figure 4.3: Multiple linear regression for total cell nitrogen as a function of the two most important model explanatory variables: flow cytometric red fluorescence and side scatter (see Table 4.1 and Fig. 4.2). Optical values are in relative units and normalized by mean optical values of the flow cytometric beads. Each point is a daily measurement at 18:00 collected from a factorial design of two independent replicate cultures for four species for two initial cell densities (R^2 = 0.868). Points and perpendicular residuals to the prediction plane are color-coded for the four different species

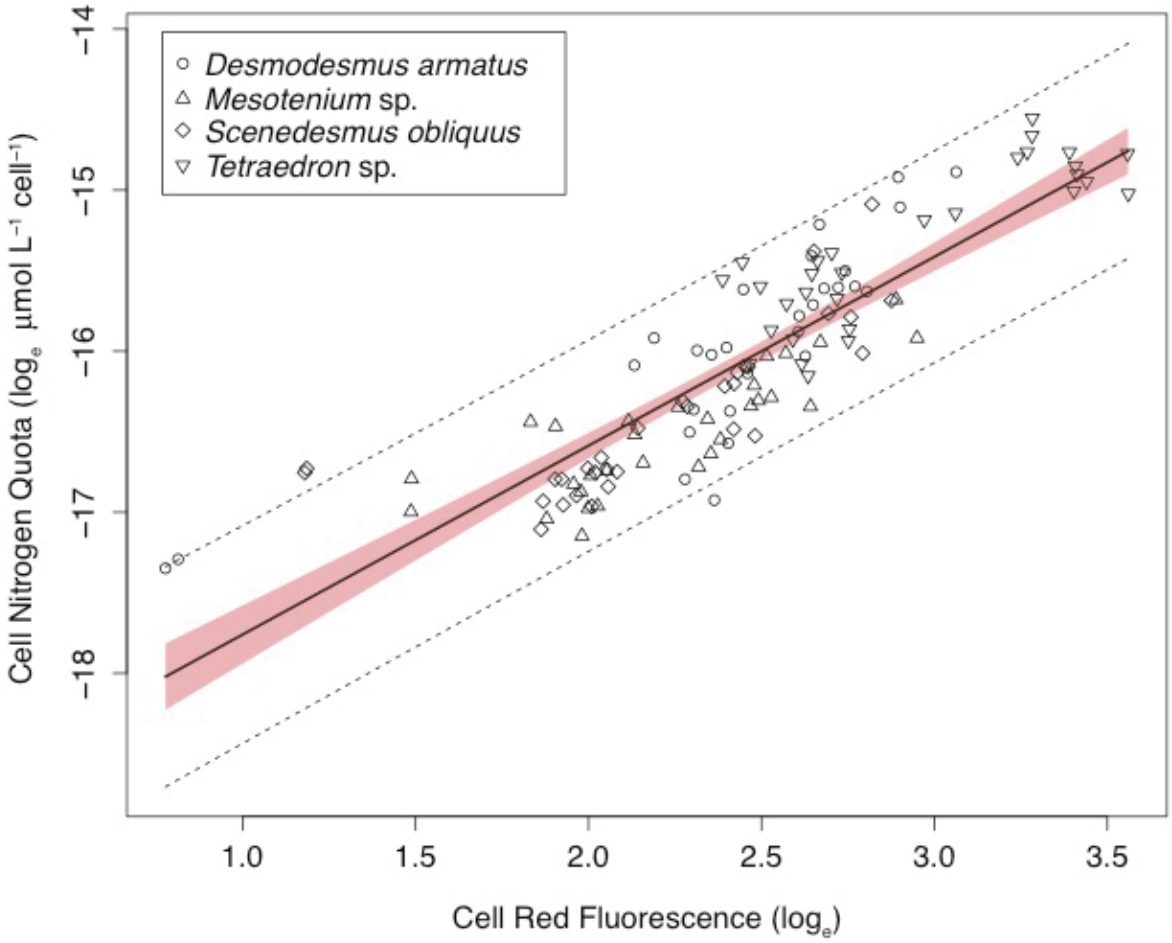

Figure 4.4: Linear regression for total cell nitrogen as a function of red fluorescence with 95% confidence intervals (red envelop) and 95% projection intervals (dashed lines). Optical values are in relative units and are normalized by mean optical values of flow cytometric beads. Each point is a daily measurement of a species at 18:00 from two independent replicate cultures at two initial cell densities ($R^2 = 0.77$).

Chapter 5: Improving dynamic phytoplankton reserve-utilization models with an indirect proxy for internal nitrogen.

Introduction

Proxy variables are commonly used in ecology as a way to quantify processes that would otherwise be difficult or impossible to monitor directly (Caro 2010; Lindenmayer, Barton & Pierson 2015). For instance, indirect proxies can facilitate mapping ecosystem services over large scales (Eigenbrod et al. 2010; Stephens et al. 2015). This is especially true for vegetation maps: It is now common in ecology to use observations from remote sensors onboard of satellites as an indirect optical proxies for different canopy attributes (e.g. net primary production, plant biomass, photosynthetically active radiations) to overcome many long-standing monitoring challenges, for example evaluation of impervious regions, such as Arctic and Antarctic (Santin-Janin et al. 2009; Epstein et al. 2012), or fragmented and isolated areas (Pereira Coltri *et al.* 2013; Li *et al.* 2014b), or very extended territories (Son *et al.* 2014; Stephens *et al.* 2015). Anther use of indirect proxies in ecology is to quantify the overall performance of a species. For instance, trait-based approaches use different types of measurable ecophysiological and life-history traits (e.g. growth, body mass, fecundity) as a proxy of the ecological capabilities of a species (e.g. competitive ability) and about complex processes at higher organizational levels (e.g. community structure, ecosystem functioning, energy flow: McGill *et al.* 2006; Violle *et al.* 2007). For example, the colony shape of a coral species is a

proxy for its susceptibility to mortality from physical dislodgment (Madin *et al.* 2014). Proxies can also be used to quantify the condition of an individual organism. For instance, the size of the liver and its lipid concentration is a good proxy for the health of a fish (Dempster *et al.* 2011). Also, whole-organism oxygen consumption rate is a traditional proxy for metabolic activity or energy consumption (Brown *et al.* 2004; Salin *et al.* 2015) and various biochemical indices have been used as proxies for specific growth rate and overall activity of an organism (Runge & Roff 2000; Holmborn *et al.* 2009). Hence, indirect proxies serve different purposes in ecology across different scales, ranging from biomes, to species, to individuals.

The use of indirect proxies is particularly important when studying organisms that are difficult to measure directly, such as phytoplankton. The productivity of phytoplankton populations is critical to sustain life on the planet and their rate of cell division is often regulated by the availability of inorganic nutrients to a cell. However, phytoplankton cells are also adapted to store nutrients to support growth in periods of low nutrient availability (Caperon *et al.* 1972; Droop 1973; Droop 1983), which complicates the analysis of nutrient utilization and population dynamics. Quota models are the most successful representation of phytoplankton nutrient utilization to date, because of their ability to incorporate internal nutrient storage within single cells that can temporarily support cell division even in the absence of sufficient external nutrients (Droop 1973; Leadbeater 2006; Pahlow *et al.* 2013). The key assumption of Quota models is largely biologically justified: phytoplankton cells are adapted to respond to nutrient-limited conditions by relocating resources from storage molecules (e.g. lipids, carbohydrates, pigments, RNA) to vital metabolic functions (e.g. cell division; Dortch *et al.* 1984). However, analyzing phytoplankton nutrient utilization by fitting Quota models to data also

requires monitoring the internal nutrient status of a cell, which is the most stringent limitation to this modeling technique. Estimating nutrient concentrations within phytoplankton cells is technically complicated, costly, destructive, and time-consuming (Sattayatewa, Arnaldos & Pagilla 2011; American Public Health Association 2012). For instance, a performance study of this technique reviewing 55 laboratories revealed that around half of the participating laboratories produced inconsistent results, and the coefficient of variation among the reliable laboratories was up to 20% for nitrogen and 60% for phosphorous concentrations (Aminot, Kirkwood & Carlberg 1997). Alternatively, Quota models can be fitted to data even when internal quota are not directly monitored (Ducobu *et al.* 1998; Malerba *et al.* 2012; Malerba *et al.* 2015). This is possible because the dynamics of internal nutrients in closed systems can sometimes be inferred from population densities and ambient nutrient depletion (Brand 1991; Fujimoto *et al.* 1997; De La Rocha *et al.* 2010). However, this approach is limited to highly controlled laboratory settings and it generally requires more data and more complex experimental designs. Hence, overcoming the limitations involved with direct measurements of cell internal nutrients could substantially enhance our ability to understand and predict dynamics of phytoplankton populations.

A recent study by Malerba *et al.* (2016) proposed a new way to fit Quota models to phytoplankton population dynamics, by using cell optical properties as an indirect proxy for internal nitrogen status. Nitrogen status is known to alter many physiological and morphological aspects of a cell (e.g. cell volume, cell roundness, pigment composition, quantities of internal organelles, concentrations of storage molecules; Vanucci *et al.* 2010; Adams *et al.* 2013). Flow cytometric optical analysis provides a means to directly quantify these anatomical and physiological

changes that are intrinsically linked to the nitrogen quota of a single cell (Collier 2000; Dubelaar *et al.* 2000; Veldhuis *et al.* 2000). In particular, flow cytometric red fluorescence from four phytoplankton species grown in nitrogen-limited batch cultures explained 77% of the variability in per-cell internal nitrogen, across species and a range of initial nutrient concentrations (Malerba *et al.* 2016). Monitoring red fluorescence emission from phytoplankton cells has many practical advantages: it is instantaneous, non-destructive, precise, non-biased by inorganic particles, feasible to monitor automatically, and often routinely measured as part of the protocol for estimating total population densities (Collier 2000; Dubelaar *et al.* 2000; Veldhuis *et al.* 2000). However, inferring a state variable from an indirect proxy also requires accounting for an additional source of error, due to the use of a calibration curve to convert between a variable and its proxy. Hence, while incorporating red fluorescence as a proxy for cell nitrogen quota could extend the utilization of Quota models, it is unknown how the added uncertainty of using a calibration curve could affect parameter identifiability, precision, and accuracy when fitting Quota models to phytoplankton time-series.

The aim of the present study was to evaluate the use of flow cytometric red fluorescence in Quota models as a proxy for internal nutrient status. To this end, we conducted two different analytical approaches. In the first analysis, we generated data by simulation, so that the three models could be compared using mean squared error (MSE) from the difference between the estimated parameter values and the known, true parameter values used to generate the data. Phytoplankton allometric relationships were used to generate parameter values from a phytoplankton community spanning several orders of magnitude in cell size. In the second analysis, we used the data collected in chapter 4 from laboratory cultures of four

green algal species (i.e. *Desmodesmus armatus*, *Mesotaenium* sp., *Scenedesmus obliquus*, and *Tetraedron* sp.), each started at two initial conditions. This study illustrates the usefulness of incorporating red fluorescence as a proxy for cell nitrogen quota to improve the applicability and performance of phytoplankton models. This study illustrates the usefulness of incorporating red fluorescence as a proxy for cell nitrogen quota to improve the applicability and performance of phytoplankton models.

Material and Methods

Model development

In this study we derived three forms of Quota models: the "Nitrogen-Quota" model, "Virtual-Quota" model, and the "Fluorescence-Quota" model. The three different models were derived from the original Quota model by Droop (1973), as:

$$\frac{dN}{dt} = -f\big(N(t)\big)\times B(t) \qquad \text{(eq. 5.1 a)}$$

$$\frac{dQ}{dt} = f\big(N(t)\big) - g\big(Q(t)\big)\times Q(t) \qquad \text{(eq. 5.1 b)}$$

$$\frac{dB}{dt} = g\big(Q(t)\big)\times B(t) \qquad \text{(eq. 5.1 c)}$$

where $N(t)$, $Q(t)$, and $B(t)$ indicate ambient nitrogen, per-cell internal nitrogen quota, and population density, respectively. Functional responses $f(N(t))$ and $g(Q(t))$ describe the per-cell uptake rate and growth rate as a function of external and internal nitrogen, and are represented with two saturating functional responses:

$$f\big(N(t)\big) = v_{max}\times\frac{N(t)}{N(t)+k} \qquad \text{(eq. 5.2 a)}$$

$$g\big(Q(t)\big) = \mu_{max} \times \left(1 - \frac{Q_{min}}{Q(t)}\right) \qquad \text{(eq. 5.2 b)}$$

where v_{max} is per-capita maximum uptake rate, k is the Michaelis-Menten half-saturation constant, μ_{max} is specific growth rate of a cell at infinite nitrogen quota, and Q_{min} is the threshold internal nitrogen concentration at which no cell division occurs.

All three models include the state variable $Q(t)$, as the nitrogen quota within a single phytoplankton cell, but differ in the way the model is calibrated to the data. The nitrogen-quota model calibrates the dynamics for $Q(t)$ to direct measurements of per-cell internal nitrogen, as:

$$Q_{obs}(t) = c \times Q(t) \qquad \text{(eq. 5.3)}$$

where $Q_{obs}(t)$ is the observed nitrogen quota within a single cell, and *c* is a positive constant accounting for bias associated with laboratory protocols when recording total cell nitrogen in phytoplankton cultures. Directly estimating cell quota has two sources of bias. Firstly, the precision of measuring the elemental composition within a cell depends on the type of chemical bonds within the molecules (e.g. nitrogen atoms connected by double bonds within molecules yield very poor recovery rate with most traditional protocols; Aminot *et al.* 1997; Raimbault *et al.* 1999b). Secondly, field and laboratory samples often present variable loads of dead cells and nutrient-rich inorganic particles in solution, which contribute to the overall reading and overestimate cell quota in living cells (Shelly *et al.* 2010). Hence, the parameter *c* represents underestimated $Q_{obs}(t)$ due to partial N recovery associated with experimental protocol (c<1), or overestimated $Q_{obs}(t)$ due to nitrogen recovered from dead cells and suspended inorganic particles within the sample

(c>1). Bias of up to 50% has been reported with organic nitrogen standards (Nydahl 1978; Langner & Hendrix 1982; Raimbault & Slawyk 1991; Raimbault *et al.* 1999b), so in each simulated dataset c was generated from a uniform distribution ranging between 0.5 and 1.5. The reason for assuming an uninformative prior distribution is because in this way the parameter c will have more flexibility to explore the range of potential values between upward and downward biases of 50%.

The uninformative prior distribution assumed for this parameter was c to explore the entire range of values. The case with no bias in $Q_{obs}(t)$ was also explored, by repeating the analysis with c fixed at 1 (see *Testing Robustness* in Results section).

The fluorescence-quota model derives $Q(t)$ from the red fluorescence signal emitted by a cell. Previously, Marra, Bidigare and Dickey (1990) showed the utility of using red fluorescence as a proxy for internal nutrient status in phytoplankton Quota models. We build on this idea by considering flow cytometric red fluorescence measured from individual cells, instead of total red fluorescence from a volume of water. In this way, the recorded value of red fluorescence signal is determined only by properties of individual cells, without the need to standardize by total population density within the culture (which would introduce additional measurement error). The relationship between $Q(t)$ and per-cell fluorescence intensity was assumed to follow the same power-law functional response documented in Malerba *et al.* (2016):

$$Q(t) = a \times F(t)^b \qquad \text{(eq. 5.4)}$$

which can be rearranged as:

$$F(t) = \left(\frac{Q(t)}{a}\right)^{\frac{1}{b}} \qquad \text{(eq. 5.5)}$$

where $F(t)$ indicates the strength of the red fluorescence signal, and *a* and *b* are shape parameters.

Finally, the virtual-quota model uses only observations of phytoplankton population size and external nitrate and ammonium concentrations, and infers changes in internal nitrogen $Q(t)$ from the fitted parameter values. This approach to infer $Q(t)$ is equivalent to Ducobu *et al.* (1998), Malerba *et al.* (2012), and Malerba *et al.* (2015). Hence, the total number of estimated parameters changes between the three models: the virtual-quota model has 4 parameters, while the nitrogen-quota model and fluorescence-quota model have 1 (i.e. *c* from eq. 5.3) and 2 (i.e. *a* and *b* from eq. 5.5) additional parameters, respectively.

Approach 1: Simulation-based analysis

Data simulations

The nitrogen-quota, the virtual-quota, and the fluorescence-quota models were compared by fitting each model to 100 simulated datasets. In this way, model performance could be calculated from the average distance between the parameter values used to generate the data ("true" parameters) and the model estimates calibrated from the same data (estimated parameters). Each simulation was generated following these steps: (1) choose a set of demographic parameters, (2) use stochastic simulations to generate trajectories for external nitrogen, cell nitrogen quota, population density, and red fluorescence, and (3) generate trajectories of the corresponding observations of these state variables incorporating the measurement

error for each state variable. Here we describe each step in more detail (please refer to Appendix B Chapter 5 for a graphical summary of each step in the analytical methods).

The first step consisted of generating the demographic parameters for a hypothetical phytoplankton species sampled from a phytoplankton community. To do that, a cell volume was selected from a uniform distribution on $\log_{10}$-scale from 10^2 to 10^5 μm^3, which is the approximate range reported in Edwards *et al.* (2012) for freshwater phytoplankton species. Then, the allometric relationships in Edwards *et al.* (2012) were used to associate the sampled cell volume to expected values for maximum nitrogen uptake (v_{max}), half-saturation rate (k), maximum theoretical growth rate (μ_{max}), and minimum nitrogen quota (Q_{min}; see Table S5.1 in Appendix A Chapter 5, and Appendix B Chapter 5). Also, to account for between-species variation around the four allometric relationships in Edwards *et al.* (2012), a residual was extracted from the error distribution of each linear regression and added to the expected parameter values (Table S5.1 in Appendix A Chapter 5).

The second step consisted in simulating the true dynamics of the system. We did that by using eq. 5.1 a-c, with the demographic parameters determined in the first step, to calculate time-series for external nitrogen ($N(t)$), population density ($B(t)$), internal nitrogen ($Q(t)$), and red fluorescence ($F(t)$). Trajectories for the red fluorescence emission (i.e. $F(t)$) of a cell were calculated based on changes in its internal nitrogen status ($Q(t)$) using eq. 5.5. The values for a and b were drawn from a bivariate uncertainty distribution from calibration of this relationship using empirical data from four phytoplankton species (Malerba *et al.* 2016). Log-normally distributed process noise was added to each of the state variables to represent the

unexplained variation due to natural stochasticity in the dynamics (Hilborn *et al.* 1997; Bolker 2008). The magnitudes of process noise were estimated from calibrating eq. 5.1 a-c to empirical data (Malerba *et al.* 2016). Each time-series was simulated for 100 days, to ensure narrow confidence intervals for all estimated parameters. The initial concentration for external nitrogen was standardized as ten times the half-saturation constant (i.e. $10\times k$) of the species. The initial population density was calculated so that medium nitrogen would become limiting half way through the time-series (i.e. between day 40 and 60). In this way, available nutrients transitioned from N-rich, to N-limited, to N-absent conditions, and growth rates transitioned from fast to zero. Finally, initial per-capita internal nitrogen was randomly selected from a uniform distribution between nitrogen deplete (i.e. $Q(t_o) = Q_{min}$) and nitrogen replete (i.e. $Q(t_o) = 10\times Q_{min}$).

The third step consisted in adding observation error to the true system dynamics calculated in step 2. Observation error was added to the dynamics of ambient nitrogen ($N(t)$), observed internal quota ($Q_{obs}(t)$), population density ($B(t)$), and red fluorescence ($F(t)$). The magnitudes of observation error were calculated from the standard deviations of the triplicate independent readings from empirical data in Malerba *et al.* (2016), which offers an independent estimate for the size of the measurement error for each state variable. They were all assumed to follow a log-normal distribution, except for medium nitrogen, which was assumed to be normally distributed based on previous work (Malerba *et al.* 2016). Time-series for observed internal quota ($Q_{obs}(t)$) were further modified to account for bias by using eq. 5.3 with a value for c sampled from a uniform distribution between 0.5 and 1.5.

Model calibration to simulated data

All three models were calibrated to 100 simulated datasets. The nitrogen-quota model was calibrated to trajectories of external nitrogen (N(t)), population density (B(t)), and observed internal quota (Q_{obs}(t)), with internal quota (Q(t)) estimated from eq. 5.3. The virtual-quota model was calibrated only to external nitrogen (N(t)) and population density (B(t)), with internal quota (Q(t)) inferred from changes in N(t) and B(t). The fluorescence-quota model was calibrated to external nitrogen (N(t)), population density (B(t)), and red fluorescence ($F(t)$), with internal quota (Q(t)) estimated from $F(t)$, using eq. 5.5.

State-space statistical estimation techniques were used to fit each model to each of the 100 datasets. State-space models allow estimating model parameters by simultaneously accounting for both process noise and observation error (Bolker 2008; Pedersen *et al.* 2011). The underlying idea behind this modeling technique is that observation error and process noise affect the variability around the model in different ways: the variability caused by observation error will remain constant through time, while the influence of process noise will compound over time. Mathematically this corresponds to:

$$Y_{t+1}^{true} = f(Y_t^{true}) + \varepsilon \qquad \text{(eq. 5.6 a)}$$

$$Y_{t+1}^{obs} = Y_{t+1}^{true} + \tau \qquad \text{(eq. 5.6 b)}$$

where ε represents the log-normally distributed process noise, τ represents the normally distributed observation error, Y_t^{true} and Y_{t+1}^{true} are the true states of the system at times t and t+1, and Y_{t+1}^{obs} is the measured state of the system at time t+1 (see Appendix B Chapter 5 for more details).

Sampling from the posterior distribution using Bayesian Markov-Chain Monte Carlo (MCMC) is a particularly suitable method to fit state-space models accounting for observation error and process noise. Each dataset was sampled 10^5 times with Gibbs sampler, following 50000 iterations for adapting the chains and 50000 for burn in, using software JAGS and R with package *rjags* (Plummer 2003; R Core Team 2014; Plummer 2015). To monitor for successful convergence, we visually inspected the iterated history, density plot, and correlation diagram of each chain in each model. Also, we graphically inspect the overlapping posterior distribution between the whole chain and the last 10%, and ensured Geweke z-scores between -2 and 2 (Geweke 1992). Chains were extended if they failed to meet convergence criteria. Software R was used with packages *coda* and *ggmcmc* for statistical analyses and plots (Plummer *et al.* 2006; Marín 2015).

The performance of each model to estimate maximum nitrogen uptake (v_{max}), half-saturation rate (k), maximum specific growth rate (μ_{max}), and minimum nitrogen quota (Q_{min}) was evaluated using mean squared error (MSE), as:

$$mean\left[\left(\hat{\theta} - \theta_{true}\right)^2\right] \quad \text{(eq. 5.7)}$$

where θ_{true} is the parameter value used to simulate the dataset, and $\hat{\theta}$ is the value of the parameter estimated from the same dataset.

Approach 2: Testing the models with real data

Data from chapter 4 were used to test the model with laboratory data. Refer to material and methods in chapter 4 for a detailed description of the experimental methods. Briefly, four green algal species (i.e. *Desmodesmus armatus*, *Mesotaenium* sp., *Scenedesmus obliquus*, and *Tetraedron* sp.) were reared in batch

culture conditions under two different initial conditions of medium nitrogen and initial population density. Triplicate readings for population density, medium nitrogen, cell internal nitrogen quota, and cell red fluorescence were collected daily at 18:00, in order to control for any diurnal fluctuations.

Model calibration to laboratory time-series

Each model was calibrated to each time-series collected in chapter 4. The Nitrogen Quota model was calibrated using observations for the internal nitrogen quota (Q_{obs}(t)), as well as medium nitrogen (N(t)) and population density (B(t)). The Red Quota mode was calibrated to data for red fluorescence (R(t)), medium nitrogen (N(t)), and population density (B(t)). Finally, the Virtual Quota model was calibrated to data for medium nitrogen (N(t)) and population density (B(t)). The models were calibrated using the same techniques for the simulated datasets (see section "Model calibration for simulated data"). However, there were not enough observations in the time-series to simultaneously account for the effects of both process noise and observation error. Therefore, we simplified the analysis by assuming that the residuals in the data were only due to observation error. This assumption is more reasonable than assuming process noise-only, because protocols to monitor per-cell internal nitrogen quota are complex and often suffer from lack of precision.

In contrast to simulated data, it is not possible to calculate an MSE for model parameters for laboratory data, as the "true" parameter values (θ_{true} in eq. 5.7) are unknown. Instead, we assumed that the observations for the internal nitrogen quota represent the "true" dynamics of the internal quota and we tested the ability of each model to fit the observed dynamics. For each calibrated model, we used the

coefficient of determination (R^2) between the observed quota and the model-inferred quota as the index for the goodness-of-fit of the model. We calculated the R2 of the model integrated over the posterior distribution of the parameters. In this way, we could evaluate both the accuracy (mean R2 value) and the precision (variability around the R2 coefficient).

Note that the above approach is biased in favor of the Nitrogen Quota model: the observations on internal quota are used for both calibrating the parameters and for evaluating the performance of the model. This is not the case for the Red Quota and Virtual Quota models, as the data on internal quota dynamics are not used for their calibrations.

Results

Simulated data

The relationship between the simulated data for red fluorescence ($F(t)$) and observed internal quota ($Q_{obs}(t)$) recorded a mean R^2 of 0.9, which is 15% higher than the corresponding coefficient from empirical data (Malerba *et al.* 2016). This indicates that a fraction of the observation error in $F(t)$, $Q_{obs}(t)$, or both, was not included in the standard deviations calculated from triplicate independent readings of the samples in Malerba *et al.* (2016). Therefore, it was necessary to simulate time-series of $F(t)$ and Q_{obs} (t) with an increased observation error estimate (note that process noise does not contribute to the precision of this relationship). To be conservative, we added equal proportions of observation error to $F(t)$ and Q(t) until

the empirically detected R^2 of 0.77 in Malerba *et al.* (2016) was reflected in the simulated data.

Analysis

The virtual-quota model performed substantially worse than either the fluorescence-quota or the nitrogen-quota models. The mean squared error of the four parameters estimated with the virtual-quota model (MSE_{virt}) were between 2 to 4 orders of magnitude higher than the error for the nitrogen-quota (MSE_{nitr}) and fluorescence-quota (MSE_{flu}) models (Fig. 5.1). The accuracy of the nitrogen-quota model was intermediate, performing consistently better than the virtual-quota model across all parameters (Fig. 5.1). Specifically, the MSE_{virt} for maximum uptake rate (v_{max}), half-saturation constant (k), and minimum quota (Q_{min}) was 2 and 4 orders of magnitude higher than MSE_{nitr} and MSE_{flu} , respectively, while maximum growth rate (μ_{max}) differed by 1 and 2 orders of magnitude, respectively (Fig. 5.1). Hence, inferring internal nitrogen dynamics from external nitrogen depletion and population density (i.e. virtual-quota model) led to less accuracy and less precision compared to including measurements of internal nitrogen or of red fluorescence.

The fluorescence-quota model showed better performance compared to the nitrogen-quota model in nearly all cases, but the difference between the two models depended on the parameter and on the cell size used to simulate the data (Fig. 5.2). For small cell sizes, the MSE_{flu} of all parameters was 2-3 orders of magnitude smaller than the MSE_{nitr} (Fig. 5.2). For large cell sizes, the differences in orders of magnitude were substantially reduced, between 0.5 and 1.5 for maximum uptake rate (v_{max}) and minimum quota (Q_{min}), and the two models performed equally for half-saturation constant (k ; Fig. 5.2 A-C). Finally, the maximum growth rate (μ_{max})

was better estimated by fluorescence-quota model compared to nitrogen-quota model, by between 2 and 3 orders of magnitude, and this difference was independent of the cell size (Fig. 5.2 D). In conclusion, the fluorescence-quota consistently outperformed the nitrogen-quota model, especially for small cell sizes.

The reason for an effect of cell size on the relative performance of fluorescence-quota and nitrogen-quota models is because small cells are more likely to reach stationarity at the end of the simulations, compared to larger cells. The onset of N-limitation, standardized in this study to occur half-way through the simulated dataset, leads to a gradual transition toward an equilibrium state of the system (i.e. absence of medium nitrogen, and constant levels of internal nitrogen and biomass). Larger cells have higher capacity to maintain cell division in the absence of external nutrients. Therefore, the high internal N storage in large cells leads to a slower transition toward steady-state conditions compared to small cells. This means that a dataset of 100 observations for a large cell is more likely to include less information about the carrying capacity of the system, and this leads to lower precision in the demographic parameters for the species. Differently to the nitrogen-quota model, the necessity of the fluorescence-quota model to calibrate a relationship between two different quantities (i.e. red fluorescence and internal N quota) makes this model more susceptible to limited information on steady-state conditions in the data. Indeed, excluding the datasets with population trajectories not stabilizing at carrying capacity removed the negative effect of cell size on model relative performance (data not shown).

Testing Robustness

The analysis was repeated by modifying the effect of the parameter *c*, quantifying the magnitude of bias when measuring $Q_{obs}(t)$ from $Q(t)$. Repeating the analysis with no bias in $Q_{obs}(t)$ (i.e. fixing c=1) produced virtually identical conclusions to the main analysis (data not shown). Hence, the bias-effect of the parameter *c* did not influence the overall performance of the nitrogen-quota model.

Laboratory data

All three models fit time-series for medium nitrogen and population density very accurately (most R^2 higher than 0.8; see Fig. S5.1-5.4 in Appendix C). The mean goodness-of-fit between model-inferred quota dynamics and observations on internal nitrogen was highest in the Nitrogen Quota model (R^2 = 0.55), followed by the Red Quota model (R^2 = 0.47) and the Virtual Quota model (R^2 = 0.32; horizontal bars in Fig. 5.3). Moreover, all R^2 coefficients for the Virtual Quota model presented higher uncertainty compared to the Nitrogen Quota and the Red Quota models (Fig. 5.3). These results further validate the use of red fluorescence as a proxy for internal nitrogen within Quota models.

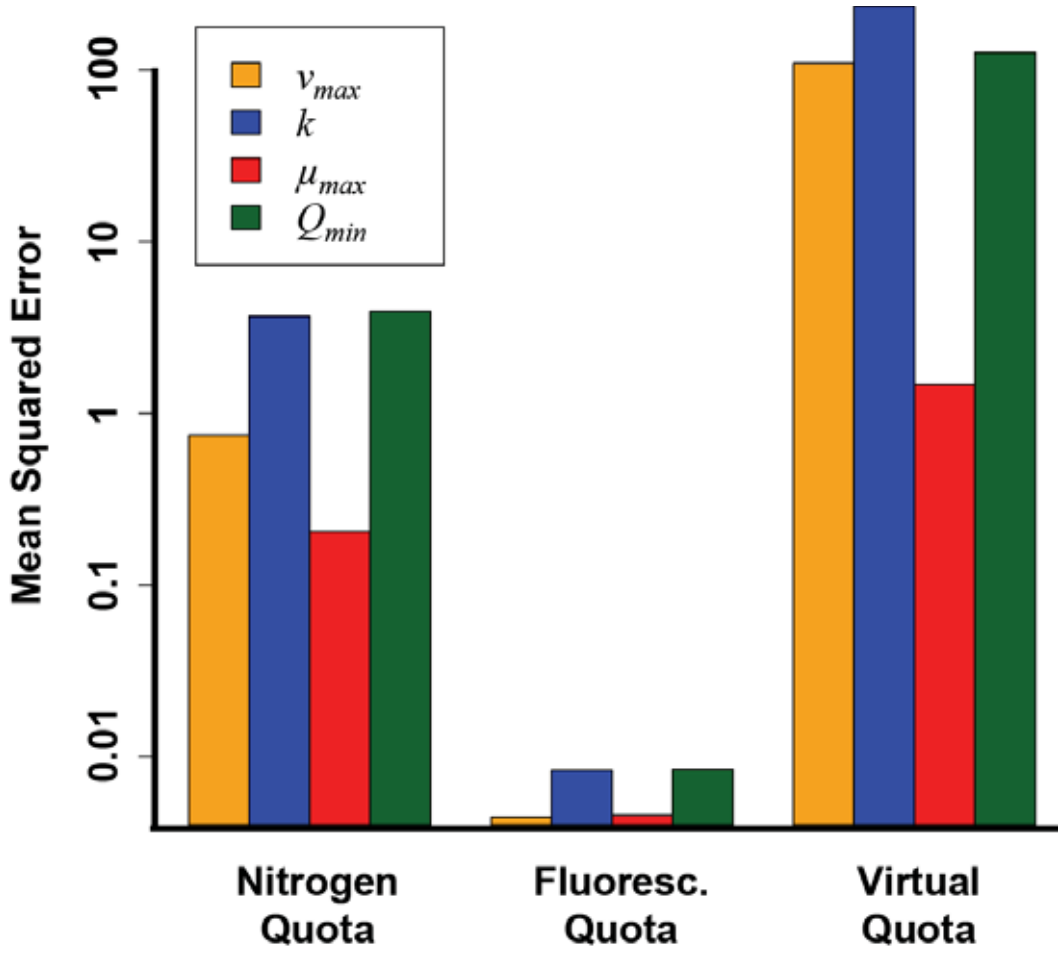

Figure 5.1: Mean Squared Error, calculated as $mean\left[\left(\hat{\theta}-\theta_{true}\right)^2\right]$, where θ_{true} is the value used to generate the data and $\hat{\theta}$ is the value estimated from the data, associated with v_{max}, k, μ_{max}, *and* Q_{min} calibrated with the three alternative models. Colors indicate equivalent parameters calibrated with different models. The total error for each parameter was calculated by summing up results from 100 calibrated datasets for each model.

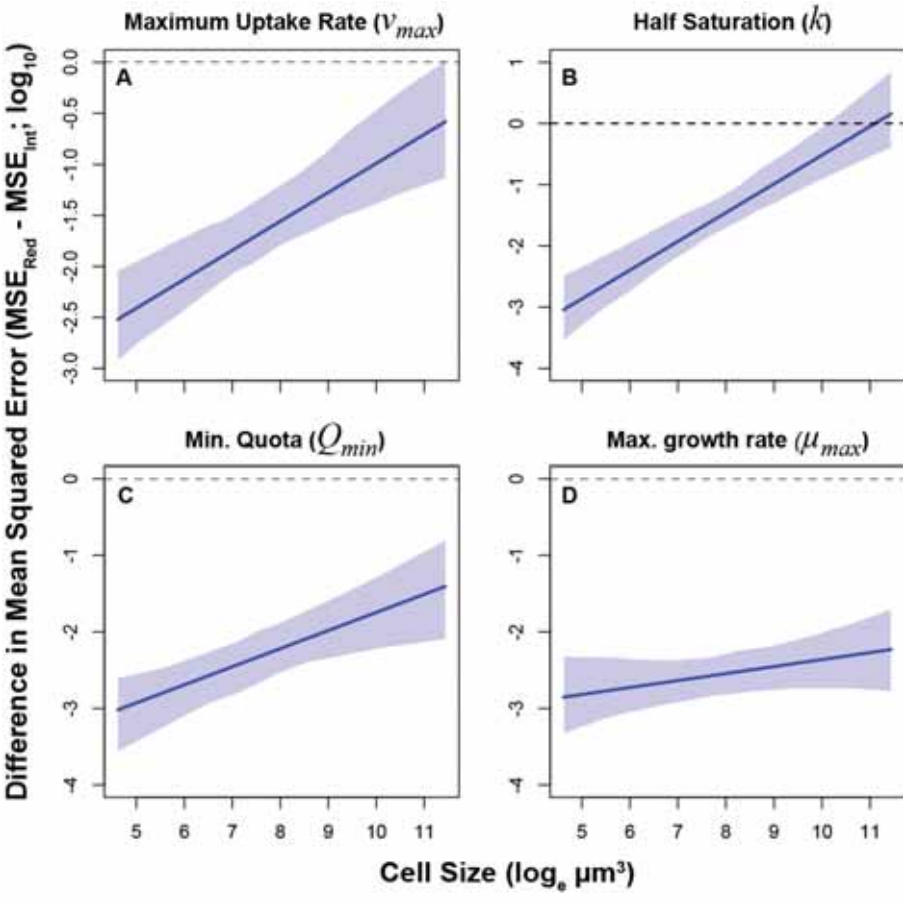

Figure 5.2: Mean and 95% confidence intervals for the difference in Mean Squared Error between the two best-performing models, the Fluorescence-Quota model and the Nitrogen-Quota model ($MSE_{flu} - MSE_{nitr}$), as a function of the cell size used to simulate the datasets for per-cell maximum nitrogen uptake rate (A), Michaelis-Menten half-saturation constant for the nitrate uptake functional response (B), per-cell minimum internal quota (C), and maximum specific growth rate (D). Negative Y-axis values indicate better performance of the Fluorescence-Quota model ($MSE_{flu} < MSE_{nitr}$), while positive values show better performance of the Nitrogen-Quota model ($MSE_{flu} > MSE_{nitr}$). Confidence intervals were calculated with Bayesian linear regressions, by subtracting the posterior distributions between Mean Squared Error and cell size across all 100 simulations for the two models.

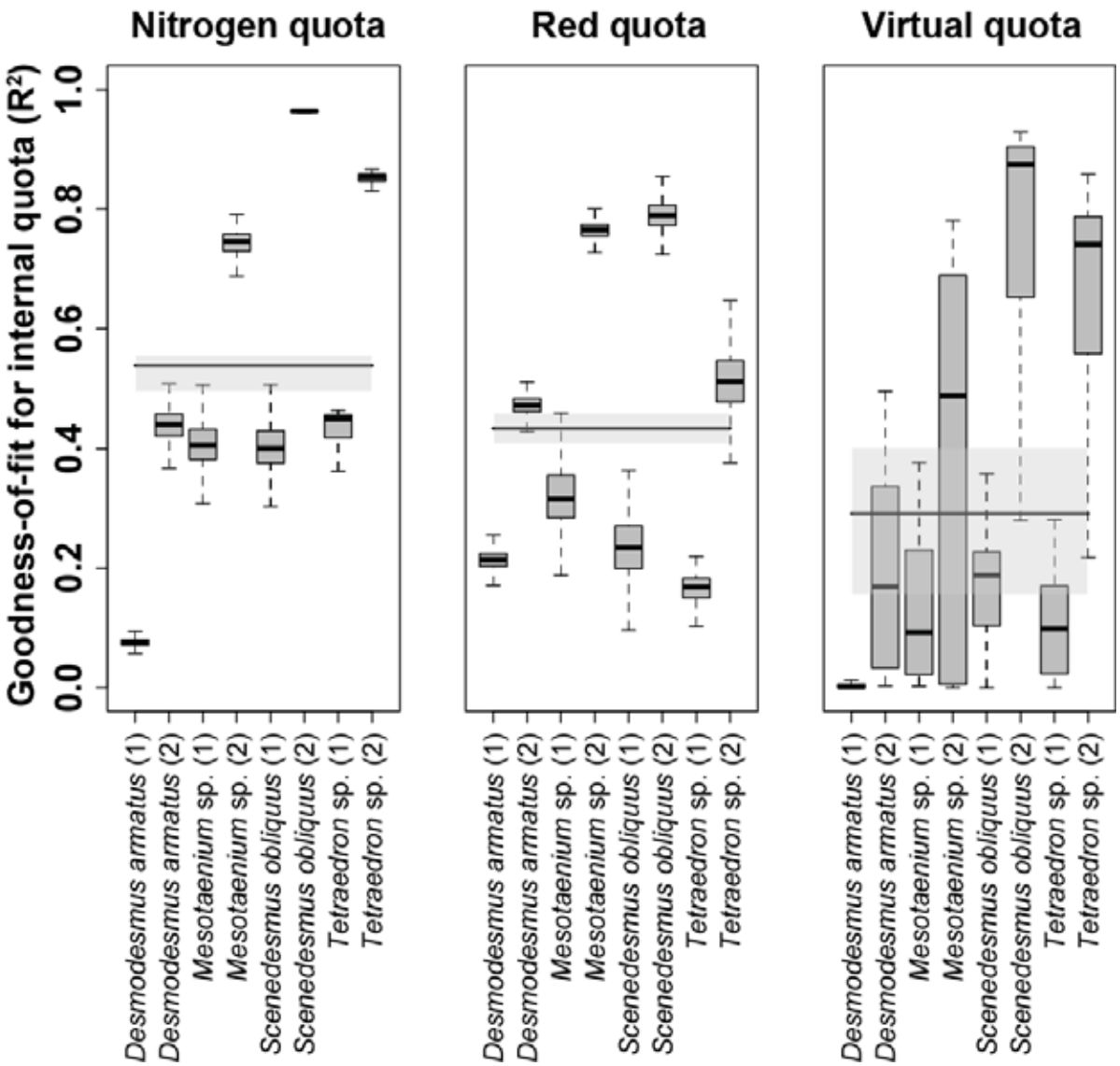

Figure 5.3: Goodness-of-fit between model inferred-quota and observed-quota integrated over the posterior distribution for the three different models calibrated to the time-series collected in chapter 4 (i.e. 4 green algal species, each grown at two initial conditions). The horizontal line represents the weighted mean over all R^2 distributions (±95% confidence intervals). Refer to panel C and F in Fig. S5.1-S5.4 in Appendix C for the graphical representation of the model fits.

Discussion

This study showed that including per-cell red fluorescence as a proxy for internal N (fluorescence-quota model) can improve the performance of Quota models while still accounting for the ability of a cell to store nitrogen intracellularly. The analysis based on simulated dataset showed that the higher instrumental precision for red fluorescence, compared to measuring internal nitrogen directly, makes the fluorescence-quota model superior even to the classic nitrogen-quota model. Furthermore, fitting Quota models to laboratory time-series showed that including information on red fluorescence can improve the ability of the model to predict the internal quota dynamics within a cell.

Replacing direct monitoring of internal N quota with per-cell red fluorescence can expand the applicability and the precision of Quota models. Firstly, protocols for measuring flow cytometric red fluorescence are non-destructive, allowing monitoring the same sample over time, which cannot be done with direct measurements for cell internal nitrogen. Secondly, technological advances in nutrient probes and automated submersible flow cytometers (cytobot; Olson *et al.* 2003) make possible the use of Quota models for real-time forecasting of phytoplankton dynamics in natural and engineered systems. In contrast, protocols for monitoring total internal N quota are more complex to automate. Thirdly, red fluorescence is an optical property intrinsic to living photoautotrophic cells, so suspended matter in water solution does not bias its reading (Collier 2000; Dubelaar *et al.* 2000; Veldhuis *et al.* 2000). Conversely, directly estimating total elemental composition from samples with variable loads of dead cells or dissolved nutrient-

rich inorganic/organic particles can substantially overestimate nutrient quota for living cells (Beardall *et al.* 2001; Shelly *et al.* 2010). Fourthly, it is feasible to separately monitor red fluorescence intensity for mixed species with non-overlapping optical ranges (Trask, Engh & Elgershuizen 1982). This could allow calibration of Quota models from time-series of interacting species. In contrast, direct methods for total nitrogen quota can only estimate the total elemental composition within a sample. These many advantages make the proposed fluorescence-quota model a promising way to reduce some of the limitations of modeling phytoplankton dynamics.

Laboratory studies have documented factors other than nitrogen status that can affect the phenomenon of phytoplankton chlorophyll fluorescence, such as light intensity, diel cycle, pigment composition, and other limiting nutrients (Sosik *et al.* 1989; DuRand *et al.* 1998; Mas *et al.* 2008). However, the analysis of per-cell fluorescence has received relatively little attention compared to other types of fluorescence (e.g. total fluorescence, Pulse Amplitude Modulated fluorometry), as the use of flow cytometers was established in phytoplankton ecology relatively recently (Veldhuis *et al.* 2000; Sosik, Olson & Armbrust 2010). Flow cytometers automatically record fluorescence intensity whenever they are used to estimate the population density of a phytoplankton sample. At present, time-series of per-cell red fluorescence are rarely of interest and scientific publications mostly do not report them. New evidence indicates that flow cytometric red fluorescence can not only reveal physiological mechanisms of a cell but also improve current phytoplankton models (Malerba *et al.* 2016). Promoting the publication and use of per-cell red fluorescence data can provide more opportunities for further verification and a

better evaluation of using flow cytometric fluorescence proxies in phytoplankton models.

The simulated datasets including observation error and process noise recorded a mean R^2 between red fluorescence ($F(t)$) and observed internal quota ($Q_{obs}(t)$) that was 15% higher than the coefficient recorded from laboratory experiments in Malerba *et al.* (2016). It cannot be determined from the data how and where this additional observation error between measurements of $F(t)$ and/or Q_{obs} (t) entered the system. However, details about the experimental protocols provide some indications. Multiple aspects contribute to the overall magnitude of observation error for measuring internal nitrogen quota: the precision of the spectrophotometer when recording reaction intensity (instrumental error), the accuracy of dispensing reagents or diluting samples (manipulative error), and the rate of chemical degradation in all chemical reactions (chemical error). While instrumental and manipulative errors were fully replicated in the experimental methods and thus reflected in the estimate of observation error from the triplicate readings, chemical error can potentially be mis-represented by triplicate readings: the same reagents and stock standards are used at each day, and chemical decay can cause an increase in observation error that is not included in the standard deviations of the replicate measurements. Also, standard stocks for measuring cell internal nitrogen require organic stock standards (i.e. glycine), which are less stable than more traditional inorganic controls. Conversely, the observation error associated with measuring red fluorescence only depends only by the instrumental error from the flow cytometer, which is well characterized by multiple independent sample readings. In fact, red fluorescence originates from exposing untreated cells to blue light at a wavelength of 488 nm and any inconsistencies involved with handling the sample can only

influence estimates for cell densities, not for the red fluorescence emission of a cell. In conclusion, the additional observation error is more likely to be associated with measuring per-cell internal nitrogen, rather than red fluorescence. Hence, our approach to add equal proportions of observation error to $F(t)$ and $Q(t)$ until the empirically detected R^2 of 0.77 in Malerba *et al.* (2016) makes the analysis conservative, as it is likely to overestimate the error in $F(t)$ and underestimate that in $Q(t)$.

Our study presents a novel approach to incorporating and evaluating indirect proxies in dynamic models. Specifically, present findings showed that red fluorescence can substantially improve the estimation of phytoplankton demographic parameters when fitting process-based Quota models to time-series data. Many other population models incorporate variables representing the condition of individual organisms. For instance, Dynamic Energy Budget models rely on the assumption that energy and resources can be stored within organisms (Nisbet *et al.* 2000; Kooijman 2010). However, variables characterizing the internal condition of individuals often require destructive and time-consuming laboratory protocols, or they may simply be impossible to measure directly (e.g. separate energy reserves for growth, reproduction, or maintenance of an individual). Consequently, most dynamic models infer changes in internal storages without testing these implied dynamics against data (i.e., they are unobserved state variables). This practice impairs the capacity to validate model performance, and it increases parameter uncertainty. Therefore, the approach applied here to evaluate an internal nitrogen proxy in phytoplankton may also be useful more broadly, for evaluating indirect proxies in other populations for which difficult-to-measure internal states strongly influence population dynamics.

Chapter 6: General Discussion

Thesis Findings and Implications

Understanding nitrogen assimilation in phytoplankton communities is critical for multiple purposes: from informing conservation policies, to quantifying global cycles, to modeling the effects of future global warming, to biotechnological applications (Hatfield & Follett 2008; Suggett, Borowitzka & Prášil 2010; Gimpel *et al.* 2013). Our ability to model the pathways of phytoplankton nitrogen assimilation and cell division is a key element to target these objectives. In the first half of my thesis, I presented a new approach to analyze phytoplankton utilization for nitrate and ammonium, the two most important ionic forms of inorganic nitrogen driving primary productivity (Gruber 2008). This approach relies on calibrating process-based models to laboratory time-series data, including multiple transitory and interactive uptake dynamics, which traditional curve-fitting techniques are unable to account for. By using this new nitrate-ammonium model, I documented and quantified the important influences of nitrogen starvation length and ammonium-induced inhibition on nitrate uptake of a cell. Moreover, I demonstrated that the nitrate-ammonium utilization of a cell changes substantially due to cell size plasticity and previous nitrogen regimes. I showed that evaluating nitrogen utilization performance without accounting for changes in mean size of a cell could substantially underestimate the actual ability of the species to cope with new conditions. In the second part of my thesis, I examined another aspect of phytoplankton models: the quantification of internal nitrogen status in phytoplankton populations. Traditional laboratory protocols present substantial

limitations in estimating the degree of nitrogen status in phytoplankton cells. Hence, I proposed and tested a new, more precise and non-destructive indirect proxy that is based on optical properties of a cell to evaluate nitrogen limitation. Finally, I showed that the higher instrumental precision associated with monitoring cell red fluorescence can substantially improve the performance of traditional phytoplankton nutrient-limited models, relative to models where internal nitrogen is directly monitored without the use of a proxy.

The overarching theme of this thesis was the use of contemporary modeling techniques for the analysis of phytoplankton time-series data. The analytical methods in many published phycological studies are often based on rates of nitrogen utilization and biomass growth calculated between each two successive observed points in time (e.g. Laws *et al.* 2011; Martinez, Pato & Rico 2012). The modeling techniques presented here represent a more comprehensive and flexible tool to quantify dynamic systems, also able to account for multiple transient and interacting processes (see chapter 2). Furthermore, my approach was specifically designed to allow calibration with only daily observations of medium nitrate, medium ammonium, and population density, rendering the models applicable to a vast number of studies where these variables are routinely monitored. Many published phytoplankton models cannot do that. For instance, anyone attempting to rigorously estimate the dozens of parameters of the phytoplankton models in Flynn *et al.* (1997b) and Flynn *et al.* (1997a) would require additional complicated, expensive and time consuming experiments. Indeed, there have been no attempts to comprehensively estimate these parameters for any study species, despite the >15 years since the original publications. Thus, this thesis also filled the need for a more

tractable modeling approach, sacrificing the explicit characterization of biochemical pathways in order to be applicable with routinely monitored variables.

Broader Implications

This work has both applied and fundamental implications. An improved understanding of nitrate-ammonium assimilation by phytoplankton species could help better manage the risk of algal bloom formation, by regulating nitrate-polluting (e.g. land clearing, agriculture) and ammonium-polluting activities (e.g. human waste discharge, intensive livestock) in coastal areas (Cloern 2001; Domingues *et al.* 2011). Throughout my thesis, I elaborated a general modeling framework to represent the process of phytoplankton nitrogen assimilation. This work could contribute to investigating the causal links between dynamics of phytoplankton communities and nitrogen eutrophication in natural environments. More fundamentally, large-scale models for global nutrient cycles rely on nitrogen budgets where the role of phytoplankton is highly simplified. For instance, the ability of phytoplankton cells to store resources is particularly difficult to include in biogeochemical models. This is mainly because monitoring phytoplankton storage conditions is not feasible for large areas (Shelly *et al.* 2010). In consequence, many biogeochemical models simplify total primary production to follow a non-linear function of the ambient concentration of the most limiting resource (e.g. Follows *et al.* 2007; Weitz *et al.* 2015). In the second part of this thesis I address this limitation by integrating into current mathematical models a new approach that is more precise, non-destructive, and easier to perform to quantify nitrogen storage in phytoplankton cells. This alternative approach relies on measuring changes in red fluorescence from single cells that now can be continuously monitored from

automated submersible units from natural phytoplankton assemblages (Olson *et al.* 2003; Hunter-Cevera *et al.* 2014). Given the important contribution of phytoplankton to the balance of the biosphere, an improved characterization of how cells can use intracellular nutrient storages to grow can substantially enhance our ability to detect cycles and trends and make long-term predictions.

Robustness of Results and Future Directions

All experiments in this thesis ensured that nitrogen was the only limiting factor for cell division. Therefore, altering experimental conditions (e.g. light, temperature, other nutrients) will also cause a change in the parameter values estimated by fitting the models. However, the mathematical structure of these models was based on prior physiological knowledge of the principles regulating phytoplankton nitrogen assimilation. Therefore, the model structures represent the dynamics of phytoplankton under the general conditions of nitrogen limitation and should not be specific to my choices of species and environmental parameters. However, further testing under different experimental conditions is needed to verify the generality of the models.

The effects of light are especially important for nitrogen utilization of phytoplankton cells. Light availability determines the inflow of photosynthetic energy to a cell and regulates its metabolic activities (Al-Qasmi *et al.* 2012). As a consequence, altering light regimes could influence many of the results documented in this thesis. Firstly, the assimilation of nitrate depends on light conditions because the incorporation of this type of nitrogen is dependent on photosynthetically-driven chemical reductions (Berges 1997; Crawford *et al.* 2000). Hence, exposing a species to different light conditions could lead to very different dynamics in the nitrate-

ammonium utilization of a cell, requiring re-calibration of all functional responses. Secondly, increasing or decreasing light exposure could lead to variations in the relative and total pigment concentration of a cell (MacIntyre *et al.* 2002; Lutz *et al.* 2003). For instance, many phytoplankton species can mitigate damages from excessive light by increasing the production of photo-protective accessory pigments, such as the carotenoids xanthophylls and carotenes (Polimene *et al.* 2012; Christaki *et al.* 2013). However, most non-chlorophyll pigments are unlikely to alter the optical properties of cells used in this thesis, as they do not include nitrogen in their elemental structure and they contribute very little to the red fluorescence emission (at 670 nm) of a cell (Takaichi 2011; Devred *et al.* 2013). Nonetheless, cells exposed to different light conditions will also optimize their photosynthetic capacity by regulating the density of light-trapping chlorophyll pigments, which will affect the red fluorescence signal emitted by a cell (Demmig-Adams & Adams 2000; Bonilla, Rautio & Vincent 2009). Furthermore, the allocation of nitrogen can change depending on light availability: more nitrogen will be allocated to pigments and associated protiens in light-limited cells compared to light-saturated cells (see Wirtz and Pahlow 2010), affecting the reliability of a calibration curve between red fluorescence and nitrogen status. Testing of the relationship between red fluorescence and internal cell nitrogen would therefore be required for cells undergoing light adaptation. Finally, changes in light conditions and chlorophyll pigments could also change the precision of the calibration curve, affecting the employability of red fluorescence as a proxy for internal nitrogen. Because phytoplankton species are adapted to thrive in very different conditions (from benthic to pelagic, from single cells to colonies), the influence of different light exposures on the accuracy of the calibration curve between red fluorescence and

internal nitrogen is likely to be group- and species-specific. Thus, further studies are particularly needed to analyze how the strength of the relationship between red fluorescence and total cell nitrogen changes across different species and experimental settings.

A final consideration goes to the choice of species. All datasets used in this thesis were collected from Chlorophytes and Charophyte freshwater green algae. These species are fast-growing and often dominate algal communities of lakes, rivers, and estuaries (Graham 2000). They are also commonly used in bioengineering research, especially in industrial production of renewable energy, human and animal nutrition, high-value pharmaceutical compounds, and environmental bioremediation (Becker 1994; Ghirardi 2000; Rosenberg *et al.* 2008). Generalizing the present work beyond green algae would require repeating these studies with more phylogenetically distant species. However, the pathways for nitrate-ammonium assimilation are equivalent across phytoplankton groups and it is likely that the proposed models will still capture the qualitative nitrogen utilization dynamics of other species (except for species adapted to fix nitrogen gas; Crawford *et al.* 2000). Also the use of red fluorescence as a proxy for internal nitrogen is likely to extend to other species and taxonomic groups, for two reasons. Firstly, chlorophyll molecules are particularly rich in nitrogen and its concentration should therefore be dependent on the nitrogen status of a cell (Sachs, Repeta & Goericke 1999; Young & Beardall 2003b). Secondly, the red fluorescence emitted by phytoplankton species across all major taxonomic groups is mainly produced by chlorophyll *a* (and to some extent also chlorophyll *b*), which consistently peaks in a surprisingly narrow range across very distantly related species (673 to 679 nm; Johnsen & Sakshaug 2007). So, despite large variation in pigment composition

across taxonomic groups, red fluorescence measured at 670 nm can be monitored for other species in the same way it was documented for green algae in chapter 4, and the same principles applied in this thesis to green algae are likely to apply also for other taxonomic groups.

Implications for Multi-Species Assemblages

A clear next step from this thesis is to apply the techniques presented here to experimental settings of mixed-species assemblages. An interesting question that remains unsolved is how important is the contribution of nitrogen partitioning in promoting species coexistence. The models developed in the first part of this thesis may help to answer this question. For instance, phytoplankton communities reared in continuous (chemostat) cultures at different relative concentration of nitrate and ammonium can test the hypothesis of whether nitrogen partitioning favors higher species diversity. Another important ecological question is how fluctuations in relative nitrogen composition can affect the stability of a phytoplankton community. In this case, the tested hypothesis would be that generalist species are advantaged over specialized species under fluctuating concentrations of nitrogen types.

Another potential application emerging from this research is the use of red fluorescence for studying cell internal nitrogen from individual species when reared in mixed cultures. Direct estimation using traditional laboratory protocols cannot allow separately monitoring nutrient storages of mixed species. Conversely, indirect estimation from optical properties of mixed phytoplankton species with non-overlapping values can easily be partitioned, quantifying the contribution of each individual species (Trask *et al.* 1982; Petersen *et al.* 2012). There is a large body of theoretical work examining the role of resource storage in community ecology and

its interaction with temporal and spatial variability (Grover 2011; Grover, Hsu & Wang 2012). The methodologies and the models explained in the second part of this thesis may help to test theoretical predictions with empirical laboratory experiments.

Conclusions

The link between nitrogen and phytoplankton biomass is complex. Fitting Quota models to time-series is a powerful and flexible tool to investigate the main processes regulating nitrogen utilization in single cells. In this thesis, I addressed two main limitations of classic Quota models: I explicitly included two sources of inorganic nitrogen, and I integrated red fluorescence as a more precise and non-destructive method to monitor cell nitrogen quota. Overall, I showed that Quota models could be extended to suit the specific experimental setting in a way that remained mathematically tractable and that allowed calibration from commonly measured time-series. Before this thesis, the only alternatives to traditional Quota models were highly detailed biochemical models, whose large numbers of parameters and state variables prevented calibration from experimental data. In conclusion, as future research further clarifies the role of nitrogen for phytoplankton population dynamics, this thesis showed that Quota models could represent a suitable tool to incorporate new processes and investigate their roles in the dynamics of phytoplankton populations.

References

Adams, C., Godfrey, V., Wahlen, B., Seefeldt, L. & Bugbee, B. (2013) Understanding precision nitrogen stress to optimize the growth and lipid content tradeoff in oleaginous green microalgae. *Bioresource Technology,* **131,** 188-194.

Aksnes, D.L. & Egge, J.K. (1991) A theoretical-model for nutrient-uptake in phytoplankton. *Marine Ecology Progress Series,* **70,** 65-72.

Al-Qasmi, M., Raut, N., Talebi, S., Al-Rajhi, S. & Al-Barwan, T. (2012) A review of effect of light on microalgae growth. *Proceedings of the World Congress on Engineering - WCE 2012, July 4 - 6, 2012, London, U.K.*

Albert, C.H., Grassein, F., Schurr, F.M., Vieilledent, G. & Violle, C. (2011) When and how should intraspecific variability be considered in trait-based plant ecology? *Perspectives in Plant Ecology Evolution and Systematics,* **13,** 217-225.

Albert, C.H., Thuiller, W., Yoccoz, N.G., Douzet, R., Aubert, S. & Lavorel, S. (2010) A multi-trait approach reveals the structure and the relative importance of intra- vs. interspecific variability in plant traits. *Functional Ecology,* **24,** 1192-1201.

American Public Health Association (2012) *Standard methods for the examination of water and wastewater (22nd edition)*. APHA-AWWA-WEF, Washington, D.C.

Aminot, A., Kirkwood, D. & Carlberg, S. (1997) The quasimeme laboratory performance studies (1993-1995): Overview of the nutrients section. *Marine Pollution Bulletin,* **35,** 28-41.

Balfoort, H.W., Berman, T., Maestrini, S.Y., Wenzel, A. & Zohary, T. (1992) Flow-cytometry - instrumentation and application in phytoplankton research. *Hydrobiologia,* **238,** 89-97.

Barton, A.D., Finkel, Z.V., Ward, B.A., Johns, D.G. & Follows, M.J. (2013) On the roles of cell size and trophic strategy in north atlantic diatom and dinoflagellate communities. *Limnology and Oceanography*, **58,** 254-266.

Barton, K. (2014) R package "mumin": Model selection and model averaging based on information criteria (AICc and alike).

Beardall, J., Young, E. & Roberts, S. (2001) Approaches for determining phytoplankton nutrient limitation. *Aquatic Sciences*, **63,** 44-69.

Becker, E.W. (1994) *Microalgae : Biotechnology and microbiology*. Cambridge University Press, Cambridge.

Berg, M. & Ellers, J. (2010) Trait plasticity in species interactions: A driving force of community dynamics. *Evolutionary Ecology,* **24,** 617-629.

Berges, J.A. (1997) Minireview: Algal nitrate reductases. *European Journal Of Phycology,* **32,** 3-8.

Bertilsson, S., Berglund, O., Karl, D.M. & Chisholm, S.W. (2003) Elemental composition of marine Prochlorococcus and Synechococcus: Implications for the ecological stoichiometry of the sea. *Limnology and Oceanography,* **48,** 1721-1731.

Bittar, T.B., Lin, Y.J., Sassano, L.R., Wheeler, B.J., Brown, S.L., Cochlan, W.P. & Johnson, Z.I. (2013) Carbon allocation under light and nitrogen resource gradients in two model marine phytoplankton. *Journal of Phycology,* **49,** 523-535.

Bolker, B. (2008) Dynamic models. *Ecological models and data in R* (ed. B. Bolker), pp. vii, 396. Princeton University Press, Princeton, N.J.

Bolnick, D.I., Yang, L.H., Fordyce, J.A., Davis, J.M. & Svanback, R. (2002) Measuring individual-level resource specialization. *Ecology,* **83,** 2936-2941.

Bonilla, S., Rautio, M. & Vincent, W.F. (2009) Phytoplankton and phytobenthos pigment strategies: Implications for algal survival in the changing arctic. *Polar Biology,* **32,** 1293-1303.

Bordi, F., Neeck, S. & Scolese, C. (1999) Contribution of eos terra to earth science. *Sensors, systems, and next-generation satellites* (eds H. Fujisada & J.B. Lurie), pp. 260-268. Spie-Int Soc Optical Engineering, Bellingham.

Boudsocq, S., Niboyet, A., Lata, J.C., Raynaud, X., Loeuille, N., Mathieu, J., Blouin, M., Abbadie, L. & Barot, S. (2012) Plant preference for ammonium versus nitrate: A neglected determinant of ecosystem functioning? *American Naturalist,* **180,** 60-69.

Bozdogan, H. (1987) Model selection and akaike information criterion (AIC) - the general-theory and its analytical extensions. *Psychometrika,* **52,** 345-370.

Brand, L.E. (1991) Minimum iron requirements of marine-phytoplankton and the implications for the biogeochemical control of new production. *Limnology and Oceanography,* **36,** 1756-1771.

Bronk, D.A., See, J.H., Bradley, P. & Killberg, L. (2007) DON as a source of bioavailable nitrogen for phytoplankton. *Biogeosciences,* **4,** 283-296.

Brookes, J.D., Geary, S.M., Ganf, G.G. & Burch, M.D. (2000) Use of FDA and flow cytometry to assess metabolic activity as an indicator of nutrient status in phytoplankton. *Marine and Freshwater Research,* **51,** 817-823.

Brown, J.H., Gillooly, J.F., Allen, A.P., Savage, V.M. & West, G.B. (2004) Toward a metabolic theory of ecology. *Ecology,* **85,** 1771-1789.

Burnham, K.P. & Anderson, D.R. (2002) *Model selection and multimodel inference: A practical information-theoretic approach,* 2nd edn. Springer-Verlag New York.

Caperon, J. (1968) Population growth response of *Isochrysis galbana* to nitrate variation at limiting concentrations. *Ecology,* **49,** 866-872.

Caperon, J. & Meyer, J. (1972) Nitrogen-limited growth of marine phytoplankton—ii. Uptake kinetics and their role in nutrient limited growth of phytoplankton. *Deep Sea Research and Oceanographic Abstracts,* **19,** 619–632.

Capone, D.G., Bronk, D.A., Mulholland, M.R. & Carpenter, E.J. (2008) *Nitrogen in marine environement,* 2 edn. Elsevier.

Caro, T. (2010) *Conservation by proxy: Indicator, umbrella, keystone, flagship, and other surrogate species*. Island Press, Washington, DC.

Carpenter, E.J. & Capone, D.G. (2008) Nitrogen fixation in the marine environment. *Nitrogen in marine environement* (eds D.G. Capone, D.A. Bronk, M.R. Mulholland & E.J. Carpenter). Elsevier.

Cataldo, D.A., Haroon, M., Schrader, L.E. & Youngs, V.L. (1975) Rapid colorimetric determination of nitrate in plant-tissue by nitration of salicylic-acid. *Communications in Soil Science and Plant Analysis,* **6,** 71-80.

Cavender-Bares, K.K., Mann, E.L., Chisholm, S.W., Ondrusek, M.E. & Bidigare, R.R. (1999) Differential response of equatorial pacific phytoplankton to iron fertilization. *Limnology and Oceanography,* **44,** 237-246.

Chevan, A. & Sutherland, M. (1991) Hierarchical partitioning. *American Statistician,* **45,** 90-96.

Christaki, E., Bonos, E., Giannenas, I. & Florou-Paneri, P. (2013) Functional properties of carotenoids originating from algae. *Journal of the Science of Food and Agriculture,* **93,** 5-11.

Clescerl, L.S., Greenberg, A.E. & Eaton, A.D. (1999) 4500 NO_3 nitrogen (nitrate). *Standard methods for examination of water and wastewater* (eds APHA, AWWA & WPCF). Amer. Public Health. Assn.

Cleveland, J.S. & Perry, M.J. (1987) Quantum yield, relative specific absorption and fluorescence in nitrogen-limited *Chaetoceros gracilis*. *Marine Biology,* **94,** 489-497.

Cloern, J.E. (2001) Our evolving conceptual model of the coastal eutrophication problem. *Marine Ecology Progress Series,* **210,** 223–253.

Cochlan, W.P. & Harrison, P.J. (1991) Uptake of nitrate, ammonium, and urea by nitrogen-starved cultures of *Micromonas pusilla* (*Prasinophyceae*) - transient responses. *Journal of Phycology,* **27,** 673-679.

Collier, J.L. (2000) Flow cytometry and the single cell in phycology. *Journal of Phycology,* **36,** 628-644.

Collos, Y. & Berges, J.A. (2002) Nitrogen metabolism in phytoplankton. *Encyclopedia of life support systems* (ed. C.M. Duarte). EOLSS Publishers (UNESCO), Oxford.

Collos, Y., Gagne, C., Laabir, M., Vaquer, A., Cecchi, P. & Souchu, P. (2004) Nitrogenous nutrition of *Alexandrium catenella* (Dinophyceae) in cultures and in thau lagoon, southern france. *Journal of Phycology,* **40,** 96-103.

Collos, Y., Mornet, F., Sciandra, A., Waser, N., Larson, A. & Harrison, P.J. (1999) An optical method for the rapid measurement of micromolar concentrations of nitrate in marine phytoplankton cultures. *Journal of Applied Phycology,* **11,** 179-184.

Collos, Y., Vaquer, A., Bibent, B., Slawyk, G., Garcia, N. & Souchu, P. (1997) Variability in nitrate uptake kinetics of phytoplankton communities in a mediterranean coastal lagoon. *Estuarine Coastal and Shelf Science,* **44,** 369-375.

Collos, Y., Vaquer, A. & Souchu, P. (2005) Acclimation of nitrate uptake by phytoplankton to high substrate levels. *Journal of Phycology,* **41,** 466-478.

Cox, T.J.S., Maris, T., Soetaert, K., Conley, D.J., Van Damme, S., Meire, P., Middelburg, J.J., Vos, M. & Struyf, E. (2009) A macro-tidal freshwater ecosystem recovering from hypereutrophication: The schelde case study. *Biogeosciences,* **6,** 2935-2948.

Crawford, N.M., Kahn, M.L., Leustek, T. & Long, S.R. (2000) Nitrogen and sulfur. *Biochemistry & molecular biology of plants* (eds B.B. Buchanan, W. Gruissem & R.L. Jones), pp. 786-849. American Society of Plant Physiologists, Rockville, Md. ; [Great Britain].

Cuddington, K., Fortin, M.J., Gerber, L.R., Hastings, A., Liebhold, A., O'Connor, M. & Ray, C. (2013) Process-based models are required to manage ecological systems in a changing world. *Ecosphere,* **4**.

Cullimore, J.V. & Sims, A.P. (1981) Glutamine-synthetase of chlamydomonas - its role in the control of nitrate assimilation. *Planta,* **153,** 18-24.

da Silva, T.L., Roseiro, J.C. & Reis, A. (2012) Applications and perspectives of multi-parameter flow cytometry to microbial biofuels production processes. *Trends in Biotechnology,* **30,** 225-232.

Dassow, P.v., Chepurnov, V.A. & Armbrust, E.V. (2006) Relationships between growth rate, cell size, and induction of spermatogenesis in the centric diatom *Thalassiosira weissflogii* (Bacillariophyta). *Journal of Phycology,* **42,** 887-899.

Davey, M., Tarran, G.A., Mills, M.M., Ridame, C., Geider, R.J. & LaRoche, J. (2008) Nutrient limitation of picophytoplankton photosynthesis and growth in the tropical north atlantic. *Limnology and Oceanography,* **53,** 1722-1733.

de la Jara, A., Mendoza, H., Martel, A., Molina, C., Nordstron, L., de la Rosa, V. & Diaz, R. (2003) Flow cytometric determination of lipid content in a marine dinoflagellate, *Crypthecodinium cohnii*. *Journal of Applied Phycology,* **15,** 433-438.

De La Rocha, C.L., Terbruggen, A., Volker, C. & Hohn, S. (2010) Response to and recovery from nitrogen and silicon starvation in *Thalassiosira weissflogii*: Growth rates, nutrient uptake and C, Si and N content per cell. *Marine Ecology Progress Series,* **412,** 57-68.

Delia, C.F., Steudler, P.A. & Corwin, N. (1977) Determination of total nitrogen in aqueous samples using persulfate digestion. *Limnology and Oceanography,* **22,** 760-764.

Demers, S., Davis, K. & Cucci, T.L. (1989) A flow cytometric approach to assessing the environmental and physiological status of phytoplankton. *Cytometry,* **10,** 644-652.

Demmig-Adams, B. & Adams, W.W., 3rd (2000) Harvesting sunlight safely. *Nature,* **403,** 371, 373-374.

Dempster, T., Sanchez-Jerez, P., Fernandez-Jover, D., Bayle-Sempere, J., Nilsen, R., Bjorn, P.A. & Uglem, I. (2011) Proxy measures of fitness suggest coastal fish farms can act as population sources and not ecological traps for wild gadoid fish. *Plos One,* **6,** e15646.

Devred, E., Turpie, K., Moses, W., Klemas, V., Moisan, T., Babin, M., Toro-Farmer, G., Forget, M.-H. & Jo, Y.-H. (2013) Future retrievals of water column bio-optical properties using the hyperspectral infrared imager (hyspiri). *Remote Sensing,* **5,** 6812-6837.

DeWitt, T.J. (1998) Costs and limits of phenotypic plasticity: Tests with predator-induced morphology and life history in a freshwater snail. *Journal of Evolutionary Biology,* **11,** 465-480.

Doan, T.T.Y. & Obbard, J.P. (2011) Enhanced lipid production in *Nannochloropsis* sp. using fluorescence-activated cell sorting. *Global Change Biology Bioenergy,* **3,** 264-270.

Dodds, W.K., Strauss, E.A. & Lehmann, R. (1993) Nutrient dilution and removal bioassays to estimate phytoplankton response to nutrient control. *Archiv Fur Hydrobiologie,* **128,** 467-481.

Domingues, R.B., Barbosa, A.B., Sommer, U. & Galvao, H.M. (2011) Ammonium, nitrate and phytoplankton interactions in a freshwater tidal estuarine zone: Potential effects of cultural eutrophication. *Aquatic Sciences,* **73,** 331-343.

Donald, D.B., Bogard, M.J., Finlay, K. & Leavitt, P.R. (2011) Comparative effects of urea, ammonium, and nitrate on phytoplankton abundance, community composition, and toxicity in hypereutrophic freshwaters. *Limnol Oceanogr,* **56,** 2161-2175.

Donk, E.v., Lürling, M. & Lampert, W. (1999) Consumer-induced changes in phytoplankton: Inducibility, costs, benefits and the impact on grazers. *The ecology and evolution of inducible defenses* (eds R. Tollrian & C.D. Harvell), pp. 89-103. Princeton University Press, Princeton/USA.

Dortch, Q. (1990) The interaction between ammonium and nitrate uptake in phytoplankton. *Marine Ecology Progress Series,* **61,** 183-201.

Dortch, Q., Clayton, J.R., Thoresen, S.S. & Ahmed, S.I. (1984) Species-differences in accumulation of nitrogen pools in phytoplankton. *Marine Biology,* **81,** 237-250.

Dortch, Q., Clayton, J.R., Thoreson, S.S., Bressler, S.L. & Ahmed, S.I. (1982) Response of marine-phytoplankton to nitrogen deficiency - decreased nitrate uptake vs enhanced ammonium uptake. *Marine Biology,* **70,** 13-19.

Droop, M.R. (1968) Vitamin B12 and marine ecology. Iv. The kinetics of uptake, growth and inhibition in *Monochrysis lutheri*. *Journal of the Marine Biological Association of the UK,* **48,** 689-733.

Droop, M.R. (1973) Some thoughts on nutrient limitation in algae. *Journal of Phycology,* **9,** 264-272.

Droop, M.R. (1974) The nutrient status of algal cells in continuous culture. *Journal of the Marine Biological Association of the United Kingdom,* **54,** 825-855.

Droop, M.R. (1983) 25 years of algal growth-kinetics - a personal view. *Botanica Marina,* **26,** 99-112.

Droop, M.R. (2003) In defence of the cell quota model of micro-algal growth. *Journal of Plankton Research,* **25,** 103-107.

Duarte, C.M., Agusti, S. & Canfield, D.E. (1990) Size plasticity of fresh-water phytoplankton - implications for community structure. *Limnology and Oceanography,* **35,** 1846-1851.

Duarte, C.M. & Cebrian, J. (1996) The fate of marine autotrophic production. *Limnology and Oceanography,* **41,** 1758-1766.

Dubelaar, G.B.J. & Jonker, R.R. (2000) Flow cytometry as a tool for the study of phytoplankton. *Scientia Marina,* **64,** 135-156.

Ducobu, H., Huisman, J., Jonker, R.R. & Mur, L.R. (1998) Competition between a prochlorophyte and a cyanobacterium under various phosphorus regimes: Comparison with the droop model. *Journal of Phycology,* **34,** 467-476.

Dugdale, R.C., Wilkerson, F.P., Hogue, V.E. & Marchi, A. (2007) The role of ammonium and nitrate in spring bloom development in san francisco bay. *Estuarine, Coastal and Shelf Science,* **73,** 17-29.

DuRand, M.D., Green, R.E., Sosik, H.M. & Olson, R.J. (2002) Diel variations in optical properties of *Micromonas pusilla* (Prasinophyceae). *Journal of Phycology,* **38,** 1132-1142.

Durand, M.D. & Olson, R.J. (1996) Contributions of phytoplankton light scattering and cell concentration changes to diel variations in beam attenuation in the equatorial pacific from flow cytometric measurements of pico-, ultra- and nanoplankton. *Deep-Sea Research Part Ii-Topical Studies in Oceanography,* **43,** 891-906.

DuRand, M.D. & Olson, R.J. (1998) Diel patterns in optical properties of the chlorophyte nannochloris sp.: Relating individual-cell to bulk measurements. *Limnology and Oceanography,* **43,** 1107-1118.

Dusenberry, J.A., Olson, R.J. & Chisholm, S.W. (1999) Frequency distributions of phytoplankton single-cell fluorescence and vertical mixing in the surface ocean. *Limnology and Oceanography,* **44,** 431–436.

Eaton, A., Clesceri, L., Rice, E. & Greenberg, A. (2005) Protocol 4500-n c. Persulfate method. *Standard methods for the examination of water and wastewater* (eds APHA, AWWA & WPCF). Amer. Public Health. Assn.

Edwards, K.F., Thomas, M.K., Klausmeier, C.A. & Litchman, E. (2012) Allometric scaling and taxonomic variation in nutrient utilization traits and maximum growth rate of phytoplankton. *Limnology and Oceanography,* **57,** 554-566.

Eigenbrod, F., Armsworth, P.R., Anderson, B.J., Heinemeyer, A., Gillings, S., Roy, D.B., Thomas, C.D. & Gaston, K.J. (2010) The impact of proxy-based methods on mapping the distribution of ecosystem services. *Journal of Applied Ecology,* **47,** 377–385.

Epstein, H.E., Raynolds, M.K., Walker, D.A., Bhatt, U.S., Tucker, C.J. & Pinzon, J.E. (2012) Dynamics of aboveground phytomass of the circumpolar arctic tundra during the past three decades. *Environmental Research Letters,* **7**.

Falkowski, P.G., Barber, R.T. & Smetacek, V.V. (1998) Biogeochemical controls and feedbacks on ocean primary production. *Science,* **281,** 200-207.

Fan, C., Glibert, P.M., Alexander, J. & Lomas, M.W. (2003) Characterization of urease activity in three marine phytoplankton species, *Aureococcus anophagefferens*, *Prorocentrum minimum*, and *Thalassiosira weissflogii*. *Marine Biology,* **142,** 949-958.

Field, C.B., Behrenfeld, M.J., Randerson, J.T. & Falkowski, P. (1998) Primary production of the biosphere: Integrating terrestrial and oceanic components. *Science,* **281,** 237-240.

Flynn, K.J. (1999) Nitrate transport and ammonium-nitrate interactions at high nitrate concentrations and low temperature. *Marine Ecology Progress Series,* **187,** 283-287.

Flynn, K.J. & Fasham, M.J.R. (1997a) A short version of the ammonium-nitrate interaction model. *Journal of Plankton Research,* **19,** 1881-1897.

Flynn, K.J., Fasham, M.J.R. & Hipkin, C.R. (1997b) Modelling the interactions between ammonium and nitrate uptake in marine phytoplankton. *Philosophical Transactions of the Royal Society B,* **352,** 1625-1645.

Flynn, K.J., Zapata, M., Garrido, J.L., Opik, H. & Hipkin, C.R. (1993) Changes in carbon and nitrogen physiology during ammonium and nitrate nutrition and nitrogen starvation in *Isochrysis galbana*. *European Journal of Phycology,* **28,** 47-52.

Folke, C., Carpenter, S., Walker, B., Scheffer, M., Elmqvist, T., Gunderson, L. & Holling, C.S. (2004) Regime shifts, resilience, and biodiversity in ecosystem management. *Annual Review of Ecology, Evolution, and Systematics,* **35,** 557-581.

Follows, M.J., Dutkiewicz, S., Grant, S. & Chisholm, S.W. (2007) Emergent biogeography of microbial communities in a model ocean. *Science,* **315,** 1843-1846.

Fowler, D., Coyle, M., Skiba, U., Sutton, M.A., Cape, J.N., Reis, S., Sheppard, L.J., Jenkins, A., Grizzetti, B., Galloway, J.N., Vitousek, P., Leach, A., Bouwman, A.F., Butterbach-Bahl, K., Dentener, F., Stevenson, D., Amann, M. & Voss, M. (2013) The global nitrogen cycle in the twenty-first century. *Philosophical Transactions of the Royal Society B,* **368**.

Fujimoto, N., Sudo, R., Sugiura, N. & Inamori, Y. (1997) Nutrient-limited growth of microcystis aeruginosa and phormidium tenue and competition under various N:P supply ratios and temperatures. *Limnology and Oceanography,* **42,** 250-256.

Gelman, A. & Rubin, D.B. (1992) Inference from iterative simulation using multiple sequences. *Statistical Science,* **7,** 457-472.

Geweke, J.F. (1992) Evaluating the accuracy of sampling-based approaches to the calculation of posterior moments. *Bayesian statistics 4* (eds J.O. Berger, J.M. Bernardo, A.P. Dawid & A.F.M. Smith). Clarendon Press, Oxford, UK.

Ghirardi, M. (2000) Microalgae: A green source of renewable H_2. *Trends in Biotechnology,* **18,** 506-511.

Gimpel, J.A., Specht, E.A., Georgianna, D.R. & Mayfield, S.P. (2013) Advances in microalgae engineering and synthetic biology applications for biofuel production. *Current Opinion in Chemical Biology,* **17,** 489-495.

Gouveia, L., Marques, A.E., da Silva, T.L. & Reis, A. (2009) *Neochloris oleabundans* utex #1185: A suitable renewable lipid source for biofuel production. *Journal of Industrial Microbiology and Biotechnology,* **36,** 821-826.

Graham, J.M. (2000) Phytoplankton ecology. *Algae* (eds L.E. Graham & L.W. Wilcox). Prentice Hall, Upper Saddler River, NJ.

Graziano, L.M., Geider, R.J., Li, W.K.W. & Olaizola, M. (1996) Nitrogen limitation of north atlantic phytoplankton: Analysis of physiological condition in nutrient enrichment experiments. *Aquatic Microbial Ecology,* **11,** 53-64.

Griffiths, M.J., van Hille, R.P. & Harrison, S.T. (2014) The effect of nitrogen limitation on lipid productivity and cell composition in *Chlorella vulgaris*. *Applied Microbiology and Biotechnology*, **98,** 2345-2356.

Gromping, U. (2006) Relative importance for linear regression in R: The package relaimpo. *J. Stat. Softw.*, **17**.

Gromping, U. (2007) Estimators of relative importance in linear regression based on variance decomposition. *American Statistician,* **61,** 139-147.

Grover, J.P. (1991) Resource competition in a variable environment - phytoplankton growing according to the variable-internal-stores model. *American Naturalist,* **138,** 811-835.

Grover, J.P. (2011) Resource storage and competition with spatial and temporal variation in resource availability. *American Naturalist,* **178,** E124-148.

Grover, J.P., Hsu, S.B. & Wang, F.B. (2012) Competition between microorganisms for a single limiting resource with cell quota structure and spatial variation. *Journal of Mathematical Biology,* **64,** 713-743.

Gruber, N. (2008) The marine nitrogen cycle: Overview and challanges. *Nitrogen in marine environement* (eds D.G. Capone, D.A. Bronk, M.R. Mulholland & E.J. Carpenter). Elsevier.

Guerrero, M.G., Vega, J.M. & Losada, M. (1981) The assimilatory nitrate-reducing system and its regulation. *Annual Review of Plant Physiology and Plant Molecular Biology,* **32,** 169-204.

Hall, B. (2008) Laplacesdemon: An R package for bayesian inference.

Hatfield, J.L. & Follett, R.F. (2008) *Nitrogen in the environment: Sources, problems, and management,* 2 edn. Elsevier, New York.

Hayes, P.K., Whitaker, T.M. & Fogg, G.E. (1984) The distribution and nutrient status of phytoplankton in the southern-ocean between 20-degrees and 70-degrees-W. *Polar Biology*, **3,** 153-165.

Hecky, R. & Kilham, P. (1988) Nutrient limitation of phytoplankton in freshwater and marine environments: A review of recent evidence on the effects of enrichment. *Limnology and Oceanography,* **33,** 796-822.

Hessen, D.O. & Vandonk, E. (1993) Morphological-changes in scenedesmus induced by substances released from daphnia. *Archiv Fur Hydrobiologie,* **127,** 129-140.

Hilborn, R. & Mangel, M. (1997) *The ecological detective: Confronting models with data*. Princeton University Press, Princeton, N.J. ; Chichester.

Hockin, N.L., Mock, T., Mulholland, F., Kopriva, S. & Malin, G. (2012) The response of diatom central carbon metabolism to nitrogen starvation is different from that of green algae and higher plants. *Plant Physiolgy,* **158,** 299-312.

Holmborn, T., Dahlgren, K., Holeton, C., Hogfors, H. & Gorokhova, E. (2009) Biochemical proxies for growth and metabolism *Inacartia bifilosa* (Copepoda, Calanoida). *Limnology and Oceanography: Methods,* **7,** 785-794.

Holt, R.D. (2008) Theoretical perspectives on resource pulses. *Ecology,* **89,** 671-681.

Hooten, M.B. & Hobbs, N.T. (2015) A guide to bayesian model selection for ecologists. *Ecological Monographs,* **85,** 3-28.

Howarth, R.W. (1988) Nutrient limitation of net primary production in marine ecosystems. *Annual Review of Ecology, Evolution, and Systematics,* **19,** 89-110.

Hunter-Cevera, K.R., Neubert, M.G., Solow, A.R., Olson, R.J., Shalapyonok, A. & Sosik, H.M. (2014) Diel size distributions reveal seasonal growth dynamics of a coastal phytoplankter. *Proceedings of the National Academy of Sciences,* **111,** 9852-9857.

Hyka, P., Lickova, S., Pribyl, P., Melzoch, K. & Kovar, K. (2013) Flow cytometry for the development of biotechnological processes with microalgae. *Biotechnology Advances,* **31,** 2-16.

Ikaran, Z., Suárez-Alvarez, S., Urreta, I. & Castañón, S. (2015) The effect of nitrogen limitation on the physiology and metabolism of *Chlorella vulgaris* var l3. *Algal Research,* **10,** 134-144.

Irwin, A.J., Finkel, Z.V., Schofield, O.M.E. & Falkowski, P.G. (2006) Scaling-up from nutrient physiology to the size-structure of phytoplankton communities. *Journal of Phytoplankton Research,* **28,** 459-471.

Jackson, L.E., Schimel, J.P. & Firestone, M.K. (1989) Short-term partitioning of ammonium and nitrate between plants and microbes in an annual grassland. *Soil Biol Biochem,* **21,** 409-415.

Jacquet, S., Lennon, J.F., Marie, D. & Vaulot, D. (1998) Picoplankton population dynamics in coastal waters of the northwestern mediterranean sea. *Limnology and Oceanography,* **43,** 1916–1931.

Johnsen, G. & Sakshaug, E. (2007) Biooptical characteristics of psii and psi in 33 species (13 pigment groups) of marine phytoplankton, and the relevance for pulse-amplitude-modulated and fast-repetition-rate fluorometry. *Journal of Phycology,* **43,** 1236-1251.

Jung, V., Violle, C., Mondy, C., Hoffmann, L. & Muller, S. (2010) Intraspecific variability and trait-based community assembly. *Journal of Ecology,* **98,** 1134-1140.

Kallqvist, T. & Svenson, A. (2003) Assessment of ammonia toxicity in tests with the microalga, *Nephroselmis pyriformis*, Chlorophyta. *Water Research,* **37,** 477-484.

Kass, R.E. & Raftery, A.E. (1995) Bayes factors. *Journal of the American Statistical Association,* **90,** 773-795.

Klausmeier, C.A., Litchman, E., Daufresne, T. & Levin, S.A. (2004) Optimal nitrogen-to-phosphorus stoichiometry of phytoplankton. *Nature,* **429,** 171-174.

Kleyer, M., Bekker, R.M., Knevel, I.C., Bakker, J.P., Thompson, K., Sonnenschein, M., Poschlod, P., Van Groenendael, J.M., Klimeš, L., Klimešová, J., Klotz, S., Rusch, G.M., Hermy, M., Adriaens, D., Boedeltje, G., Bossuyt, B., Dannemann, A., Endels, P., Götzenberger, L., Hodgson, J.G., Jackel, A.K., Kühn, I., Kunzmann, D., Ozinga, W.A., Römermann, C., Stadler, M., Schlegelmilch, J., Steendam, H.J., Tackenberg, O., Wilmann, B., Cornelissen, J.H.C., Eriksson, O., Garnier, E. & Peco, B. (2008) The LEDA traitbase: A database of life-history traits of the northwest european flora. *Journal of Ecology,* **96,** 1266-1274.

Kolber, Z., Zehr, J. & Falkowski, P. (1988) Effects of growth irradiance and nitrogen limitation on photosynthetic energy conversion in photosystem II. *Plant Physiol,* **88,** 923-929.

Kooijman, S.A.L.M. (2010) *Dynamic energy budget theory for metabolic organisation,* 3 edn. Cambridge University Press.

Krebs, R.A. & Feder, M.E. (1997) Natural variation in the expression of the heat-shock protein HSP70 in a population of drosophila melanogaster and its correlation with tolerance of ecologically relevant thermal stress. *Evolution,* **51,** 173-179.

L'Helguen, S., Maguer, J.-F. & Caradec, J. (2008) Inhibition kinetics of nitrate uptake by ammonium in size-fractionated oceanic phytoplankton communities: Implications for new production and F-ratio estimates. *Journal of Plankton Research,* **30,** 1179-1188.

Langner, C.L. & Hendrix, P.F. (1982) Evaluation of a persulfate digestion method for particulate nitrogen and phosphorus. *Water Research,* **16,** 1451-1454.

Lanoul, A., Coleman, T. & Asher, S.A. (2002) UV resonance raman spectroscopic detection of nitrate and nitrite in wastewater treatment processes. *Analytical Chemistry,* **74,** 1458-1461.

Lardon, L.A., Helias, A., Sialve, B., Stayer, J.P. & Bernard, O. (2009) Life-cycle assessment of biodiesel production from microalgae. *Environmental Science & Technology,* **43,** 6475-6481.

Largier, J.L. (1993) Estuarine fronts - how important are they. *Estuaries,* **16,** 1-11.

Lavorel, S., McIntyre, S., Landsberg, J. & Forbes, T.D. (1997) Plant functional classifications: From general groups to specific groups based on response to disturbance. *Trends in Ecology and Evolution,* **12,** 474-478.

Laws, E.A., Pei, S.F., Bienfang, P. & Grant, S. (2011) Phosphate-limited growth and uptake kinetics of the marine prasinophyte *Tetraselmis suecica* (Kylin) butcher. *Aquaculture,* **322,** 117-121.

Leadbeater, B.S. (2006) The 'Droop equation'--Michael Droop and the legacy of the 'cell-quota model' of phytoplankton growth. *Protist,* **157,** 345-358.

Li, G., Brown, C.M., Jeans, J.A., Donaher, N.A., McCarthy, A. & Campbell, D.A. (2014a) The nitrogen costs of photosynthesis in a diatom under current and future pCO. *New Phytologist,* **205,** 533-543.

Li, Q., Zhang, H., Du, X., Wen, N. & Tao, Q. (2014b) County-level rice area estimation in southern China using remote sensing data. *Journal of Applied Remote Sensing,* **8**.

Lindenmayer, D., Barton, P. & Pierson, J. (2015) *Indicators and surrogates of biodiversity and environmental change*. CSIRO Publishing.

Lindstrom, J., Kokko, H., Ranta, E. & Linden, H. (1999) Density dependence and the response surface methodology. *Oikos,* **85,** 40-52.

Litchman, E. & Klausmeier, C.A. (2008) Trait-based community ecology of phytoplankton. *Annual Review of Ecology Evolution and Systematics,* **39,** 615-639.

Litchman, E., Klausmeier, C.A., Miller, J.R., Schofield, O.M. & Falkowski, P.G. (2006) Multi-nutrient, multi-group model of present and future oceanic phytoplankton communities. *Biogeosciences Discussions, European Geosciences Union,* **3,** 607-663.

Litchman, E., Klausmeier, C.A., Schofield, O.M. & Falkowski, P.G. (2007) The role of functional traits and trade-offs in structuring phytoplankton communities: Scaling from cellular to ecosystem level. *Ecology Letters,* **10,** 1170-1181.

Liu, S.W. & Qiu, B.S. (2012) Different responses of photosynthesis and flow cytometric signals to iron limitation and nitrogen source in coastal and oceanic *Synechococcus strains* (Cyanophyceae). *Marine Biology,* **159,** 519-532.

Lomas, M.W. (2004) Nitrate reductase and urease enzyme activity in the marine diatom *Thalassiosira weissflogii* (Bacillariophyceae): Interactions among nitrogen substrates. *Marine Biology,* **144,** 37-44.

Luning, K. (2005) Endogenous rhythms and daylength effects in macroalgal development. *Algal culturing techniques* (ed. R.A. Andersen), pp. 347-364. Elsevier/Academic Press, Burlington, MA.

Lutz, V.A., Sathyendranath, S., Head, E.J.H. & Li, W.K.W. (2003) Variability in pigment composition and optical characteristics of phytoplankton in the labrador sea and the central north atlantic. *Marine Ecology Progress Series,* **260,** 1-18.

Lyczkowski, E.R. & Karp-Boss, L. (2014) Allelopathic effects of *Alexandrium fundyense* (Dinophyceae) on *Thalassiosira* cf. *gravida* (Bacillariophyceae): A matter of size. *Journal of Phycology,* **50,** 376-387.

MacIntyre, H.L., Kana, T.M., Anning, T. & Geider, R.J. (2002) Photoacclimation of photosynthesis irradiance response curves and photosynthetic pigments in microalgae and cyanobacteria1. *Journal of Phycology,* **38,** 17-38.

Madin, J.S., Baird, A.H., Dornelas, M. & Connolly, S.R. (2014) Mechanical vulnerability explains size-dependent mortality of reef corals. *Ecology Letters,* **17,** 1008-1015.

Maguer, J.F., L'Helguen, S., Madec, C., Labry, C. & Corre, P.L. (2007) Nitrogen uptake and assimilation kinetics in *Alexandrium minutum* (Dynophyceae): Effect of N-limited growth rate on nitrate and ammonium interactions. *Journal of Phycology,* **43,** 295-303.

Malerba, M.E., Connolly, S.R. & Heimann, K. (2012) Nitrate-nitrite dynamics and phytoplankton growth: Formulation and experimental evaluation of a dynamic model. *Limnology and Oceanography,* **57,** 1555-1571.

Malerba, M.E., Connolly, S.R. & Heimann, K. (2015) An experimentally validated nitrate-ammonium-phytoplankton model including effects of starvation length and ammonium inhibition on nitrate uptake. *Ecological Modelling,* **317,** 30-40.

Malerba, M.E., Connolly, S.R. & Heimann, K. (2016) Standard flow cytometry as a rapid and non-destructive proxy for cell nitrogen quota. *Journal of Applied Phycology*.

Maranon, E. (2015) Cell size as a key determinant of phytoplankton metabolism and community structure. *Annual Review of Marine Science, Vol 7,* **7,** 241-264.

Maranon, E., Cermeno, P., Lopez-Sandoval, D.C., Rodriguez-Ramos, T., Sobrino, C., Huete-Ortega, M., Blanco, J.M. & Rodriguez, J. (2013) Unimodal size scaling of phytoplankton growth and the size dependence of nutrient uptake and use. *Ecol Lett,* **16,** 371-379.

Marín, X.F.I. (2015) Ggmcmc: Graphical tools for analyzing markov chain monte carlo simulations from bayesian inference. http://xavier-fim.net/packages/ggmcmc.

Marra, J., Bidigare, R.R. & Dickey, T.D. (1990) Nutrients and mixing, chlorophyll and phytoplankton growth. *Deep Sea Research Part A. Oceanographic Research Papers,* **37,** 127-143.

Martinez, B., Pato, L.S. & Rico, J.M. (2012) Nutrient uptake and growth responses of three intertidal macroalgae with perennial, opportunistic and summer-annual strategies. *Aquatic Botany,* **96,** 14-22.

Martinez, R. (1991) Transient nitrate uptake and assimilation in skeletonema-costatum cultures subject to nitrate starvation under low irradiance. *Journal of Plankton Research,* **13,** 499-512.

Mas, S., Roy, S., Blouin, F., Mostajir, B., Therriault, J.C., Nozais, C. & Demers, S. (2008) Diel variations in optical properties of *Imantonia rotunda* (Haptophyceae) and *Thalassiosira pseudonana* (Bacillariophyceae) exposed to different irradiance levels. *Journal of Phycology,* **44,** 551-563.

Mata, T.M., Martins, A.A. & Caetano, N.S. (2010) Microalgae for biodiesel production and other applications: A review. *Renewable and Sustainable Energy Reviews,* **14,** 217-232.

McGill, B.J., Enquist, B.J., Weiher, E. & Westoby, M. (2006) Rebuilding community ecology from functional traits. *Trends Ecol Evol,* **21,** 178-185.

Merila, J., Laurila, A. & Lindgren, B. (2004) Variation in the degree and costs of adaptive phenotypic plasticity among rana temporaria populations. *Journal of Evolutionary Biology,* **17,** 1132-1140.

Michalczyk, A., Kersebaum, K., Roelcke, M., Hartmann, T., Yue, S.C., Chen, X.P. & Zhang, F.S. (2014) Model-based optimisation of nitrogen and water management for wheat-maize systems in the north China plain. *Nutrient Cycling in Agroecosystems,* **98,** 203-222.

Mommer, L., Lenssen, J.P.M., Huber, H., Visser, E.J.W. & De Kroon, H. (2006) Ecophysiological determinants of plant performance under flooding: A comparative study of seven plant families. *Journal of Ecology,* **94,** 1117-1129.

Moore, J.K., Doney, S.C., Kleypas, J.A., Glover, D.M. & Fung, I.Y. (2002) An intermediate complexity marine ecosystem model for the global domain. *Deep-Sea Research Part Ii-Topical Studies in Oceanography,* **49,** 403-462.

Morris, I. & Syrett, P.J. (1963) The development of nitrate reductase in *Chlorella* and its repression by ammonium. *Archiv Fur Mikrobiologie,* **47,** 32-41.

Morris, I. & Syrett, P.J. (1965) The effect of nitrogen starvation on the activity of nitrate reductase and other enzymes in *Chlorella*. *Journal of General and Applied Microbiology,* **38,** 21-28.

Mulholland, M.R. & Lomas, M.W. (2008) Nitrogen uptake and assimilation. *Nitrogen in marine environement* (eds D.G. Capone, D.A. Bronk, M.R. Mulholland & E.J. Carpenter), pp. 303–384. Elsevier.

Mullaney, P.F., Dilla, M.A.V. & Coulter, J.R. (1969) Cell sizing: A light scattering photometer for rapid volume determination. *Review of Scientific Instruments,* **40**.

Nichols, H.W. (1973) Growth media - freshwater. *Handbook of phycological methods* (ed. J. Stein), pp. 448. Cambridge University Press, Cambridge.

Nisbet, R.M., Muller, E.B., Lika, K. & Kooijman, S.A.L.M. (2000) From molecules to ecosystems through dynamic energy budget models. *Journal of Animal Ecology,* **69,** 913-926.

Nydahl, F. (1978) On the peroxodisulphate oxidation of total nitrogen in waters to nitrate. *Water Research,* **12,** 1123-1130.

Olson, R.J., Shalapyonok, A. & Sosik, H.M. (2003) An automated submersible flow cytometer for analyzing pico- and nanophytoplankton: Flowcytobot. *Deep-Sea Research Part I-Oceanographic Research Papers,* **50,** 301-315.

Pahlow, M. & Oschlies, A. (2013) Optimal allocation backs Droop's cell-quota model. *Marine Ecology Progress Series,* **473,** 1-5.

Parker, R.A. (1993) Dynamic-models for ammonium inhibition of nitrate uptake by phytoplankton. *Ecological Modelling,* **66,** 113-120.

Parsons, T.R., Perry, R.I., Nutbrown, E.D., Hsieh, W. & Lalli, C.M. (1983) Frontal zone analysis at the mouth of saanich inlet, british-columbia, canada. *Marine Biology,* **73,** 1-5.

Pedersen, M.W., Berg, C.W., Thygesen, U.H., Nielsen, A. & Madsen, H. (2011) Estimation methods for nonlinear state-space models in ecology. *Ecological Modelling,* **222,** 1394-1400.

Pereira Coltri, P., Zullo, J., Ribeiro do Valle Goncalves, R., Romani, L.A.S. & Pinto, H.S. (2013) Coffee crop's biomass and carbon stock estimation with usage of high resolution satellites images. *IEEE Journal of Selected Topics in Applied Earth Observations and Remote Sensing,* **6,** 1786-1795.

Petersen, T.W., Brent Harrison, C., Horner, D.N. & van den Engh, G. (2012) Flow cytometric characterization of marine microbes. *Methods,* **57,** 350-358.

Pistorius, E.K., Funkhouser, E.A. & Voss, H. (1978) Effect of ammonium and ferricyanide on nitrate utilization by *Chlorella vulgaris*. *Planta,* **141,** 279-282.

Plummer, M. (2003) Jags: A program for analysis of bayesian graphical models using gibbs sampling.

Plummer, M. (2015) Rjags: Bayesian graphical models using MCMC. *R package version 3-15.* http://CRAN.R-project.org/package=rjags.

Plummer, M., Best, N., Cowles, K. & Vines, K. (2006) Coda: Convergence diagnosis and output analysis for MCMC. *R News,* **6,** 7-11.

Polimene, L., Brunet, C., Allen, J.I., Butenschon, M., White, D.A. & Llewellyn, C.A. (2012) Modelling xanthophyll photoprotective activity in phytoplankton. *Journal of Plankton Research,* **34,** 196-207.

Priddle, J., Whitehouse, M.J., Atkinson, A., Brierley, A.S. & Murphy, E.J. (1997) Diurnal changes in near-surface ammonium concentration—interplay between zooplankton and phytoplankton. *Journal Of Plankton Research,* **19,** 1305-1330.

R Core Team (2014) R: A language and environment for statistical computing. R foundation for statistical computing, vienna, austria. Url http://www.R-project.Org/.

R Core Team (2015) R: A language and environment for statistical computing. R foundation for statistical computing, vienna, austria. Url http://www.R-project.Org/.

Raimbault, P., Diaz, F., Pouvesle, W. & Boudjellal, B. (1999a) Simultaneous determination of particulate organic carbon, nitrogen and phosphorus collected on filters, using a semi-automatic wet-oxidation method. *Marine Ecology Progress Series,* **180,** 289-295.

Raimbault, P., Pouvesle, W., Diaz, F., Garcia, N. & Sempere, R. (1999b) Wet-oxidation and automated colorimetry for simultaneous determination of organic carbon, nitrogen and phosphorus dissolved in seawater. *Marine Chemistry,* **66,** 161-169.

Raimbault, P. & Slawyk, G. (1991) A semiautomatic, wet-oxidation method for the determination of particulate organic nitrogen collected on filters. *Limnology and Oceanography,* **36,** 405-408.

Rigano, C., Dimartinorigano, V., Vona, V. & Fuggi, A. (1979) Glutamine-synthetase activity, ammonia assimilation and control of nitrate reduction in the unicellular red alga *Cyanidium caldarium*. *Archives of Microbiology,* **121,** 117-120.

Rigano, C. & Violante, U. (1973) Effect of nitrate, ammonia and nitrogen starvation on regulation of nitrate reductase in cyanidium-caldarium. *Archiv Fur Mikrobiologie*, **90,** 27-33.

Rodolfi, L., Zittelli, G.C., Bassi, N., Padovani, G., Biondi, N., Bonini, G. & Tredici, M.R. (2009b) Microalgae for oil: Strain selection, induction of lipid synthesis and outdoor mass cultivation in a low-cost photobioreactor. *Biotechnology and Bioengineering,* **102,** 100-112.

Roenneberg, T. & Mittag, M. (1996) The circadian program of algae. *Seminars in Cell & Developmental Biology,* **7,** 753-763.

Rosenberg, J.N., Oyler, G.A., Wilkinson, L. & Betenbaugh, M.J. (2008) A green light for engineered algae: Redirecting metabolism to fuel a biotechnology revolution. *Current Opinion in Biotechnology*, **19,** 430-436.

RStudio (2013) Version 0.98.507, boston (ma), url http://www.Rstudio.Org/.

Runge, J.A. & Roff, J.C. (2000) The measurement of growth and reproductive rates. *Ices zooplankton methodology manual* (eds R. Harris, P. Wiebe, J. Lenz, H.R. Skjoldal & M. Huntley), pp. 401–454. Academic Press, San Diego.

Sachs, J.P., Repeta, D.J. & Goericke, R. (1999) Nitrogen and carbon isotopic ratios of chlorophyll from marine phytoplankton. *Geochimica et Cosmochimica Acta*, **63,** 1431-1441.

Salin, K., Auer, S.K., Rey, B., Selman, C. & Metcalfe, N.B. (2015) Variation in the link between oxygen consumption and atp production, and its relevance for animal performance. *Proceedings Biological Sciences*, **282**.

Santin-Janin, H., Garel, M., Chapuis, J.L. & Pontier, D. (2009) Assessing the performance of ndvi as a proxy for plant biomass using non-linear models: A case study on the Kerguelen archipelago. *Polar Biology*, **32,** 861-871.

Sattayatewa, C., Arnaldos, M. & Pagilla, K. (2011) Measurement of organic nitrogen and phosphorus fractions at very low concentrations in wastewater effluents. *Water Environment Research,* **83,** 675-683.

Schimel, J.P. & Bennett, J. (2004) Nitrogen mineralization: Challenges of a changing paradigm. *Ecology*, **85,** 591-602.

Schwarz, G.E. (1978) Estimating the dimension of a model. *Annals of Statistics*, **6,** 461–464.

Shapiro, H.M. (2005) Parameters and probes. *Practical flow cytometry* (ed. H.M. Shapiro), pp. 736. John Wiley & Sons.

Sharpless, T.K. & Melamed, M.R. (1976) Estimation of cell size from pulse shape in flow cytofluorometry. *J. Histochem Cytochem*, **24**.

Sharpless, T.K., Traganos, F., Darzynkiewicz, Z. & Malemed, M.R. (1975) Flow cytofluorimetry: Discrimination between single cells and cell aggregates by direct size measurements. *Acta Cytol.,* **19,** 577-581.

Shelly, K., Holland, D. & Beardall, J. (2010) Assessing nutrient status of microalgae using chlorophyll a fluorescence. *Chlorophyll a fluorescence in aquatic sciences methods and applications* (eds D.J. Suggett, M. Borowitzka & O. Prášil), pp. 223-236. Springer, New York.

Shuter, B.J. (1978) Size-dependence of phosphorus and nitrogen subsistence quotas in unicellular micro-organisms. *Limnol. Oceanogr.,* **23,** 1248–1255.

Sinclair, G.A., Kamykowski, D., Milligan, E. & Schaeffer, B. (2006) Nitrate uptake by karenia brevis. I. Influences of prior environmental exposure and biochemical state on diel uptake of nitrate. *Marine Ecology Progress Series,* **328,** 117-124.

Smith, V. (1998) Cultural eutrophication of inland, estuarine and coastal waters. *Successes, limitations and frontiers of ecosystem science* (eds M. Pace & P. Groffman), pp. 7-49. Springer-Verlag, New York.

Solidoro, C., Pecenik, G., Pastres, R., Franco, D. & Dejak, C. (1997) Modelling macroalgae (ulva rigida) in the venice lagoon: Model structure identification and first parameters estimation. *Ecological Modelling,* **94,** 191-206.

Solorzano, L. & Sharp, J.H. (1980) Determination of total dissolved nitrogen in natural-waters. *Limnology and Oceanography,* **25,** 751-754.

Son, N.T., Chen, C.F., Chen, C.R., Minh, V.Q. & Trung, N.H. (2014) A comparative analysis of multitemporal MODIS EVI and NDVI data for large-scale rice yield estimation. *Agricultural and Forest Meteorology,* **197,** 52-64.

Sosik, H.M., Chisholm, S.W. & Olson, R.J. (1989) Chlorophyll fluorescence from single cells - interpretation of flow cytometric signals. *Limnology and Oceanography,* **34,** 1749-1761.

Sosik, H.M., Olson, R.J. & Armbrust, E.V. (2010) Flow cytometry in phytoplankton research. *Chlorophyll a fluorescence in aquatic sciences methods and applications* (eds D.J. Suggett, M. Borowitzka & O. Prášil), pp. 171-186. Springer, New York.

Spiegelhalter, D.J., Best, N., Carlin, B.P. & Linde, A.V.d. (2002) Bayesian measures of model complexity and fit. *Journal of the Royal Statistical Society B,* **64,** 583–640.

Stephens, P.A., Pettorelli, N., Barlow, J., Whittingham, M.J. & Cadotte, M.W. (2015) Management by proxy? The use of indices in applied ecology. *Journal of Applied Ecology,* **52,** 1-6.

Stolte, W. & Riegman, R. (1995) Effect of phytoplankton cell size on transientstate nitrate and ammonium uptake kinetics. *Microbiology,* **141,** 1221-1229.

Stolte, W. & Riegman, R. (1996) A model approach for size-selective competition of marine phytoplankton for fluctuating nitrate and ammonium. *Journal of Phycology,* **32,** 732-740.

Strong, D.R., Whipple, A.V., Child, A.L. & Dennis, B. (1999) Model selection for a subterranean trophic cascade: Root-feeding caterpillars and entomopathogenic nematodes. *Ecology,* **80,** 2750-2761.

Suggett, D.J., Borowitzka, M. & Prášil, O. (2010) *Chlorophyll a fluorescence in aquatic sciences methods and applications*. Springer, New York.

Syrett, P.J. (1981) Nitrogen metabolism of microalgae. *Physiological bases of phytoplankton ecology* (ed. T. Platt), pp. 182-210. Canadian Government Publishing Center, Hull, Quebec, Canada.

Syrett, P.J. & Morris, I. (1963) The inhibition of nitrate assimilation by ammonium in *Chlorella*. *Biochimica et Biophysica Acta,* **67,** 566–575.

Takaichi, S. (2011) Carotenoids in algae: Distributions, biosyntheses and functions. *Marine Drugs,* **9,** 1101-1118.

Tantanasarit, C., Englande, A.J. & Babel, S. (2013a) Nitrogen, phosphorus and silicon uptake kinetics by marine diatom *Chaetoceros calcitrans* under high nutrient concentrations. *Journal of Experimental Marine Biology and Ecology,* **446,** 67-75.

Thacker, A. & Syrett, P.J. (1972) Assimilation of nitrate and ammonium by *Chlamydomonas reinhardi*. *New Phytologist,* **71,** 423-&.

Thyssen, M., Gregori, G.J., Grisoni, J.M., Pedrotti, M.L., Mousseau, L., Artigas, L.F., Marro, S., Garcia, N., Passafiume, O. & Denis, M.J. (2014) Onset of the spring bloom in the northwestern mediterranean sea: Influence of environmental pulse events on the in situ hourly-scale dynamics of the phytoplankton community structure. *Front Microbiol,* **5,** 387.

Timmermans, K.R., Davey, M.S., Wagt, B.v.d., Snoek, J., Geider, R.J., Veldhuis, M.J.W., Gerringa, L.J.A. & Baar, H.J.W.d. (2001) Co-limitation by iron and light of *Chaetoceros brevis*, *C. dichaeta* and *C. calcitrans* (Bacillariophyceae). *Marine Ecology Progress Series,* **217,** 287-297.

Trask, B.J., Engh, G.J.v.d. & Elgershuizen, J.H.B.W. (1982) Analysis of phytoplankton by flow cytometry. *Cytometry,* **2,** 258-264.

Turchin, P. (1996) Nonlinear time-series modeling of vole population fluctuations. *Researches on Population Ecology,* **38,** 121-132.

Turpin, D.H. (1991) Effects of inorganic n availability on algal photosynthesis and carbon metabolism. *Journal of Phycology,* **27,** 14-20.

Vaddella, V.K., Ndegwa, P.M. & Jiang, A. (2011) An empirical model of ammonium ion dissociation in liquid dairy manure. *Transactions of the American Society of Agricultural and Biological Engineers,* **54,** 1119-1126.

Vanucci, S., Guerrini, F., Milandri, A. & Pistocchi, R. (2010) Effects of different levels of n- and p-deficiency on cell yield, okadaic acid, DTX-1, protein and carbohydrate dynamics in the benthic dinoflagellate prorocentrum lima. *Harmful Algae,* **9,** 590-599.

Varela, D.E. & Harrison, P.J. (1999) Effect of ammonium on nitrate utilization by emiliania huxleyi, a coccolithophore from the oceanic northeastern pacific. *Marine Ecology Progress Series,* **186,** 67-74.

Veldhuis, M.J.W. & Kraay, G.W. (2000) Application of flow cytometry in marine phytoplankton research: Current applications and future perspectives. *Scientia Marina,* **64,** 121-134.

Vieira, N., Poff, N., LeRoy, C., Moulton, S., Koski, M. & Kondratieff, C. (2006) A database of lotic invertebrate traits for north america: US geological survey data series 187.

Violle, C., Navas, M.-L., Vile, D., Kazakou, E., Fortunel, C., Hummel, I. & Garnier, E. (2007) Let the concept of trait be functional! *Oikos,* **116,** 882-892.

von Dassow, P., van den Engh, G., Iglesias-Rodriguez, D. & Gittins, J.R. (2012) Calcification state of coccolithophores can be assessed by light scatter depolarization measurements with flow cytometry. *Journal of Plankton Research,* **34,** 1011-1027.

Wayne, R.P. (1993) *Chemistry of atmospheres,* 2nd edn. Oxford University Press, New York.

Weitz, J.S., Stock, C.A., Wilhelm, S.W., Bourouiba, L., Coleman, M.L., Buchan, A., Follows, M.J., Fuhrman, J.A., Jover, L.F., Lennon, J.T., Middelboe, M., Sonderegger, D.L., Suttle, C.A., Taylor, B.P., Frede Thingstad, T., Wilson, W.H. & Eric Wommack, K. (2015) A multitrophic model to quantify the effects of marine viruses on microbial food webs and ecosystem processes. *ISME J,* **9,** 1352-1364.

Wirtz, K.W. (2011) Non-uniform scaling in phytoplankton growth rate due to intracellular light and CO2 decline. *Journal of Plankton Research,* **33,** 1325-1341.

Yang, J., Xu, M., Zhang, X., Hu, Q., Sommerfeld, M. & Chen, Y. (2011) Life-cycle analysis on biodiesel production from microalgae: Water footprint and nutrients balance. *Bioresour Technol,* **102,** 159-165.

Yentsch, C.M., Horan, P.K., Muirhead, K., Dortch, Q., Haugen, E., Legendre, L., Murphy, L.S., Perry, M.J., Phinney, D.A., Pomponi, S.A., Spinrad, R.W., Wood, M., Yentsch, C.S. & Zahuranec, B.J. (1983) Flow-cytometry and cell

sorting - a technique for analysis and sorting of aquatic particles. *Limnology and Oceanography,* **28,** 1275-1280.

Yoshiyama, K. & Sharp, J.H. (2006) Phytoplankton response to nutrient enrichment in an urbanized estuary: Apparent inhibition of primary production by overeutrophication. *Limnology and Oceanography,* **51,** 424-434.

Young, E.B. & Beardall, J. (2003a) Photosynthetic function in *Dunaliella tertiolecta* (Chlorophyta) during a nitrogen starvation and recovery cycle. *Journal of Phycology,* **39,** 897-905.

Young, E.B. & Beardall, J. (2003b) Rapid ammonium- and nitrate-induced perturbations to chl a fluorescence in nitrogen-stressed *Dunaliella tertiolecta* (Chlorophyta). *Journal of Phycology,* **39,** 332-342.

Zamon, J.E. (2002) Tidal changes in copepod abundance and maintenance of a summer coscinodiscus bloom in the southern san juan channel, san juan islands, USA. *Marine Ecology Progress Series,* **226,** 193-210.

Zehr, J.P. & Ward, B.B. (2002) Nitrogen cycling in the ocean: New perspectives on processes and paradigms. *Applied and Environmental Microbiology,* **68,** 1015-1024.

Zettler, E.R., Olson, R.J., Binder, B.J., Chisholm, S.W., Fitzwater, S.E. & Gordon, R.M. (1996) Iron-enrichment bottle experiments in the equatorial pacific: Responses of individual phytoplankton cells. *Deep-Sea Research Part II-Topical Studies in Oceanography,* **43,** 1017-1029.

Zhang, Y.M., Chen, H., He, C.L. & Wang, Q. (2013) Nitrogen starvation induced oxidative stress in an oil-producing green alga *Chlorella sorokiniana* C3. *PLoS One,* **8,** e69225.

Zhou, Q., Chen, W., Zhang, H.Y., Peng, L., Liu, L.M., Han, Z.G., Wan, N., Li, L. & Song, L.R. (2012) A flow cytometer based protocol for quantitative analysis of bloom-forming cyanobacteria (microcystis) in lake sediments. *Journal of Environmental Sciences-China,* **24,** 1709-1716.

Zuur, A., Ieno, E.N., Walker, N., Saveliev, A.A. & Smith, G.M. (2009) *Mixed effects models and extensions in ecology with R.* Springer, New York.

Appendices

Appendix Chapter 3

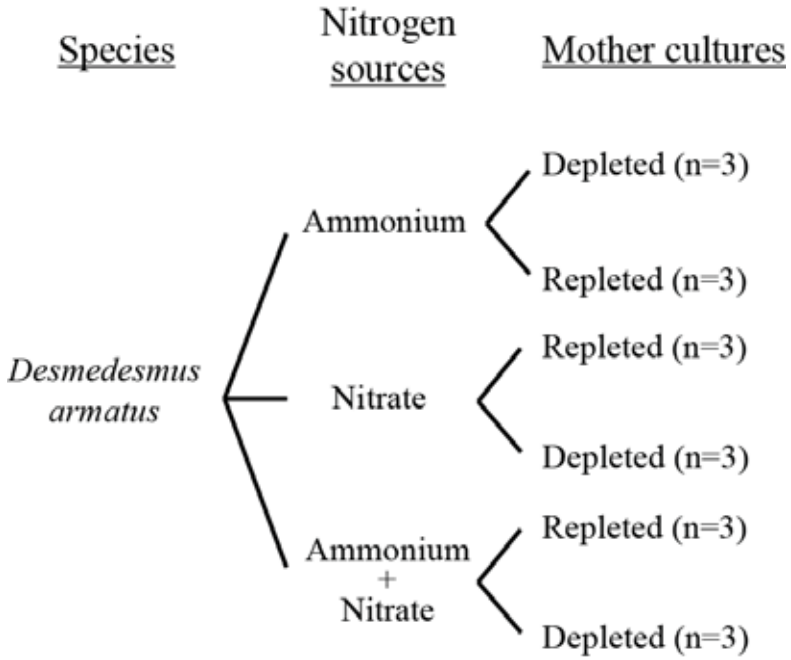

Figure S3.1: Diagram for the 3 × 2 factorial experimental design.

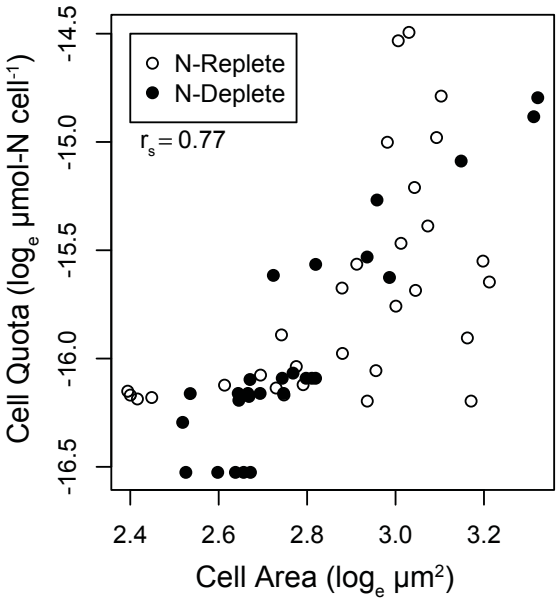

Figure S3.2: Correlation between internal quota dynamics extracted from the best-fitting "Allometric N-history" model and observed mean population cell size. Different symbols represent nitrogen-replete and nitrogen-replete experimental conditions. Also reported is the Spearman's rho correlation coefficient (r_s).

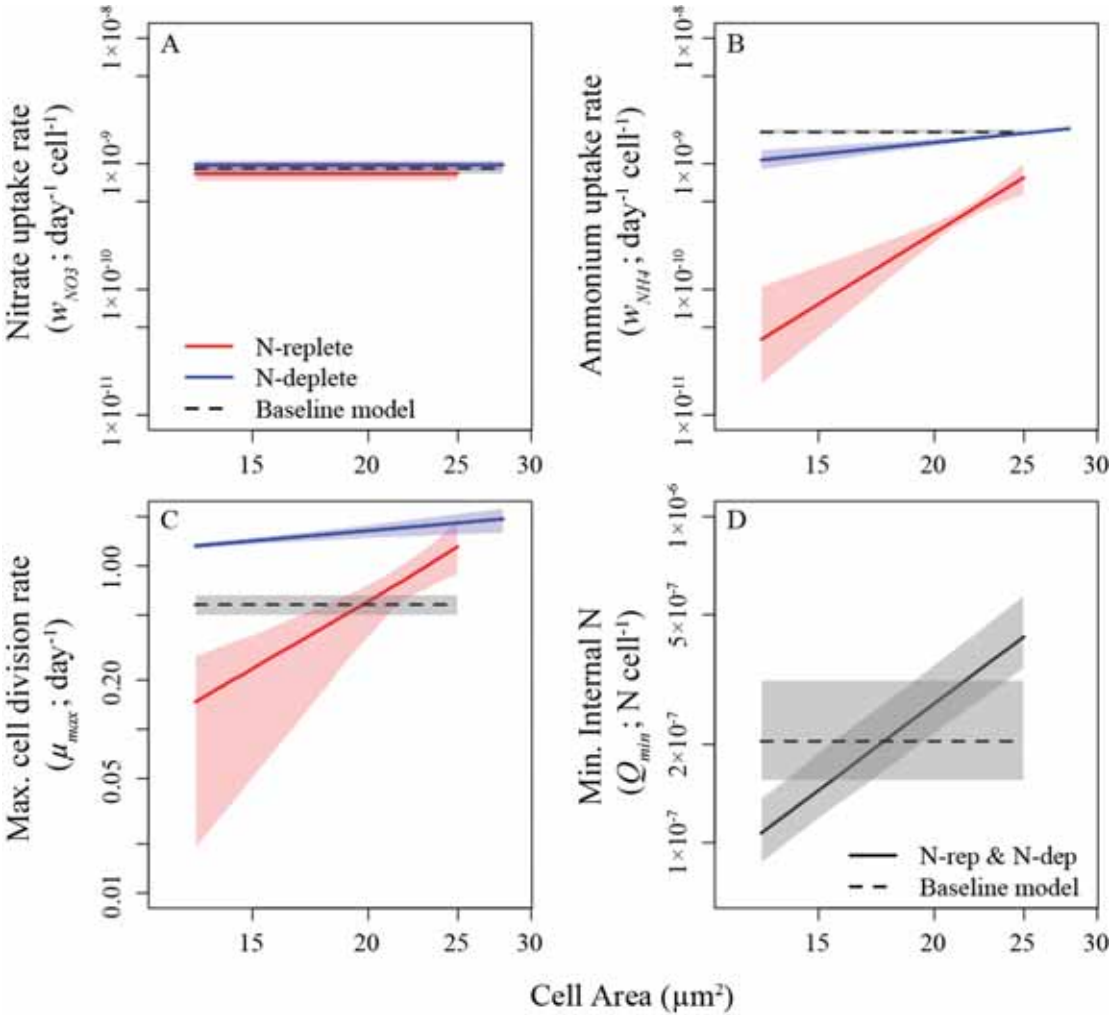

Figure S3.3: Comparison for the best-estimates for demographic parameters (median ±95% confidence intervals) calculated with process noise-only likelihood functions for the "baseline" model (dashed lines) and with the best-fitting "Allometric N-history" model (solid lines). Parameters represent rates of per-cell uptake for nitrate (A) and ammonium (B), growth rate at infinite stored internal nitrogen (C), and minimum internal nitrogen (D). Two solid lines in the same pannel represent the effect of cell size on the demographic parameters between N-replete (red) and N-deplete (blue) previous N-history. Dashed line is the corresponsive parameter estimated with the "baseline" model, which assumes independence with cell size and nutrient history. See Fig. 3.1 in Chapter 3 for more details.

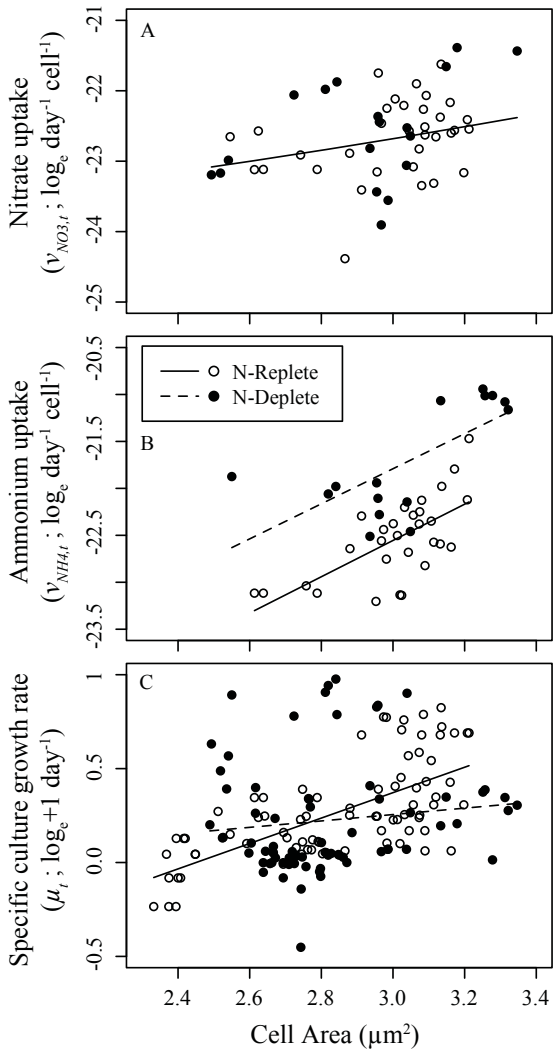

Figure S3.4: Effects of cell size and nutrient history on the observed per-cell rates for (A) nitrate uptake, $v_{NO3,t}$, (B) ammonium uptake, $v_{NH4,t}$, and (C) specific culture growth rate, μ_t. Each point is the mean between three replicate measurements for each replicate culture, for each day, for each experimental treatment. All plotted lines represent significant linear models at $p<0.05$.

Appendix A Chapter 5

Table S5.1: Models used to generate demographic parameters for simulating the datasets. A linear model was used to calculate a deterministic prediction for each parameter. Then, a random residual was extracted from a normal distribution with the standard deviation reported in the table. All coefficients were taken from freshwater phytoplankton communities in Edwards et al. (2013).

Par	Allometric model for $\log_{10}$(Par)	Stand. Deviation
v_{max}	$1.3 \times \log_{10}(\text{cell size}) - 8.8$	0.75
k	$0.52 \times \log_{10}(\text{cell size}) - 0.71$	0.34
μ_{max}	$-0.36 \times \log_{10}(\text{cell size}) + 0.69$	0.27
Q_{min}	$0.68 \times \log_{10}(\text{cell size}) - 8.7$	0.14

Appendix B Chapter 5

Graphical explanation for each step of the analytical methods

Step 1. Randomly select the cell volume of a species with uniform distribution on $\log_{10}$-scale between 10^2 and 10^5

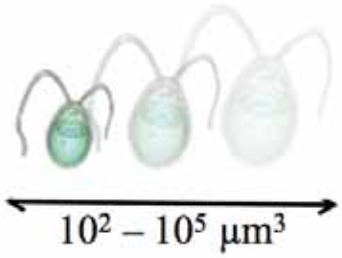

Step 2. For each model parameter, use allometric relationships in Edwards et al. (2012) to estimate a parameter value from the cell size of the species, also including uncertainty around the published allometric relationship.

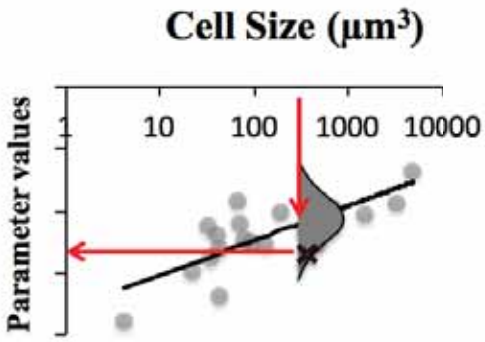

Step 3. Use the classic Quota model (eq. 1 a-c in main text) to generate the dataset for external N ($N(t)$), per-cell internal N ($Q(t)$), and population density ($B(t)$).

$$\frac{dN}{dt} = -f(N(t)) \times B(t)$$

$$\frac{dQ}{dt} = f(N(t)) - g(Q(t)) \times Q(t)$$

$$\frac{dB}{dt} = g(Q(t)) \times B(t)$$

Step 4. Simulate true trajectories (white dots): simulate deterministic trajectories (*Det.*) between each time step (arrows) and include stochastic process noise (red dashed line). Run simulations for 100 days.

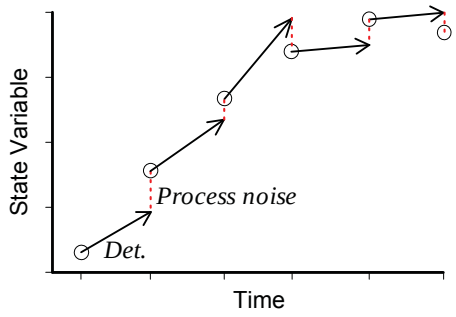

Step 5. Simulate observed trajectories (black dots):
add observation error (black dashed line) to each true value (white dots).

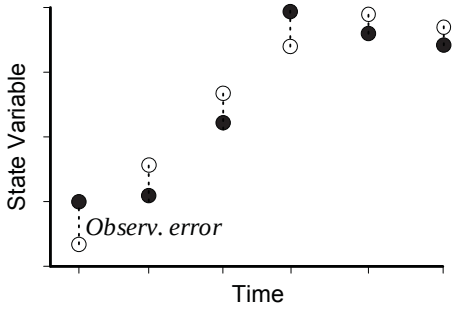

Step 6. A dataset for the three state variables, simulated with both process noise and observation error

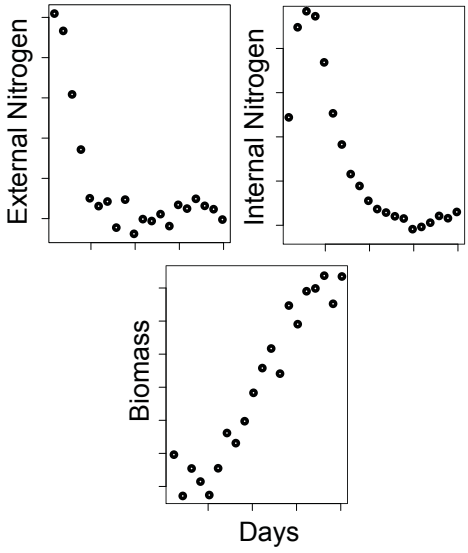

Step 7. Use the calibration curve documented in Malerba et al. (2015) and convert values of internal per-cell nitrogen to per-cell red fluorescence. Ensure a final R^2 of 0.77 between the two variables, equivalent to the relationship recorded empirically. If the precision of the relationship is higher than empirical data, increase observation error by increasing empirically-recorded observation error estimates[1] for both variables by keeping the ratio constant (*conservative option*[2])

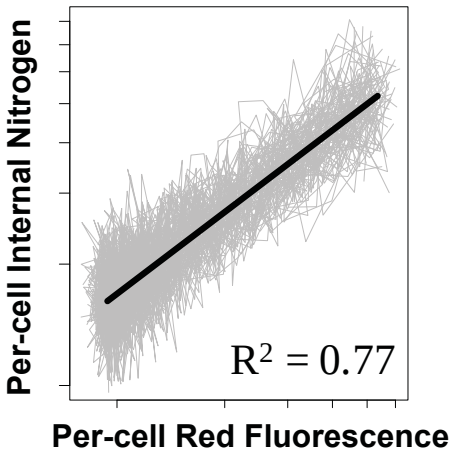

[1] The standard deviation from collecting triplicate independent readings of a sample offers an independent estimate of the magnitude of the observation error characterizing the laboratory procedure.

[2] This approach is conservative because details on laboratory protocols indicate that unrecorded observation error is more likely to be associated with measuring per-cell internal nitrogen, rather than red fluorescence. See first paragraph of the results in main text.

Step 8. Calibrate the three alternative models from different combinations of simulated state variables:

- Virtual-Quota model: External Nitrogen + Biomass
- Nitrogen-Quota model: External Nitrogen + Biomass + Internal Nitrogen
- Fluorescence-Quota model: External Nitrogen + Biomass + Per-cell red florescence

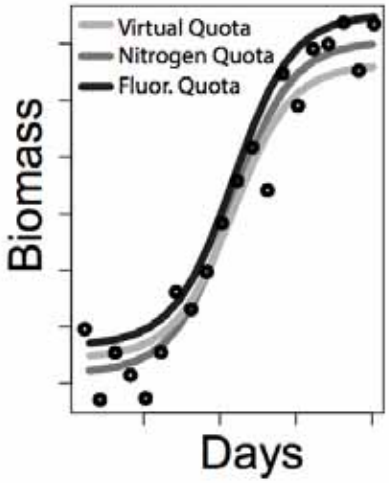

Step 9. Calculate the Mean Squared Error (MSE) between the parameter best-estimate ($\hat{\theta}$) and the true parameter value used to simulate the data (θ_{true}).

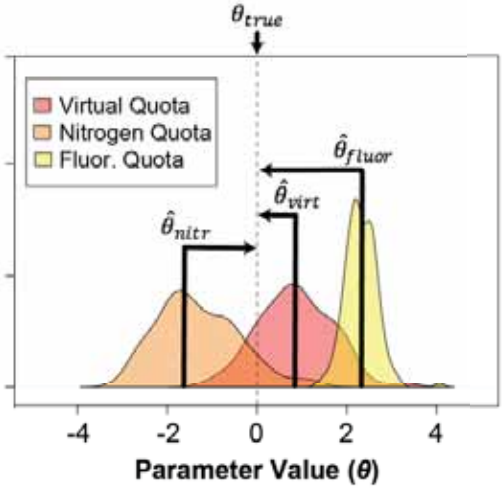

Appendix C Chapter 5

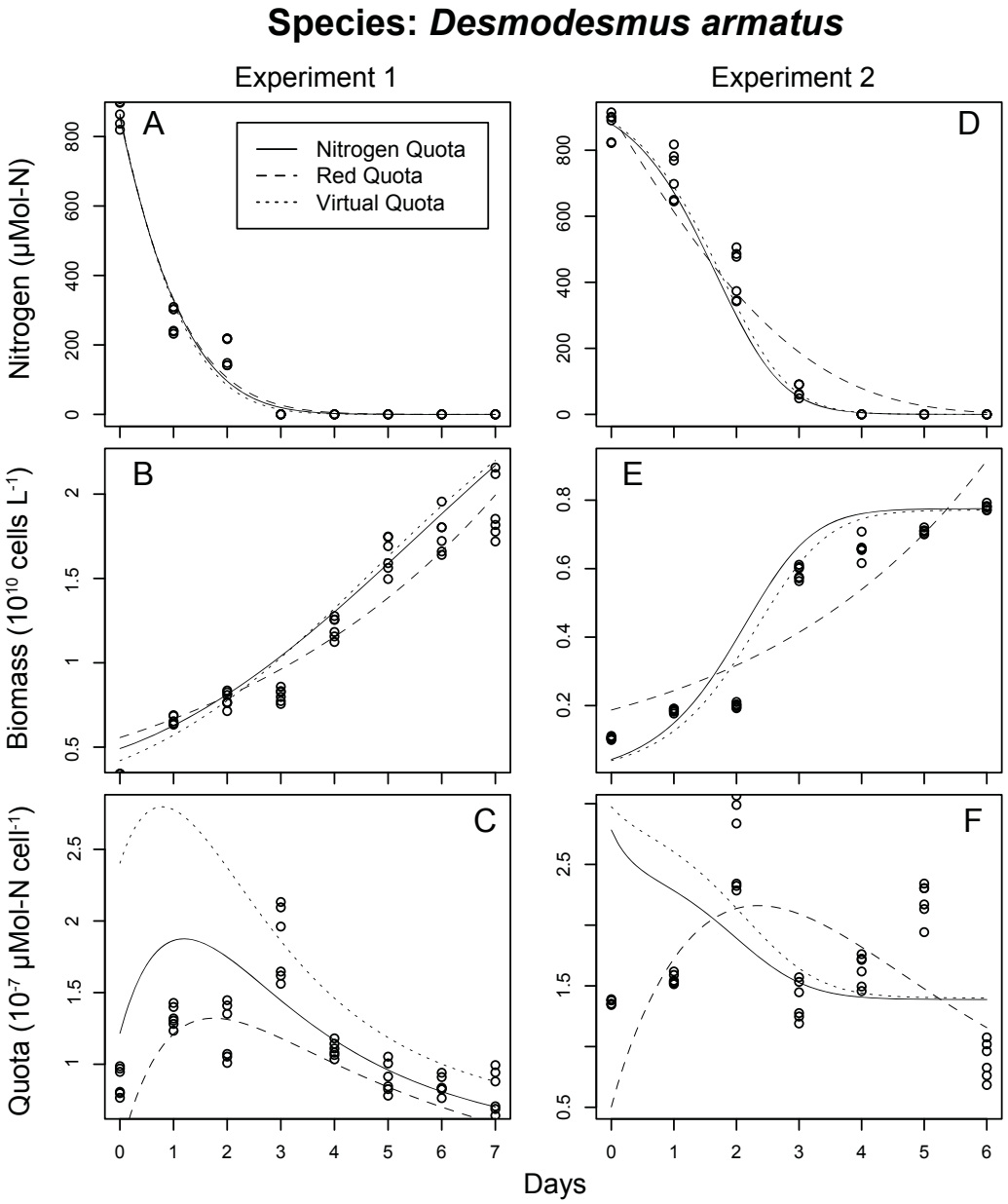

Fig. S5.1: Model fits for medium nitrogen (A, D), biomass (B, E), and nitrogen quota (C, F) for the time-series collected in chapter 4 from *Desmodesmus armatus* under two different initial conditions (Experiment 1 in A-C, and Experiment 2 in D-F). All models were calibrated assuming observation error-only. Only the Nitrogen Quota model is calibrated including observations for medium

nitrogen, biomass, and internal quota (panel C and F). Instead, the Red Quota model inferred the internal quota trajectories from time-series observations of red fluorescence, as well as ambient nitrogen and biomass. The Virtual Quota model inferred quota trajectories only from changes in ambient nitrogen and biomass growth. See material and methods in chapter 4 for more details on data collection.

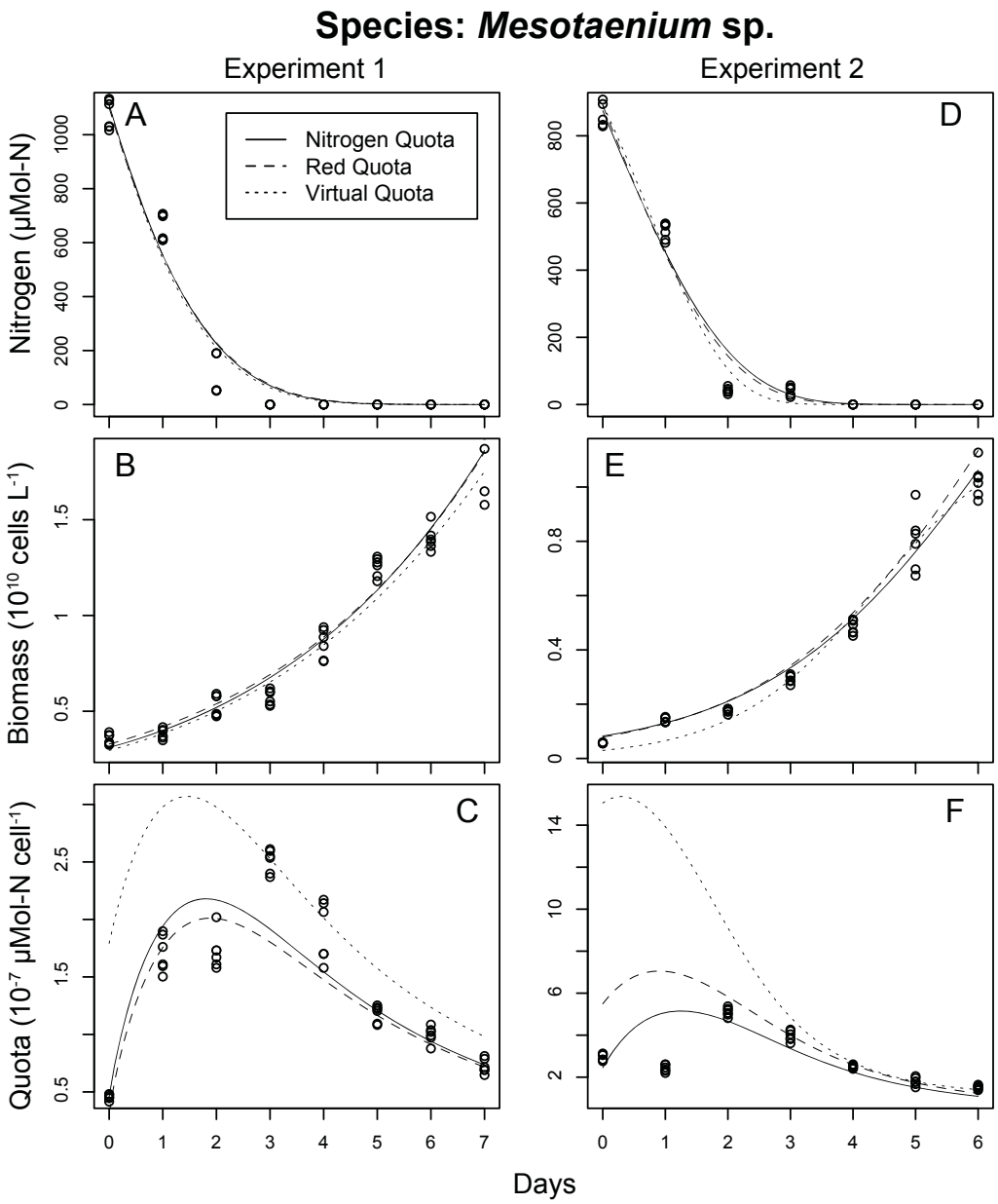

Fig. S5.2: Model fits for medium nitrogen (A, D), biomass (B, E), and nitrogen quota (C, F) for the time-series collected in chapter 4 from *Mesotaenium* sp. under two different initial conditions (Experiment 1 in A-C, and Experiment 2 in D-F). See legend in Fig. S5.1 and material and methods in chapter 4 for more details.

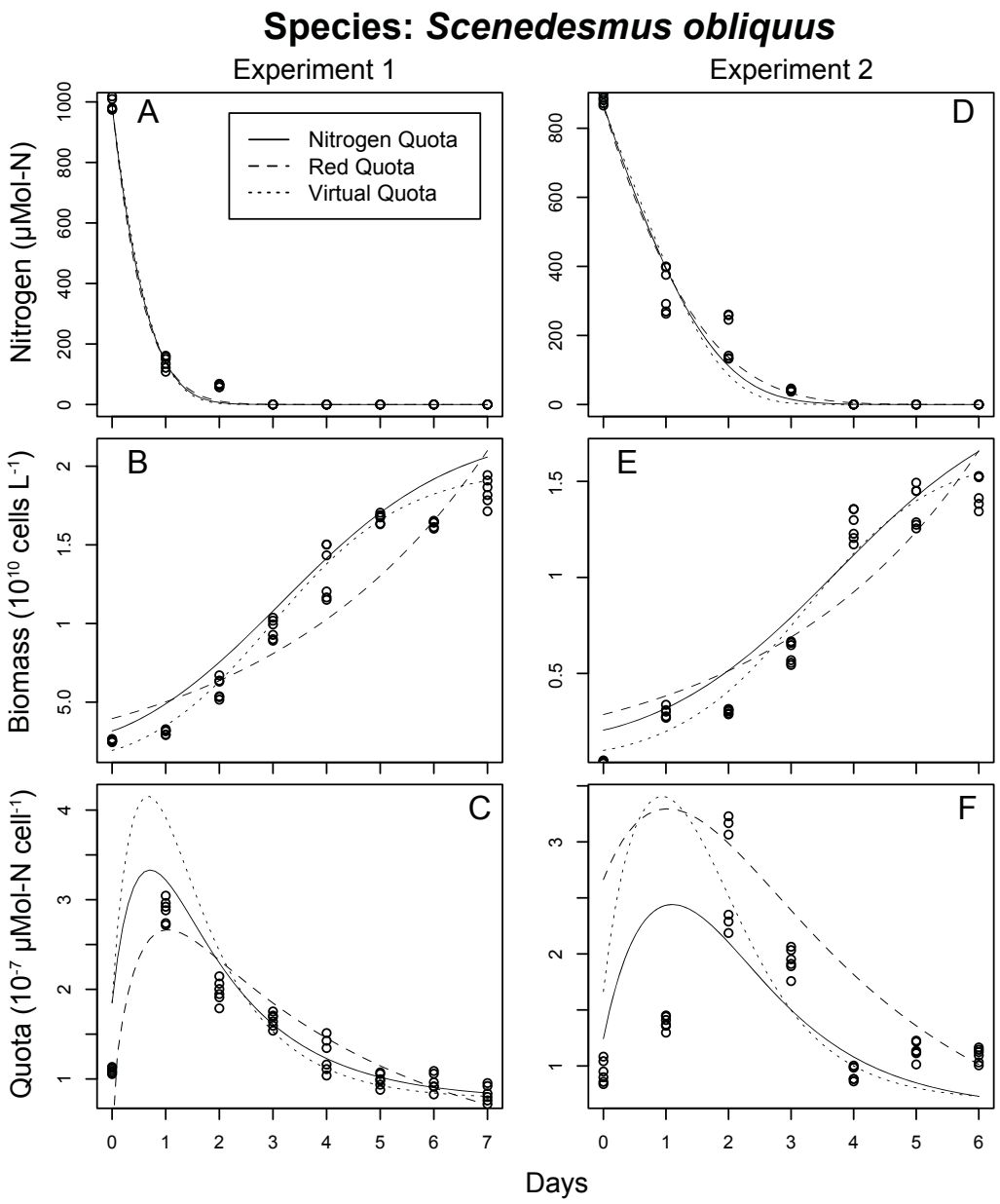

Fig. S5.3: Model fits for medium nitrogen (A, D), biomass (B, E), and nitrogen quota (C, F) for the time-series collected in chapter 4 from *Scenedesmus obliquus* under two different initial conditions (Experiment 1 in A-C, and Experiment 2 in D-F). See legend in Fig. S5.1 and material and methods in chapter 4 for more details.

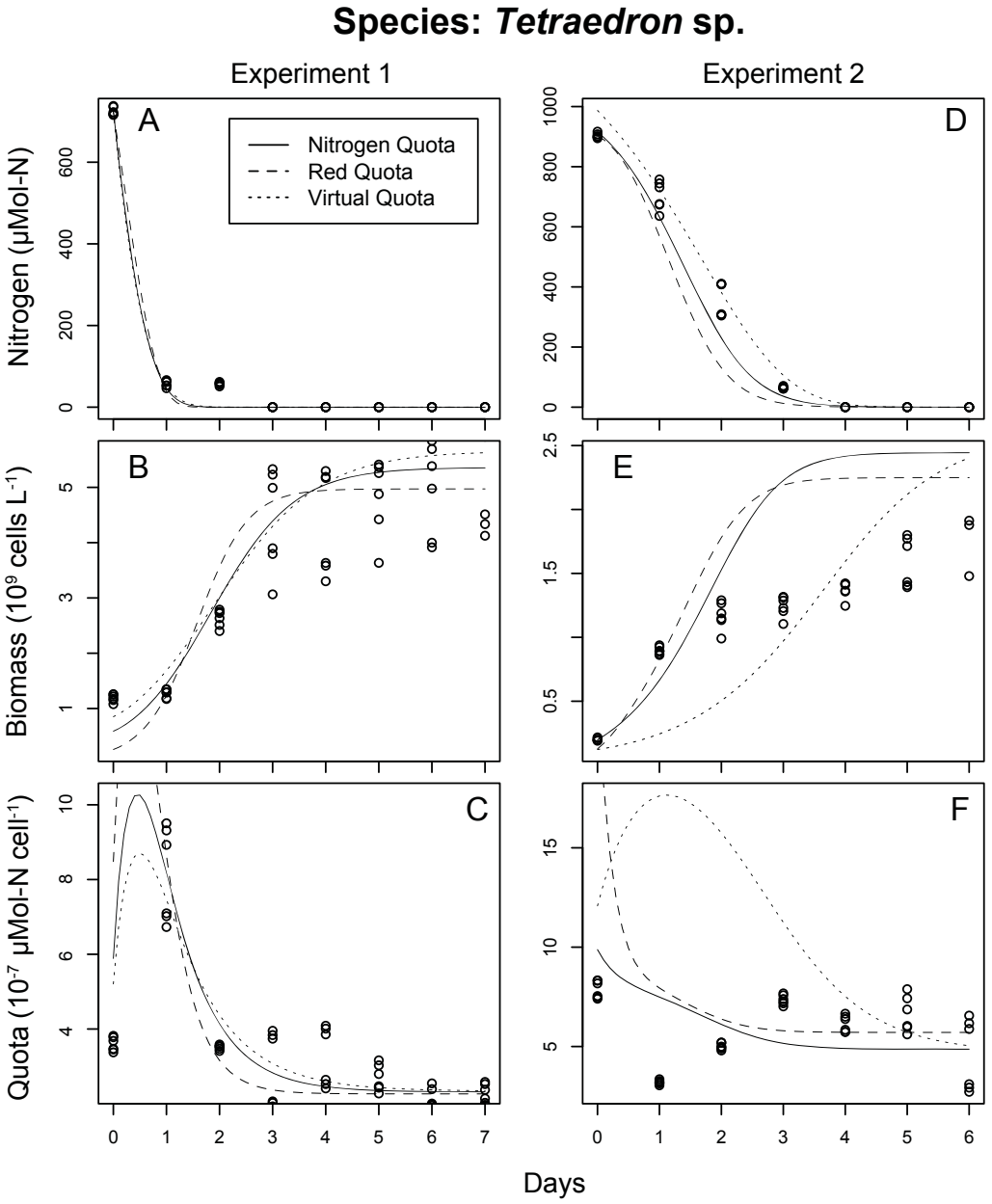

Fig. S5.4: Model fits for medium nitrogen (A, D), biomass (B, E), and nitrogen quota (C, F) for the time-series collected in chapter 4 from *Tetraedron* sp. under two different initial conditions (Experiment 1 in A-C, and Experiment 2 in D-F). See legend in Fig. S5.1 and material and methods in chapter 4 for more details.